



UNIVERSITAT DE
BARCELONA

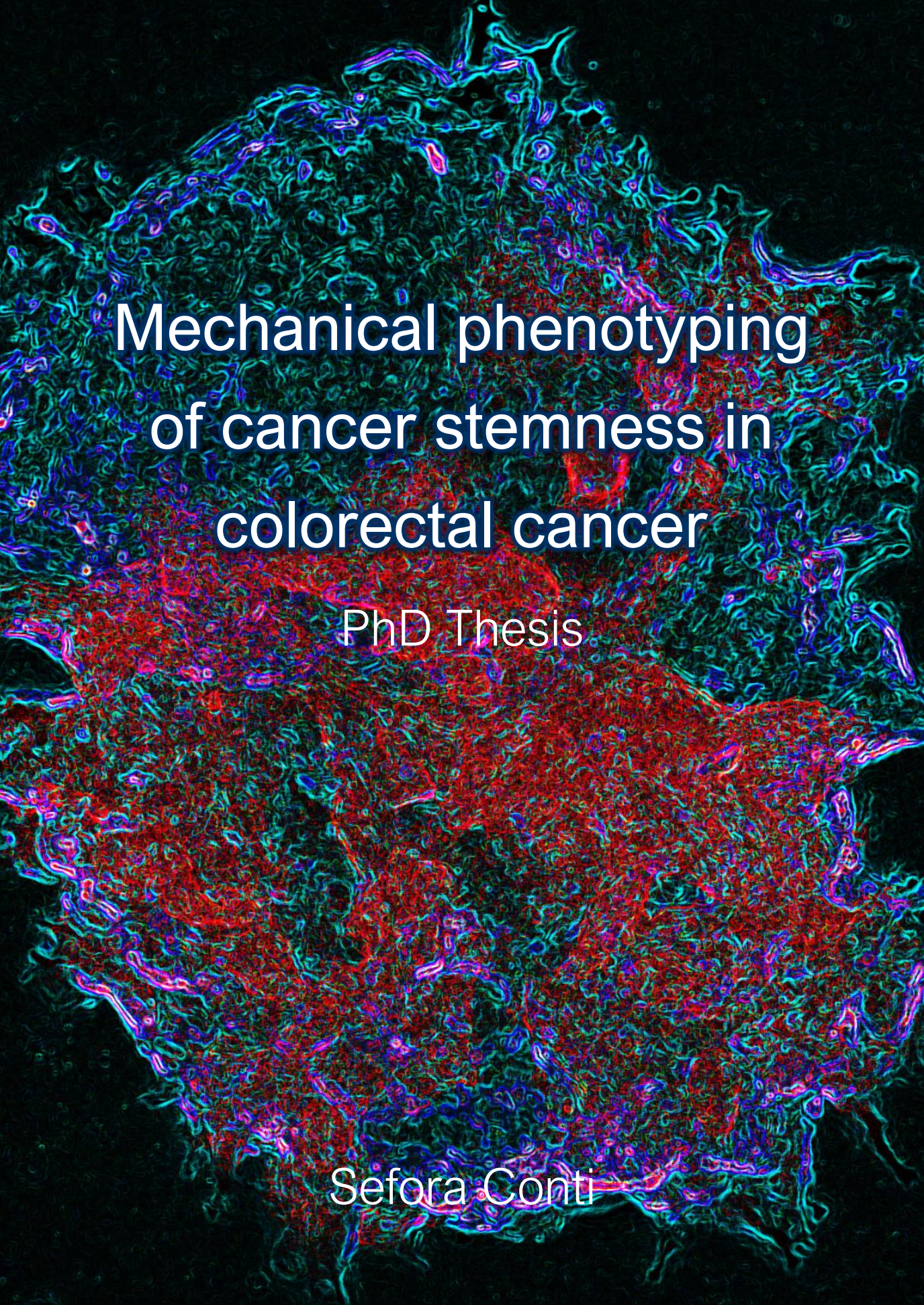
Mechanical phenotyping of cancer stemness in colorectal cancer

Sefora Conti

ADVERTIMENT. La consulta d'aquesta tesi queda condicionada a l'acceptació de les següents condicions d'ús: La difusió d'aquesta tesi per mitjà del servei TDX (www.tdx.cat) i a través del Dipòsit Digital de la UB (diposit.ub.edu) ha estat autoritzada pels titulars dels drets de propietat intel·lectual únicament per a usos privats emmarcats en activitats d'investigació i docència. No s'autoritza la seva reproducció amb finalitats de lucre ni la seva difusió i posada a disposició des d'un lloc aliè al servei TDX ni al Dipòsit Digital de la UB. No s'autoritza la presentació del seu contingut en una finestra o marc aliè a TDX o al Dipòsit Digital de la UB (framing). Aquesta reserva de drets afecta tant al resum de presentació de la tesi com als seus continguts. En la utilització o cita de parts de la tesi és obligat indicar el nom de la persona autora.

ADVERTENCIA. La consulta de esta tesis queda condicionada a la aceptación de las siguientes condiciones de uso: La difusión de esta tesis por medio del servicio TDR (www.tdx.cat) y a través del Repositorio Digital de la UB (diposit.ub.edu) ha sido autorizada por los titulares de los derechos de propiedad intelectual únicamente para usos privados enmarcados en actividades de investigación y docencia. No se autoriza su reproducción con finalidades de lucro ni su difusión y puesta a disposición desde un sitio ajeno al servicio TDR o al Repositorio Digital de la UB. No se autoriza la presentación de su contenido en una ventana o marco ajeno a TDR o al Repositorio Digital de la UB (framing). Esta reserva de derechos afecta tanto al resumen de presentación de la tesis como a sus contenidos. En la utilización o cita de partes de la tesis es obligado indicar el nombre de la persona autora.

WARNING. On having consulted this thesis you're accepting the following use conditions: Spreading this thesis by the TDX (www.tdx.cat) service and by the UB Digital Repository (diposit.ub.edu) has been authorized by the titular of the intellectual property rights only for private uses placed in investigation and teaching activities. Reproduction with lucrative aims is not authorized nor its spreading and availability from a site foreign to the TDX service or to the UB Digital Repository. Introducing its content in a window or frame foreign to the TDX service or to the UB Digital Repository is not authorized (framing). Those rights affect to the presentation summary of the thesis as well as to its contents. In the using or citation of parts of the thesis it's obliged to indicate the name of the author.



Mechanical phenotyping of cancer stemness in colorectal cancer

PhD Thesis

Sefora Conti



PhD program in Biomedicine

Mechanical phenotyping of cancer stemness in colorectal cancer

Dissertation submitted by Sefora Conti for
the degree of Doctor of Philosophy
Barcelona, 2023

A handwritten signature in black ink, appearing to read "Sefora Conti".

Supervisors:

Dr. Xavier Trepats Guixer

Dr. Anna Labernadie

A handwritten signature in black ink, likely belonging to Dr. Xavier Trepats Guixer.

A handwritten signature in black ink, likely belonging to Dr. Anna Labernadie.



To all the women of my family, past and present.

And to my Dad.

“L’acqua ch’o prendo già mai non si corse.”

Dante Alighieri, Divina Commedia

ACKNOWLEDGMENTS

Before diving into the waters of cancer mechanics, I would like to acknowledge the people that contributed to this thesis work and supported me in this journey.

Six years ago, I adventured in the field of mechanobiology almost clueless, since then I learned a lot about science and the academic world. For that I would like to thank my supervisor, Xavier Trepate, for giving me the opportunity to work in the lab, for the support and for the freedom to discover the scientist in me. Without you this journey and thesis would not have been possible.

I acknowledge the work and help of the laboratory technicians during the whole duration of my PhD. Natalia, Susana, Anghara, Oriol y Monica muchas gracias por vuestra ayuda y para constituir la base de todo el trabajo que se hace en el laboratorio. I'm also grateful for the various teams in the lab, microscopy, cell culture, protocol etc. You all dedicate time to the proper functioning of the lab, handling the frustration from failing microscopes or overbooked hoods. Mutual help and a patient approach makes our lab so enjoyable to work in.

I would like to thank my collaborators, Valeria Venturini, Verena Ruprecht, Carme Cortina, Adrià Canyellas, Eduard Batlle, Catherine Xu and Jochen Guck, for their help and scientific contribution. I learned so much from you and loved discussing science and exchanging ideas with you.

I also would like to thank my lab mates and friends. In these years we built a community, a sort of family, sharing not only science but also deep conversations, laughs, meals, hikes, trips, culture, holidays, and beers. I'm grateful for your friendship, for listening to me and supporting me in bright and dark times, for enriching me with new points of view. Some of you became true friends, and I hope our paths will cross many times more.

I'm grateful for sharing this journey and my life with my partner, Giordano. Grazie per accompagnarmi e appoggiarmi in questo viaggio di scoperte. Spero di esplorare e scoprire ancora tante cose con te accanto. I thank my family for the emotional support and advice of the past years. Sisters, siete meravigliose. Cedis, hai ascoltato quasi ogni lab meeting con interesse e dandomi infinito appoggio. Grazie per le lunghe conversazioni sulla vita. Zinis grazie per i consigli e per darmi tanti strumenti per affrontare le difficoltà. Babbo grazie per credere in me e capire il mio senso d'umorismo. **ליותר ולשאוף שלי היצירתיות את לבטא חשוב כמה אותי שלימדת תודה אמא Sansone**, for your feline love for me and for food. You make my life funnier and fluffier.

I thank the advisory board members and the jury for reading this thesis, for your questions and feedbacks.

I thank the patients that donated tumor samples to science and enabled the existence of this study and others.

And finally, I thank the reader for taking the time to read this thesis.

ABSTRACT

In this thesis work, I explored the link between cancer stemness and the mechanical properties of colorectal cancer (CRC) cells. In the last decades, the cancer stem cell (CSC) model underwent an important paradigm shift, from a static and intrinsic concept of CSCs to a more dynamic and plastic notion, integrating the influence of the microenvironment. Similarly, during the last five years, my experimental approach had to shift, from assuming that cancer stem cells are static and thus won't change in response to different culture conditions, to the realization that their stemness is largely affected by the microenvironment, and thus I had to establish the experimental conditions that would maintain the desired cellular phenotypes. This effort is not reflected in the present work, but it constitutes its foundation.

CRC tumors are composed of heterogeneous cell populations including a pool of cancer stem cells (CSCs) that express LGR5. The link between cancer cell differentiation states and their metastatic potential has been the focus of extensive investigation, with some studies pointing to microenvironmentally defined plasticity as a mechanism indispensable for metastasis formation. In this highly heterogeneous and plastic context, differences in mechanical phenotypes may favor or impair the ability of specific cell populations to progress through the metastatic cascade. However, whether distinct cell populations in CRC tumors display different mechanical properties, and how these properties might contribute to metastasis is unknown.

In the present study I performed a broad biophysical characterization of CRC patient derived organoids (PDOs) engineered to fluorescently label cells expressing LGR5. I found that LGR5⁺ and LGR5⁻ cells display distinct mechanical phenotypes. Compared to LGR5⁻ cells, LGR5⁺ cells are stiffer, adhere better to the extracellular matrix (ECM), move slower both as single cells and clusters, display higher nuclear YAP, and show a higher survival rate in response to mechanical confinement. These differences are largely explained by the downregulation of the membrane to cortex attachment proteins Ezrin/Radixin/Moesin (ERMs) in the LGR5⁺ cells. By analyzing scRNA-seq expression patterns from a patient cohort, I show that this downregulation is a robust signature of colorectal tumors. Finally, I also show that LGR5⁺ cells adhere better to the endothelial surface and form transendothelial gaps with higher efficiency than LGR5⁻ cells. Together, these results show that LGR5⁻ cells display a mechanically dynamic phenotype that favors dissemination from the primary tumor whereas LGR5⁺ cells display a mechanically stable and resilient phenotype that promotes extravasation and metastatic growth. The observed coupling between mechanical states and cancer cell heterogeneity may be an indispensable adaptive mechanism for metastatic progression.

RESUMEN

En esta tesis, he explorado la relación entre las células madre cancerosas y las propiedades mecánicas de las células del cáncer de colon. En las últimas décadas, el modelo de células madre de cancerosas ha experimentado un importante cambio de paradigma, pasando de un concepto estático e intrínseco de células madre cancerosas a una noción más dinámica y plástica, que integra la influencia del microambiente. Del mismo modo, durante los últimos cinco años, mi enfoque experimental tuvo que cambiar, pasando de suponer que las células madre cancerosas son estáticas y, por tanto, no cambiarán en respuesta a diferentes condiciones de cultivo, a la constatación de que su carácter de células madre se ve afectado en gran medida por el microambiente, por lo que tuve que establecer las condiciones experimentales que mantuvieran los fenotipos celulares deseados. Este esfuerzo no se refleja en el presente trabajo, pero constituye su fundamento.

Los tumores de cáncer colorrectal están compuestos por poblaciones celulares heterogéneas que incluyen un conjunto de células madre cancerosas, marcadas por la expresión de LGR5. La relación entre los estados de diferenciación de las células cancerosas y su potencial metastásico ha sido objeto de una amplia investigación, y algunos estudios apuntan a la plasticidad definida por el microambiente como mecanismo indispensable para la formación de metástasis. En este contexto altamente heterogéneo y plástico, las diferencias en los fenotipos mecánicos pueden favorecer o perjudicar el potencial metastático de las células cancerosas. Sin embargo, se desconoce si las distintas poblaciones celulares de los tumores de colon presentan diferentes propiedades mecánicas y cómo estas propiedades podrían contribuir a las metástasis.

En este estudio llevé a cabo una amplia caracterización biofísica de organoides derivados de pacientes de cáncer de colon diseñados para etiquetar con fluorescencia células que expresan LGR5. Descubrí que las células LGR5+ y LGR5- muestran fenotipos mecánicos distintos. En comparación con las células LGR5-, las células LGR5+ son más rígidas, se adhieren mejor a la matriz extracelular, se mueven más lentamente tanto como células individualmente que en grupo, muestran más YAP nuclear y una mayor tasa de supervivencia en respuesta al confinamiento mecánico. Estas diferencias se explican en gran medida por la regulación a la baja de las proteínas de unión de la membrana a la corteza Ezrin/Radixina/Moesina en las células LGR5+. Mediante el análisis de los patrones de expresión scRNA-seq de una cohorte de pacientes, demuestro que esta regulación a la baja es una firma robusta de los tumores colorrectales. Por último, también demuestro que las células LGR5+ se adhieren mejor a la superficie endotelial y forman brechas transendoteliales con mayor eficacia que las células LGR5-. En conjunto, estos resultados muestran que las células LGR5- presentan un fenotipo mecánicamente dinámico que favorece la diseminación desde el tumor

primario, mientras que las células LGR5+ presentan un fenotipo mecánicamente estable y resistente que favorece la extravasación y el crecimiento metastásico. El acoplamiento observado entre los estados mecánicos y la heterogeneidad de las células cancerosas puede ser un mecanismo adaptativo indispensable para la progresión metastásica.

CONTENTS

List of Figures	xv
1. INTRODUCTION	1
1.1. MECHANOBIOLOGY OF CANCER	3
1.1.1. Physical traits of cancer	3
1.1.2. Mechanical forces in the metastatic cascade	5
1.2. BIOMIMETIC SYSTEM FOR CANCER RESEARCH	9
1.2.1. 2D and 3D models	9
1.2.2. Spheroids	10
1.2.3. Tumor organoids	11
1.2.4. Tumor-on-chip	13
1.2.5. Measuring forces and mechanics of tumors	14
1.3. CANCER STEM CELLS	16
1.3.1. The cancer stem cell model	16
1.3.2. Cancer stem cells and their niche	19
1.3.3. Cancer stem cells, EMT and metastasis	20
1.3.4. Mechanical niche and cancer stem cells	22
1.3.5. Mechanics of cancer stem cells	23
1.4. COLORECTAL CANCER	25
1.4.1. Types	25
1.4.2. CRC progression and staging	25
1.4.3. Colon cancer stem cells	27
1.4.4. Metastasis in colorectal cancer	30
1.4.5. CRC CSCs and the microenvironment	32
2. OBJECTIVES	34
3. MATERIALS AND METHODS	36
3.1. EXPERIMENTAL METHODS	36
3.1.1. Patient-derived organoids culture	36
3.1.2. Flow cytometry analysis and sorting	37
3.1.3. Polyacrylamide gel preparation	38
3.1.4. Cell confinement	39
3.1.5. Mechanical characterization of cells using RT-DC	39
3.1.6. Cluster Motility assay	41

3.1.7.	HUVEC Monolayer Formation and cluster attachment assay	41
3.1.8.	Quantitative PCR (qPCR)	41
3.1.9.	Western blotting	43
3.1.10.	Generation of stable PDO line expressing inducible iMC-linker	43
3.1.11.	Immunostainings	44
3.1.12.	Antibodies	44
3.2.	DATA AND IMAGE ANALYSIS	45
3.2.1.	Image acquisition	45
3.2.2.	Cell and cluster segmentation	45
3.2.3.	LGR5+ cells Tdtomato fluorescence intensity measurements	46
3.2.4.	YAP nuclear to cytoplasmic ratio quantification.....	46
3.2.5.	Shape Analysis.....	46
3.2.6.	Cell and clusters tracking	46
3.2.7.	Traction force microscopy	47
3.2.8.	Multipole analysis of tractions	47
3.2.9.	Patient 10x single-cell analysis	47
3.2.10.	Statistical analysis	48
4.	RESULTS	50
4.1.	SINGLE CELL MECHANICAL CHARACTERIZATION	50
4.1.1.	LGR5+ and LGR5- cells display differences in morphology and adhesion	50
4.1.2.	LGR5+ and LGR5- cells display differences in YAP localization, but not in mechanosensing.....	51
4.1.3.	Cell velocities, mean traction forces and polarization	52
4.1.4.	LGR5+ cells are stiffer	55
4.2.	RESPONSE TO CONFINEMENT	57
4.2.1.	LGR5+ cells respond to confinement with higher survival.	57
4.2.2.	LGR5- cells adopt a faster amoeboid migration	59
4.3.	COLLECTIVE BEHAVIOUR	61
4.3.1.	LGR5- clusters are rounder, migrate faster and exert less tractions ...	61
4.3.2.	LGR5+ clusters adhere better to the endothelium and form transendothelial gaps.	64
4.4.	MOLECULAR MECHANISM UNDERLYING THE IDENTIFIED PHENOTYPES	
	67	

4.4.1.	Upregulation of ERMs in LGR5- cells	67
4.5.	EXPRESSION OF LGR5 AND EZRIN ARE ANTICORRELATED IN CRC PATIENTS	73
5.	DISCUSSION	77
5.1.	DYNAMIC MECHANICAL STATE vs. RESILIENCE	77
5.2.	COLLECTIVE BEHAVIOUR AND ACTIVE WETTING	80
5.3.	YAP AND CRC STEMNESS	80
5.4.	ERM PROTEINS DETERMINE THE IDENTIFIED MECHANICAL PHENOTYPES	82
5.5.	MECHANICAL ADAPTABILITY	84
6.	CONCLUSIONS	86
7.	REFERENCES	88

List of Figures

Figure 1: Biological processes influenced by mechanical forces.

Figure 2: Mechanical hallmarks of cancer.

Figure 3: Effects of adhesion on distinct aspects of metastasis.

Figure 4: Physiological relevance of cancer models.

Figure 5: Examples of applications of 3D spheroids.

Figure 6: Patient-derived cancer organoids derivation and processing.

Figure 7: Julius Cohnheim

Figure 8: The hierarchical and dynamic CSC models.

Figure 9: Heterogeneity in mechanical properties of the TME.

Figure 10: Scheme of progression of colorectal cancer.

Figure 11: Lineage tracing experiments, LGR5⁺ cells and plasticity.

Figure 12: Plasticity of LGR5⁻ cells drives metastasis in CRC.

Figure 13: Sorting and measuring TdTomato Fluorescence of LGR5⁻, LGR5^{med} and LGR5⁺ cells.

Figure 14: Scheme of dynamic cell confiner.

Figure 15: Principle and setup of RT-DC setup.

Figure 16: LGR5⁺ and LGR⁻ single cells display differences in morphology and adhesion.

Figure 17: LGR5⁺ and LGR5⁻ single cells display differences in YAP localization but not in mechanosensing.

Figure 18: LGR5⁺ and LGR5⁻ cells are equally fast in adhesive conditions and exert similar tractions, but LGR5⁺ are more polarized.

Figure 19: RT-DC experimental setup.

Figure 20: LGR5⁺ cells are stiffer.

Figure 21: LGR5⁺ cells respond to confinement with a higher survival rate.

Figure 22: LGR5⁺ cells respond to confinement with slower ameboid migration.

Figure 23: LGR5⁺ cells respond to confinement with slower ameboid migration

Figure 24: LGR5⁻ clusters are rounder, migrate faster and exert less traction.

Figure 25: LGR5⁻ clusters are rounder, migrate faster and exert less traction.

Figure 26. Setup of adhesion to endothelium experiment.

Figure 27. PDO clusters adhering to an endothelial monolayer.

Figure 28. LGR5⁺ clusters adhere better to endothelial monolayers and form transendothelial gaps.

Figure 29: Expression of genes related to adhesion and actin cytoskeleton organization.

Figure 30: ERM proteins are upregulated in the LGR5⁻ cells.

Figure 31: Levels of phosphorylated ERM proteins and Ezrin expression in sorted LGR5^{med} and LGR5⁺ cells.

Figure 32: ERM proteins determine the morphological differences between LGR5⁺ and LGR5⁻ single cells and clusters.

Figure 33: ERM proteins determine the response to confinement in LGR5⁺ and LGR5⁻ cells.

Figure 34: Expression of LGR5 and Ezrin are anticorrelated in transcriptomic data from CRC patients.

Figure 35. Expression of *Msn* and *Rdx* in CRC patients.

Figure 36. Expression of *Lgr5*, *Krt20*, *Msn* and *Rdx* in CRC patients.

Figure 37: Membrane to cortex attachment determines different mechanical phenotypes in LGR5⁺ cancer stem cells and LGR5⁻ cancer cells.

ACRONYMS

AML	acute myelogeneous leukemia
AFM	atomic force microscopy
APC	adenomatous polyposis coli
BMP	bone morphogenetic protein
CAF	cancer-associated fibroblast
CRC	colorectal Cancer
CSC	cancer stem cell
CTC	circulating tumor cell
CK20	cytokeratin20
DTR	diphtheria toxin receptor
ECM	extracellular matrix
EGF	epidermal growth factor
EGFR	epidermal growth factor receptor
EHS	engelbreth-Holm-Swarm
EMT	epithelial to mesenchymal transition
ERM	ezrin/ radixin/ moesin
FGF	fibroblast growth factor
FERM	Four point one, ERM
FRET	Förster resonance energy transfer
HCC	hepatocellular carcinoma
HNPCC	hereditary nonpolyposis colorectal cancer
HRC	high-relapse cell
HSC	hematopoietic stem cell
HUVEC	human umbilical vein endothelial cell
Ig-CAM	immunoglobulin-like cell adhesion molecule
iPSC	induced pluripotent stem cell
IFP	interstitial fluid pressure
ISC	Intestinal stem cells
L1CAM	L1 cell adhesion molecule
LGR5	leucine-rich repeat-containing G-protein coupled receptor
MAPK	mitogen-activated protein kinase
MET	mesenchymal-to-epithelial transformation
MMR	mismatch repair
NF-κB	nuclear factor kappa-light-chain-enhancer of activated B cells
PIV	particle imaging velocimetry
PDO	patient derived organoids

PAA	polyacrylamide
PDMS	polydimethylsiloxane
PI3K	phosphatidylinositol-4,5-bisphosphonate 3-kinase
RT-DC	real-time deformability cytometry
TEMED	tetramethylethylenediamine
TFM	traction force microscopy
TEM	transendothelial migration
TGF- β	transforming growth factor
TACS	tumor associated collagen signatures
TME	tumor microenvironment

1. INTRODUCTION

Mechanobiology is the study of how physical forces shape biological elements and how these elements sense and respond to physical inputs. Physiological processes such as growth, development, differentiation, and morphogenesis are all influenced by physical forces and linked to defined cellular and tissue mechanics (Figure 1). Examples for such forces are shear stresses exerted on circulating cells in blood and lymphatic vessels, pulling or pushing forces between neighboring cells, adhesion forces either intercellular or between cells and their substrate, compressive stresses, and physical confinement during migration through narrow pores or transendothelial spaces (Paul et al., 2017; Zuela-Sopilniak and Lammerding, 2022).

Cells can sense physical forces through a wide range of cellular machineries encompassing cell surface receptors such as integrins and cadherins, cytoskeletal filaments such as actin and microtubules and nuclear components including nucleopores and the nuclear lamina (Cho et al., 2017; Kirby and Lammerding, 2018). Mechanical inputs are converted to biochemical signals through mechanosensors, which induce cellular signaling that ultimately results in cellular responses. This conversion process from mechanical stimuli to signaling responses is defined “mechanotransduction”. Examples for mechanosensors are stretch-activated ion-channels, cell-cell junctions, adhesion complexes, cytoskeletal components, and nuclear components. Upon physical inputs such as extracellular matrix (ECM) stiffness, stretching, changes in ECM geometry and cell crowding, these mechanosensitive elements activate signaling pathways that modulate the expression of genes involved in cell proliferation, survival, and cell fate (Z. Sun et al., 2016; Dasgupta and McCollum, 2019; Murthy et al., 2017; Kirby and Lammerding, 2018; Swaminathan and Gloerich, 2021). Hence, there is a constant interplay between cells and their mechanical environment.

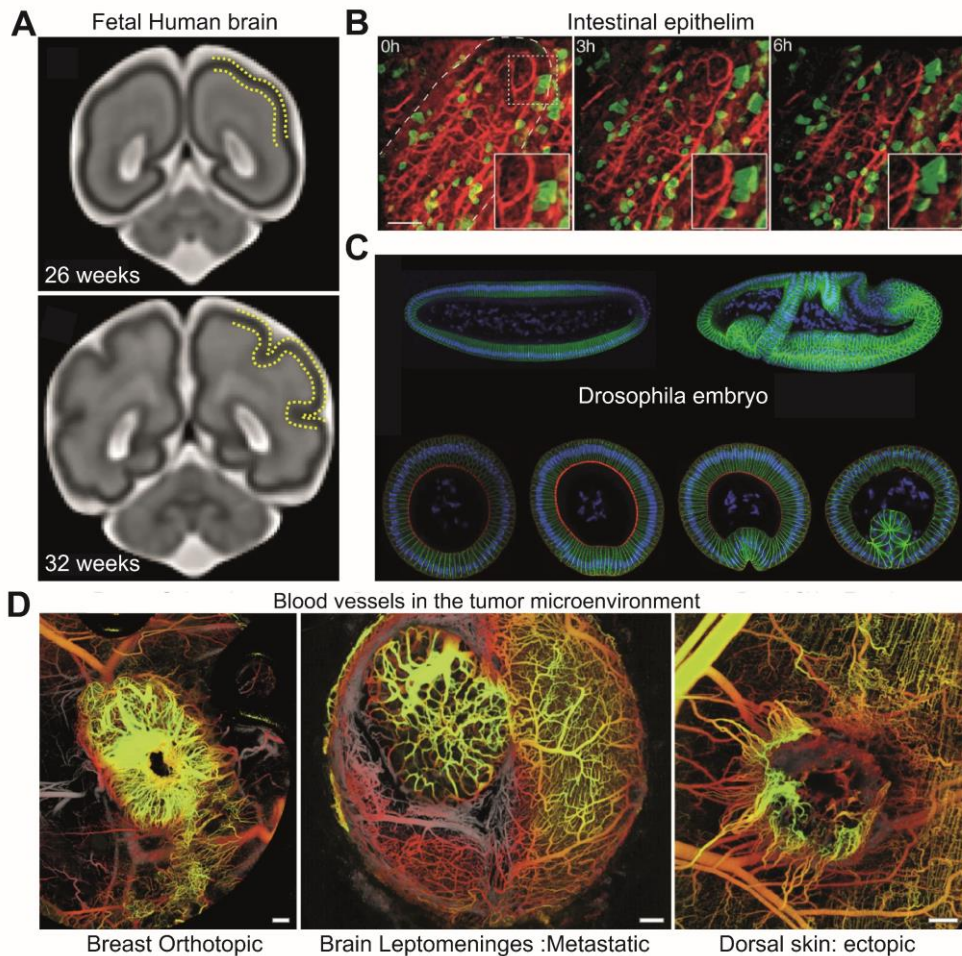


Figure 1: Biological processes influenced by mechanical forces. (A) Magnetic resonance images of the fetal human brain before and after the formation of cortical folds. Adapted from (Garcia et al., 2021) (B) Intestinal epithelial cells actively migrate up the gut villus in an actomyosin-dependent manner. Adapted from (Krndija et al., 2019). (C) Formation of the ventral furrow in the *Drosophila* embryo. Top images depict the embryo before and after gastrulation while the bottom images are cross sections showing the progression of the ventral furrow formation. Adapted from (Holcomb et al., 2021). (D) Optical frequency domain images of murine carcinoma vasculatures showing differences in vessel networks depending on the tumor microenvironment. Adapted from (Vakoc et al., 2009).

1.1. MECHANOBIOLOGY OF CANCER

1.1.1. Physical traits of cancer

Alterations in the mechanical properties of cells and their microenvironment are often associated with pathological conditions. One example of such alterations can be found in cancer. The tumor microenvironment (TME) contains three main components: cells (stromal cells, pericytes, immune cells), the ECM and the vasculature (blood and lymphatic vessels). As cancer progresses, the homeostatic biomechanical properties of the environment are increasingly disrupted leading to abnormal physical forces. At the level of the whole tissue, 4 main physical traits or hallmarks of cancer can be identified: elevated solid stress and interstitial fluid pressure, altered mechanical properties and altered microarchitecture (Figure 2) (Nia et al., 2020).

Solid stress is defined as the residual stress that remains in a solid and elastic material after all the external forces have been removed. As cells and the ECM contain solid and elastic elements, they can accumulate and transmit mechanical forces such as tensile, compressive and shear forces. In tumors, cell proliferation, deposition or swelling of matrix components (Voutouri et al., 2016) and cell contractions all contribute to the building-up of compressive and tensile solid stress (Levayer, 2020; Nia et al., 2016).

Mechanical stress can be contained and transmitted not only by solid components, but also by the tumor liquid phase. In the TME, leaky blood vessels (Baluk et al., 2003), abnormalities in the lymphatic drainage system (Leu et al., 2000; Padera et al., 2002) and vessel compression from the high solid stress lead to an increase of the osmotic and hydrostatic pressure in the tumor interstitium and thus an elevated interstitial fluid pressure (IFP) (Gutmann et al., 1992; Less et al., 1992; Curti et al., 1993; Heldin et al., 2004). Elevated IFP decreases transport across capillary walls, thus lowering the uptake of anti-carcinogenic drugs.

Another mechanical alteration that characterizes tumor tissues is an increase in stiffness or elastic modulus. In several cancer types such as breast (Evans et al., 2012), colorectal (Bauer et al., 2020), liver (Shahryari et al., 2019) and prostate (Rouvière et al., 2017) the tissue rigidity is higher in comparison to the healthy tissue. This tissue stiffening derives from increased deposition and cross-linking

of the matrix components by cancer cells and cancer associated fibroblasts (CAF) (Sahai et al., 2020), and by strain stiffening of the same components by the mechanical stresses in the TME (Han et al., 2018). As a result, CAFs are activated and their ECM deposition and modeling is further enhanced resulting ultimately in an increase in cancer cells invasiveness and thus tumor malignancy (Deng et al., 2022; Ishihara and Haga, 2022; Samuel et al., 2011).

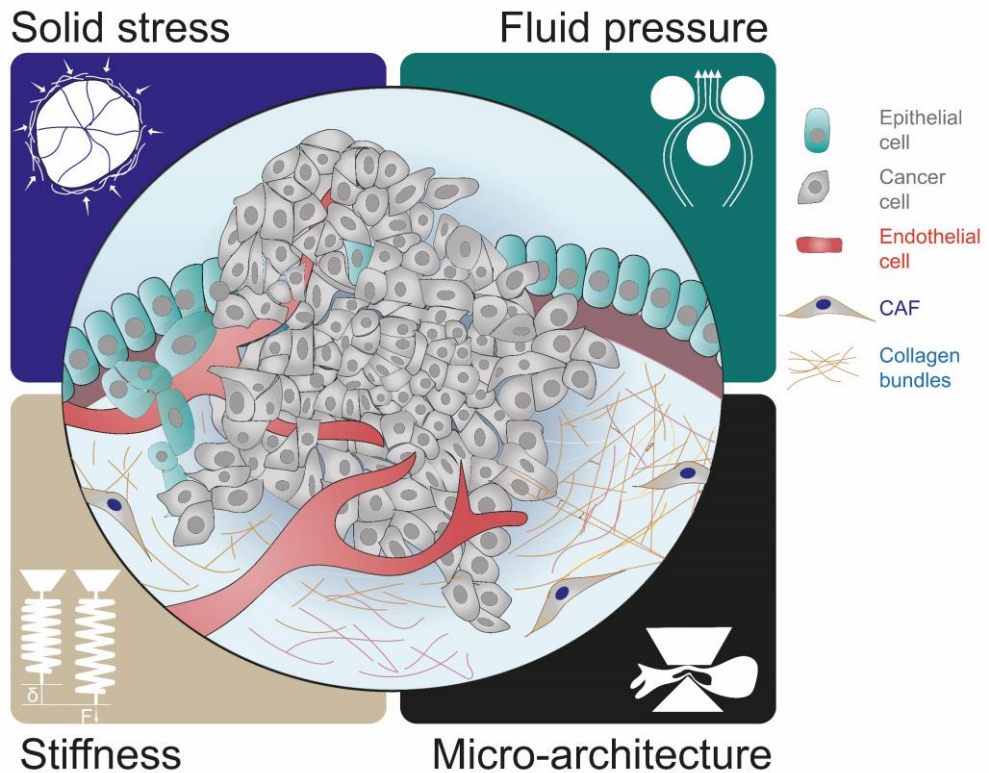


Figure 2: Mechanical hallmarks of cancer. Inspired from (Nia et al., 2020).

Despite the stiffening of the tumor tissue during cancer progression, it is well established that cancer cells tend to be softer than their healthy counterparts. This was shown already more than two decades ago, in a study comparing two normal epithelial cell lines to three bladder cancer ones. Using scanning force microscopy, Lekka *et al.* showed that the cancerous cell lines were an order of magnitude softer than the normal cells (Lekka et al., 1999). Since then, similar findings were reported for gastrointestinal (Suresh et al., 2005), breast (Guck et al., 2005; Liu et al., 2015) and ovarian cancer cell lines (Xu et al., 2012) and for patient samples of lung, breast and pancreatic cancer (Cross et al., 2008). Moreover, cells in the invasive branches and periphery of cancer organoids were

found to be softer compared with cells in the organoid core, suggesting a potential role of tumor cell mechanics in determining the invasive potential of cancer cells (Han et al., 2020).

Organs and tissues are organized following a specific structure and architecture that allow proper execution of their function and maintenance of homeostasis. As tumors progress, this structure is disrupted, and the tissue microarchitecture undergoes alterations. Some examples are changes in cell geometry and polarization (Yang and Weinberg, 2008), reorganization of ECM topology and pore size, alignment of collagen bundles and changes in cell-ECM and cell-cell adhesion (Winkler et al., 2020).

1.1.2. Mechanical forces in the metastatic cascade

Metastasis formation is a sequential process involving multiple steps including cancer cell dissemination, intravasation, survival in the bloodstream, adhesion to the vessel wall, extravasation, and colonization of distant organs (Lambert et al., 2017). In every step of this cascade, cancer cells are exposed to distinct physical forces. The crosstalk between these forces and the mechanical properties of cancer cells is determinant for their survival and metastatic potential (Gensbittel et al., 2021; Hayward et al., 2021). For instance, reduced cell stiffness contributes to cancer cell ability to migrate through confining microenvironments (Swaminathan et al., 2011), while it can be detrimental for circulating tumor cells (CTCs) survival against hemodynamic stresses during circulation in the blood stream (Moose et al., 2020).

One example of the physical forces applied on cancer cells is physical confinement. While disseminating, cancer cells encounter confining microenvironments as porous matrices, heterogeneous ECM geometries, and 3D longitudinal tracks formed by aligned collagen bundles (Paul et al., 2017). They are subjected to physical constriction also while intra or extravasating from the blood stream (Paul et al., 2017) or while migrating through perivascular (Kienast et al., 2010) and intravascular spaces (Yamauchi et al., 2005). Physical confinement induces cellular and subsequent nuclear deformations, promoting changes in signaling pathways and in migration mechanisms (Paul et al., 2017). In absence of focal adhesions, physical confinement promotes a transition from adhesion-dependent mesenchymal migration to amoeboid migration, which is

bleb based and propelled by cortical actomyosin contractility and thus, does not require adhesion to the substrate (Figure 3A) (Gabbireddy et al., 2021; Liu et al., 2015; Lomakin et al., 2020; Venturini et al., 2020). To sense the confining microenvironment, cells rely on the nucleus, the stiffest and largest organelle in a cell (Guilak et al., 2000). As cell confinement increases, the nuclear envelope unfolds and the nuclear membrane tension increases, eliciting calcium release and consecutive activation of cytosolic phospholipase A₂, an enzyme known as a mechanosensor for changes in nuclear membrane tension. Ultimately, this cascade results in reorganization of the actin cytoskeleton and enhanced cortical actomyosin contractility, leading to increased cell polarization and amoeboid migration (Lomakin et al., 2020; Venturini et al., 2020). This mechanism has been proposed as the cell escape response to compression, enabling migration plasticity while facing heterogeneous microenvironments, such as the ones encountered by cancer cells throughout the metastatic cascade.

An example of a mechanical property that affects cell metastatic potential is adhesion. Fine-tuning the balance between cell-cell and cell- ECM adhesions is required all throughout the metastatic cascade and enables motility, cell-cell interactions, and integration of mechanical stimuli from the environment (Janiszewska et al., 2020). Cell adhesion molecules can be classified in four main groups: cadherins which mediate homotypic and heterotypic cell-cell junctions, integrins which mediate cell-matrix adhesions, selectins related to immune function and mediating cell-cell adhesions and immunoglobulin-like cell adhesion molecules (Ig-CAMs) that drive heterophilic and homophilic interactions and are the only group that is calcium independent. Several studies have related malignant transformation to changes in cell-cell (Derksen et al., 2006; Eger et al., 2005; Pećina-Šlaus, 2003; Takamura et al., 2004; Vleminkx et al., 1991) and cell-ECM adhesions, especially cadherins and integrins (Desgrosellier et al., 2009; Cagnet et al., 2014; Barcus et al., 2017; Hamidi and Ivaska, 2018). In the classic view of tumor progression of epithelial cancers, the apical-basal polarity is lost, and cells acquire features that enable detachment from the tumor bulk, migration, and invasion (Lambert and Weinberg, 2021). This process is defined as epithelial to mesenchymal transition (EMT) and in terms of adhesion its hallmarks are loss of adherens junctions through genetic, epigenetic or post translational repression of E-cadherin and loss of the cell dependence on integrin-mediated anchorage to the surrounding ECM (Janiszewska et al., 2020; Yang and Weinberg, 2008). However, metastatic

lesions mostly exhibit epithelial phenotypes (Brabletz et al., 2001; Pedersen et al., 2002; Kowalski et al., 2003; Saha et al., 2007; Chao et al., 2012, 2010; Fischer et al., 2015; Puram et al., 2017), suggesting that EMT could be a transitory state from which cells revert back through a mesenchymal-to-epithelial transformation (MET) after the initial dissemination, or that other mechanisms enabling metastatic spread might be at play. Indeed, in many solid tumors, cells retain their epithelial properties, including cell-cell adhesions, leading to the hypothesis of collective invasion or the invasion of cohesive groups of cells as a dissemination mechanism (Cheung and Ewald, 2016). To support this hypothesis, polyclonal metastasis, arising from multiple cancer cell clones were reported in various cancer types including breast (Figure 3C) (Aceto et al., 2014; Cheung et al., 2016), pancreatic, prostate (Gundem et al., 2015) and colorectal cancer (Dang et al., 2020; Kok et al., 2021). Thus, changes in the adhesion properties of cancer cells affect their dissemination strategies, tipping the balance either in favor of a single cell or collective invasion format.

A crucial step of the metastatic cascade influenced by cell adhesions is extravasation of circulating tumor cells (CTCs), that are found both as single cells and clusters, the latter being less frequent but with higher metastatic potential (Figure 3B) (Aceto et al., 2015). CTCs are exposed to hostile circulatory conditions including high shear stress, anoikis, clearance by immune cells and fragmentation. A rapid escape from the circulation, through extravasation, may contribute to CTC survival (Ring et al., 2023). In order to extravasate, tumor cells need to first arrest intravascularly through the formation of weak *de novo* adhesions to endothelial cells. Then, the CTC/endothelium bond is stabilized to resist blood flow shear forces through recruitment of adhesions with higher strength (Osmani et al., 2019). Arrest is followed by transendothelial migration (TEM), which can be either paracellular (the migration of cancer cells through endothelial junctions) or transcellular (the migration through the endothelial cell body). A wide range of adhesion molecules mediate cancer cell adhesion to the endothelium in the arrest phase including selectins, cadherins, integrins, CD44 and Ig-CAMs (Reymond et al., 2013). Variability in the expression of these adhesion molecules determines the efficiency of cancer cells in the extravasation process and thus influences their metastatic potential.

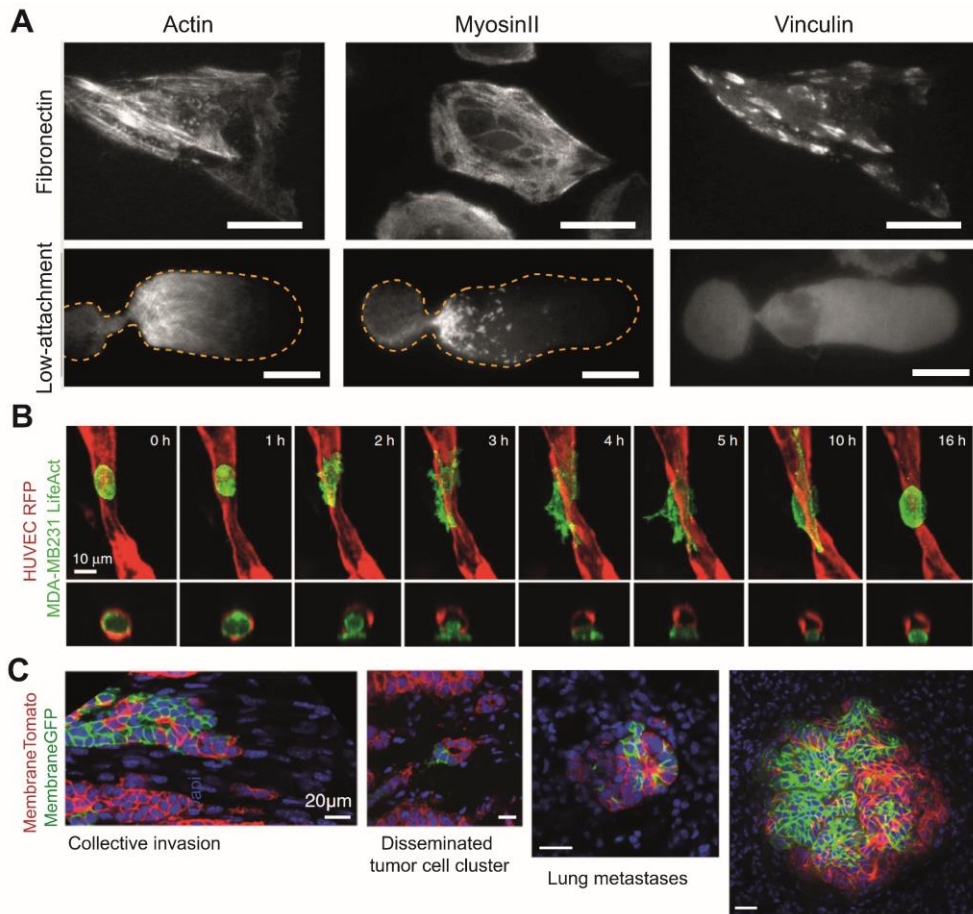


Figure 3: Effects of adhesion on distinct aspects of metastasis. (A) Migration plasticity of Hela cells depending on adhesion. On fibronectin coated glass, cells adopt a mesenchymal migration while in confinement and low attachment conditions they move in an amoeboid-like migration. Adapted from (Liu et al., 2015). (B) Breast cancer cell extravasating from a 3D vessel-like structure. In vitro model for extravasation. Adapted from (Cheung et al., 2016). (C) Polyclonal breast cancer disseminating clusters and metastasis. Adapted from (Cheung et al., 2016).

1.2. BIOMIMETIC SYSTEM FOR CANCER RESEARCH

2D and 3D models

From the latin “glass”, *in vitro* model is a broad term encompassing any model that recapitulates one or more aspects of biological systems in a dish. One of the simplest *in vitro* models for cancer research is tumor-derived cell lines (Budhwani et al., 2022). The first immortal cell line was established in 1951 from a cervical tumor biopsy taken from a patient named Henrietta Lacks (Callaway, 2013). Since then, cancer cell lines have become a fundamental tool for biological, genetic, functional cancer studies and therapeutic testing due to their simplicity, scalability, extensive characterization, reproducibility and easy and cheap maintenance. Nevertheless, their simplicity also constitutes a limitation, as often they fail to reproduce the complexity and heterogeneity of tumors and their microenvironment (Budhwani et al., 2022; Karami et al., 2019). Moreover, 2D cultures modify essential aspects of cancer cells such as morphology, gene expression, differentiation, heterogeneity and thus might lead to only a partial understanding of tumor biology (Mabry et al., 2016; Melissaridou et al., 2019; Rodrigues et al., 2021). To overcome the limitations of 2D cell lines and mimic tumor microarchitecture, more complex 3D models have been developed, the most promising being spheroids, organoids, microfluidic bioreactors and lab-on-chip approaches (Figure 4) (Budhwani et al., 2022; Karami et al., 2019).

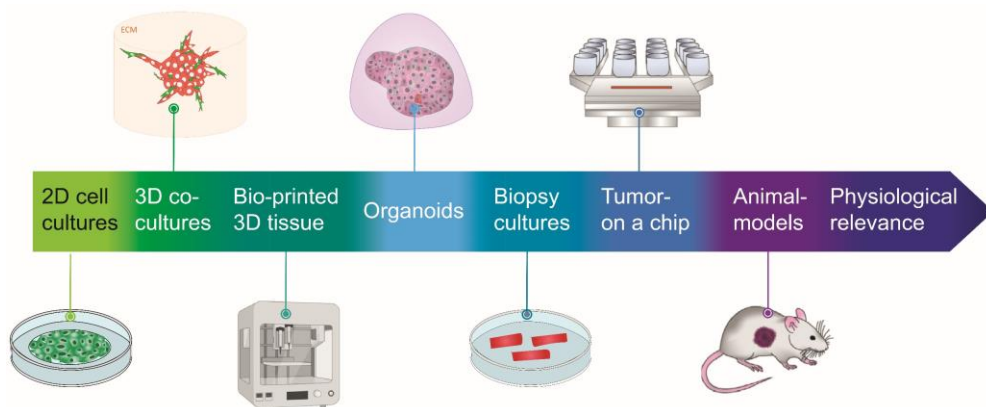


Figure 4: Physiological relevance of cancer models. Adapted and inspired from (Budhwani et al., 2022).

1.2.2. Spheroids

Spheroids are 3D structures formed by one or more cell types that can mimic distinct physiological conditions related to the 3D tumor microenvironment. Compared to 2D cultures, spheroids embedded in ECM or hydrogels can better recapitulate nutrient and oxygen gradients and 3D interactions between cancer cells and other cells such as fibroblasts, immune cells, and endothelial cells. For instance, embedded spheroids containing cancer cells and fibroblasts can be used to study cancer invasion, leader-follower dynamics, and effects of matrix deposition on cancer cells (Figure 5A, B) (Conti et al., 2021; Labernadie et al., 2017). Pre-treatment of fibroblasts with cancer-derived exosomes or TGF- β allows investigating the effects of preconditioning on the cancer-stroma interactions and invasion dynamics (Adams et al., 2021; González-Callejo et al., 2023). Tridimensional culture also provides insights to understand cellular and clonal competition in the context of cancer heterogeneity and invasive potential (Cerchiari et al., 2015; Chapman et al., 2014; Kang et al., 2021; Muciño-Olmos et al., 2020; Perrin et al., 2022; West et al., 2021).

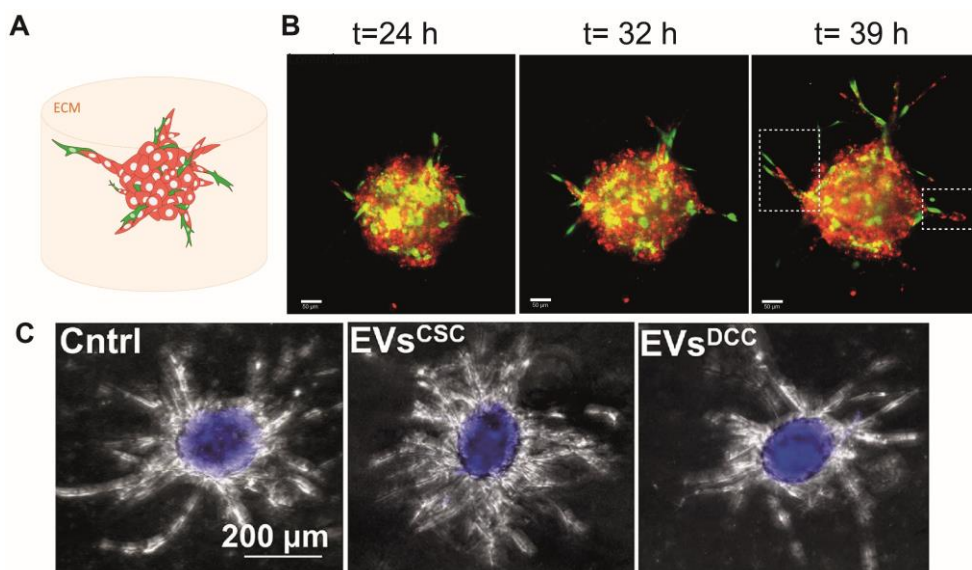


Figure 5: Examples of applications of 3D spheroids. (A) Scheme of spheroid containing cancer cells and fibroblasts embedded in matrix. (B) Invasion of fibroblasts and cancer cells in time. Adapted from (Conti et al., 2021) a method chapter I wrote which was published as part of the *Methods in Molecular Biology* book series. (C) Fibroblasts spheroids treated with exosomes derived from CSCs or non-CSC. Adapted from (González-Callejo et al., 2023), a study where I collaborated and performed the 3D spheroid invasion experiments with fibroblasts.

1.2.3. Tumor organoids

Organoids are self-organized 3D tissues that recapitulate to a certain extent the functional, biological and structural complexity of the *in vivo* organ of origin. Tumor organoids are derived from cells obtained from human or animal tissue biopsies (Zhao et al., 2022).

The first cancer organoid to be established was colon adenoma and carcinoma organoids isolated from mouse models (Sato et al., 2011). Since then, organoids from many cancer types have been established such as breast cancer (Sachs et al., 2018), ovarian cancer (Kopper et al., 2019), prostate cancer (Chua et al., 2014; Gao et al., 2014), pancreatic cancer (Boj et al., 2015), gastric cancer (Bartfeld et al., 2015) and more. They can be derived from different patient samples including primary tumors (Gao et al., 2014; Kopper et al., 2019; Sachs et al., 2018), metastasis (Sachs et al., 2018), CTCs (Gao et al., 2014) and tumor cells isolated from fluid effusions (Kopper et al., 2019). Alternatively, they can be established from normal organoids, by promoting oncogenic molecular pathways or mutating tumor suppressor genes (Artegiani et al., 2019; Dekkers et al., 2020; Li et al., 2014; Matano et al., 2015).

After collection, the sample is either dissociated to fragments, for higher maintenance of the tissue architecture and TME components, or to single cells, enabling the expansion of clonal organoids. Then the fragments or single cells are embedded in a 3D matrix which mimics the tumor native environment (Figure 6). The most common matrices used are collagen matrix and murine EHS matrix (Matrigel), a reconstituted matrix extracted from mouse sarcomas, tumors rich of ECM proteins such as laminins and collagen IV (LeSavage et al., 2022).

Tumor organoids have been validated as a model for several cancer types, showing that they are able to recapitulate genetic, histopathological and phenotypic features of the tumor of origin (Boj et al., 2015; Fujii et al., 2016; Gao et al., 2014; Sachs et al., 2018; Seino et al., 2018). Compared to 2D cultures or spheroids, not only they display higher resemblance to the *in vivo* morphology and architecture, but given the proper conditions, they are able to partially reproduce the tumor cellular diversity.

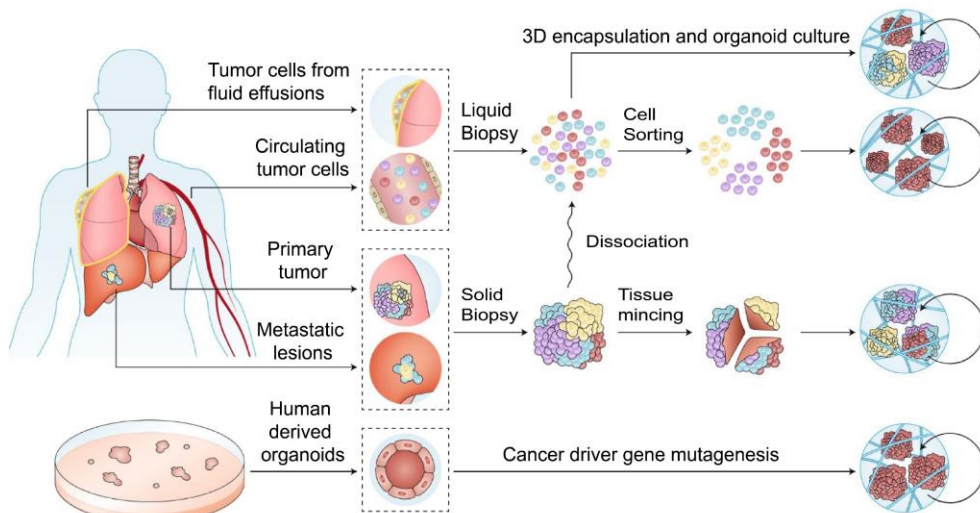


Figure 6: Patient-derived cancer organoids derivation and processing.

For example, a CRC organoid biobank, established from a range of histological subtypes and clinical stages, was shown to reproduce the differentiation capacity of the parental tumor, with organoids from well-differentiated adenocarcinomas forming cystic structures while organoids from poorly differentiated tumors forming similar morphologies *in vitro*. Moreover, each organoid line displayed different niche-dependency for its growth, and this variability was associated to the degree of transition from adenoma to advanced carcinoma (Fujii et al., 2016). Thus, cancer organoids can be used as a tool to study intra and inter- tumor heterogeneity and investigate the role of specific cancer populations in tumor initiation, proliferation, invasion and immune evasion. They can also be applied to model the TME heterogeneity and heterotypic cellular interactions, by establishing co-cultures with CAFs (Calon et al., 2015a; Öhlund et al., 2017; Seino et al., 2018) or with immune cells (Chakrabarti et al., 2018; Yuki et al., 2020).

Gene editing approaches can be combined with cancer organoids to label or/and deplete specific cell-populations, perform fate mapping *in vitro* and *in vivo* or, as previously mentioned, introduce oncogenic mutations to study cancer progression (Artegiani et al., 2019; Dekkers et al., 2020; Li et al., 2014; Matano et al., 2015). For instance, CRISPR/ Cas9 technology was used in two pioneering studies to label and selectively ablate cancer stem cells (CSCs) and differentiated-like cancer cells in CRC PDOs (Cortina et al., 2017; Shimokawa et al., 2017).

Finally, it is worth mentioning the potential clinical applications of patient-derived tumor organoids. Several studies have demonstrated the applicability of tumor organoids to predict the clinical outcome of treatments (Driehuis et al., 2020; Pasch et al., 2019; Schnalzger et al., 2019; Tiriach et al., 2018; Verissimo et al., 2016; Vlachogiannis et al., 2018; Yao et al., 2020). For example, patient-derived organoids of metastatic gastrointestinal cancer showed a high degree of genetic and phenotypic similarity with the original tumors. Moreover, their molecular profile after drug treatment were shown to match the clinical responses, thus supporting the concept that they could be implemented for personalized medicine (Vlachogiannis et al., 2018). Tumor organoids constitute a valuable model to screen libraries of engineered immune cells for immunotherapy (Schnalzger et al., 2019; Scognamiglio et al., 2019) or screen for synergistic combinations of drugs (Verissimo et al., 2016).

Despite their potential, tumor organoids have some limitations. One of them is a lack of standardization in the derivation protocols and sample collections. Sampling is often done from only one part of the tumor and thus the organoids fail to represent the extensive patient-specific heterogeneity of cancer. Other limitations include expensive culture medium and growth factors, heterogeneity in the culture matrices, especially for the animal-derived ones and limited accessibility for imaging techniques (LeSavage et al., 2022). To overcome the latter, recently, intestinal organoids cultured in 2D monolayers have been shown to retain many features of the *in vivo* intestinal epithelium, thus providing a strategy to combine the organoid cellular diversity with microscopy-based experiments (Pérez-González et al., 2021; Thorne et al., 2018). Potentially, the same strategy can be applied to tumor organoids, in order to perform 2D assays while maintaining the tumor organoid cellular heterogeneity.

1.2.4. Tumor-on-chip

Organs-on-chips (also called organ chips) are cell culture systems composed of optically clear material such as polydimethylsiloxane (PDMS) that contain microchannels where cells are grown, mimicking the complexity of organs *in vivo*. In contrast with 2D and 3D culture systems, organ chips can recapitulate physiological aspects such as tissue-tissue interfaces, multicellular architectures, chemical gradients, vascular perfusion (Sontheimer-Phelps et al., 2019) and mechanical cues such as hydrostatic pressure, fluid flow and

compression (Charelli et al., 2021). Microfluidic cancer models or tumor-on-chips have been used to reproduce and study different aspects of cancer including tumor growth (Hassell et al., 2017), interactions with stromal cells (Erdogan et al., 2017; Montanez-Sauri et al., 2013), angiogenesis (Lee et al., 2021), invasion (S. Wang et al., 2013) and intra/extravasation (Chen et al., 2017, 2016; Jeon et al., 2015). These early models used cell lines that lack cellular diversity and self-organization potential. To overcome this limitation, combining organ-on-chip technology with the cellular heterogeneity of organoids provides a novel approach to engineer more physiological, reproducible, and controlled models of cancer and the TME *in vitro* (Hofer and Lutolf, 2021). Moreover, tumor organoids on chip can be implemented to create more scalable, high throughput platforms for personalized medicine and drug screening (Takebe et al., 2017). In this context, a multisensory organoid on chip platform, able to monitor in situ and automatically physical, chemical, and optical parameters was developed (Zhang et al., 2017).

1.2.5. Measuring forces and mechanics of tumors

Cancer progression and metastasis formation are coupled with changes in the physical tumor microenvironment and in the mechanical properties of cancer cells (Nia et al., 2020). To measure these changes, several techniques are available (Nguyen and Kilian, 2020; Roca-Cusachs et al., 2017). For example, we can quantify forces exerted by migrating single cancer cells or clusters on 2D substrates through traction force microscopy (TFM), which measures deformations of soft, elastic gels and computes the tractions related to these deformations. Cellular forces can also be measured with cantilevers or micropillars, on the basis of the same principle of measuring the deformation derived from forces exerted by cells. Typically, the substrates used for TFM are polyacrylamide (PAA) and soft PDMS gels, coated with ECM proteins to allow attachment of cells. Alternatively, 3D traction force microscopy enables quantification of cellular forces that induce ECM remodeling in 3D (Gómez-González et al., 2020).

Mechanical properties of cancer cells can be measured at different scales with techniques such as atomic force microscopy (AFM), laser ablation, magnetic/optical tweezers, optical stretcher, and particle tracking micro-rheology. Although widely used, most of these techniques have a very low throughput

(Nguyen and Kilian, 2020; Roca-Cusachs et al., 2017). In contrast, microfluidic-based techniques enable the measurement of mechanical properties of thousands of cells within minutes. For instance, real-time deformability cytometry (RT-DC) relies on estimating the cell deformation resulting from hydrodynamic forces to assess the cell mechanical properties (Otto et al., 2015). RT-DC has been used previously to measure changes in cell stiffness during the transition from normal to cancer of breast epithelial cells (Guck et al., 2005). On a bigger scale, Brillouin microscopy, a type of optical elastography, is emerging as a potential tool to assess the viscoelastic properties of samples and tissues in a non-invasive, label and contact-free manner (Prevedel et al., 2019; Scarcelli and Yun, 2008; Troyanova-Wood et al., 2016).

Many other tools are available to assess mechanics and forces of tumors *in vitro* and *in vivo*. The most promising ones for *in vivo* measurements of forces are laser ablation, consisting of disrupting cellular structures with a laser beam and based on the assumption that tissues are in mechanical equilibrium; synthetic force transducers that can be inserted in the target tissue and their deformation can be tracked through imaging techniques; geometric force inference methods, which are non-invasive and are based on the topology and geometry of cell contacts, with the assumption that forces are balanced at each vertex; FRET tension sensors which are genetically encoded or synthesized molecular springs whose deformation is reported by resonant fluorophores (Floerchinger et al., 2021; Gómez-González et al., 2020; Yankaskas et al., 2021)

1.3. CANCER STEM CELLS

1.3.1. The cancer stem cell model

The cancer stem cell (CSC) concept lies its roots on tumor heterogeneity. It states that, similarly to normal tissues, tumor growth is fueled by a set of dedicated cells that are able to self-renew and give rise to short-lived differentiated progeny.

The origins of the CSC concept can be traced back to the late nineteenth century, when Julius Cohnheim (1839 - 1884), a pathology professor, proposed that tumors arose from “rudiments” or residual embryonic cells that if provided with sufficient blood supply, could grow uncontrollably and mirror embryonic development (Cohnheim, 1880). This embryonic theory of tumor formation was rooted in the observation that teratocarcinomas are composed of undifferentiated and differentiated cells, with the differentiated population resembling tissues from all three germ layers (ectoderm, endoderm, and mesoderm) (Cooper, 2009).



Figure 7: Julius Cohnheim

A few decades later, in the 1950', Leroy Stevens, a postdoctoral researcher at the Jackson Laboratory, carried out a study on the influence of mutagenic and carcinogenic agents on mice. He examined 3557 mice and reported that around 1% developed testicular teratoma, establishing the 129 mouse-strain as a model for spontaneous teratoma (Stevens and Little, 1954). Grafts of some of these tumors could induce new tumors when transplanted in other mice, forming “embryoid bodies”, with neuroepithelial cells, amnion, yolk sac epithelium and mesodermal cells. Conversely, some fertilized eggs or embryonic tissues gave rise to teratomas when transplanted into the testis of mice (Stevens, 1960). From these findings Stevens concluded that both undifferentiated germinal cells and poorly differentiated cells of the early embryo can form teratomas and

differentiate into multiple cell types. He referred to these cells as “pluripotent embryonic stem cells” (Cooper, 2009; Stevens, 1970).

In the same years, Barry Pierce conducted a series of landmark experiments showing that a subpopulation of teratocarcinomas cells is highly tumorigenic when transplanted in a compatible host and can give rise to well-differentiated, non-tumorigenic cells (Kleinsmith and Pierce, 1964). These observations led Pierce in 1988 to define neoplasms as “caricatures of tissue renewal” composed of “a mixture of malignant stem cells, which have a marked capacity for proliferation and a limited capacity for differentiation under normal homeostatic conditions, and of the differentiated, possibly benign, progeny of these malignant cells” (Pierce and Speers, 1988).

An important contribution to the formulation of the CSC concept derived from studies of hematological diseases. In 1937, Furth and Kahn showed that as few as 1 to 100 cells can generate leukemia in recipient mice (Furth et al., 1937), demonstrating the tumor-initiating ability of single transplanted cancer cells. In 1990', pioneering studies of acute myelogenous leukemia (AML) demonstrated that a few rare cells of mouse AML expressing the same surface markers as hematopoietic stem cells (HSCs), are not only able of initiating leukemia when transplanted in immunocompromised mice, but also have the potential to self-renew (Bonnet and Dick, 1997; Lapidot et al., 1994; Uckun et al., 1995). In the following years, the presence of heterogeneous cancer populations with varying differentiation and self-renewing potentials was discovered also in solid tumors, including breast cancer (Al-Hajj et al., 2003), brain cancer (Singh et al., 2004), prostate cancer (Collins et al., 2005), pancreatic cancer (Li et al., 2007), colon cancer (Dalerba et al., 2007; O'Brien et al., 2007; Ricci-Vitiani et al., 2007), ovarian (Zhang et al., 2008) and lung cancer (Eramo et al., 2008).

From these studies, a model emerged to explain tumor heterogeneity and cancer stem cells. Mirroring the rigid HSC hierarchy, this hierarchical model conceives the CSCs as a biologically distinct subset of cells with hardwired, intrinsic properties: low frequency, self-renewal, unlimited proliferation potential but rare divisions, ability to generate a progeny capable of differentiation and resistance to chemotherapy and radiotherapy. The non-CSCs, in contrast, are only able to proliferate transiently and have limited division potential, thus, they do not contribute to long-term tumor growth. In this hierarchy, plasticity, or the transition from one cell state to another, is limited as the CSCs properties are

intrinsic and cannot be attained by differentiated cancer cells (Figure 8). However, application of CSC markers and lineage tracing approaches to mark specific cells and their progeny (Kretzschmar and Watt, 2012) led to observations of higher plasticity than anticipated by the hierarchical model. Several reports observed phenotypic versatility of the non-CSCs, which in certain contexts, were able to give rise to both differentiated and undifferentiated cells, behaving *de facto* as functional CSCs (Roesch et al., 2010; Gupta et al., 2011; Scheel et al., 2011; Zomer et al., 2013; Z. A. Wang et al., 2013). These observations led to the formulation of a more dynamic CSC model, proposing cancer differentiation and stemness as dynamic and plastic states that are largely dictated by the microenvironment (Batlle and Clevers, 2017; Vermeulen et al., 2012).

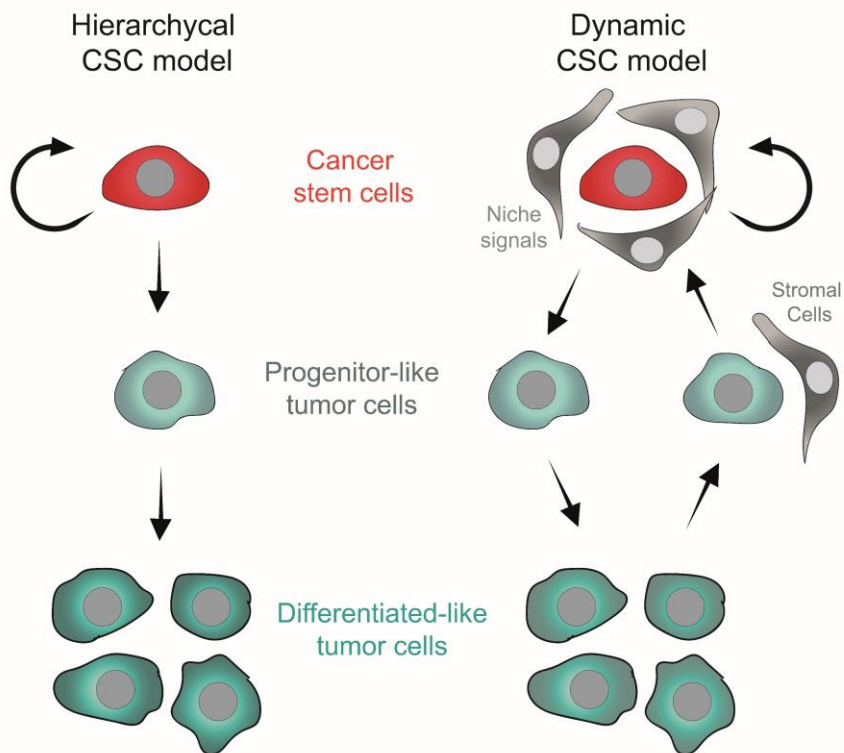


Figure 8: The hierarchical and dynamic CSC models. The hierarchical model stipulates that CSCs are able to self-renew and to differentiate into progenitor-like cells that give rise to terminally differentiated cells, which lack the capacity to self-renew and drive tumor growth. Based on the dynamic model, CSCs are not hardwired but dependent on signals from the microenvironment. Differentiated tumor cells can dedifferentiate in response to microenvironmental stimuli. Stromal cells represent myofibroblasts, endothelial cells, mesenchymal stem cells, or infiltrating immune cells. Inspired by (Vermeulen et al., 2012).

Based on this novel CSC notion, CSC state is not hardwired. Rather, cells can transit between cell states as a result of intrinsic factors (stochastic epigenetic and genetic alterations) and as an adaptive mechanism to external stimuli (Figure 8) (Jehanno et al., 2022; Vermeulen et al., 2012). Moreover, evidence from studies on melanoma (Quintana et al., 2008) and pancreatic cancer (Cr et al., 2017), indicates that in some tumor types CSCs are not necessarily rare as in the classical view. As tumor progresses and genetic mutations accumulate, subclones with tumor initiating abilities may expand, becoming the tumor bulk and thus leading to a shallower hierarchy and a more homogeneous tumorigenic population (Kreso and Dick, 2014). Hence, although tempting in the clinical perspective, the classical CSC model has shifted to a more complex concept, considering important aspects of tumor biology such as phenotypic plasticity, microenvironmental stimuli and clonal evolution. Still, the unifying notion of a population responsible for tumor initiation, long-term growth and therapy resistance provides a framework to understand tumorigenesis and tumor progression.

1.3.2. Cancer stem cells and their niche

The tumor microenvironment is a diverse ecological system composed of compartments or niches that are in constant interactions with cancer cells and provide supporting/ selective contexts for specific sub-populations, such as CSCs (Prager et al., 2019). In breast cancer and glioblastoma models, it has been shown that hypoxic and acidic conditions result in an enrichment of the CSC population, promoting stemness signaling programs, quiescence and invasion (Bhagat et al., 2016; Carcereri de Prati et al., 2017; Kim et al., 2018; Li et al., 2013; Lu et al., 2021; Zhang et al., 2016). A stemness supporting compartment is constituted also by the perivascular niche in several tumor types, including glioblastoma (Calabrese et al., 2007), melanoma (Correa et al., 2016), skin cancer (Beck et al., 2011), breast cancer (Fazilaty and Behnam, 2014) and colorectal cancer (Lu et al., 2013). Endothelial cells secrete factors that promote and maintain a stem cell-like phenotype while the CSCs drive and enhance vascularization, establishing a mutual dependency with the vascular cells (Calabrese et al., 2007; Beck et al., 2011; Zhu et al., 2011; Fazilaty and Behnam, 2014; Lu et al., 2013). Tumor associated macrophages secrete chemokines that induce stem pathways and thus support and maintain the CSCs (Jinushi et al., 2011). Similarly, cancer associated fibroblasts, an important

component of the tumor stroma, sustain the CSC population via paracrine signaling (Kinugasa et al., 2014; Chen et al., 2014; Calon et al., 2015a; Nair et al., 2017; Alguacil-Núñez et al., 2018; Álvarez-Tejreiro et al., 2018). Hence, cancer stemness is regulated and molded by the diverse niches composing the tumor ecosystem including the hypoxic core of the tumor, perivascular regions, tumor-associate immune cells and fibroblasts.

1.3.3. Cancer stem cells, EMT and metastasis

Epithelial integrity arises from tight homotypic cell-cell junctions that establish a cellular barrier, preventing leakage of molecules through interstitial spaces. The position of these tight cell-cell adhesions defines the apical-basal polarity of epithelia, and thus the tissue organization and structure (Buckley and St Johnston, 2022; Lambert and Weinberg, 2021). During development, repair and regeneration, some epithelial cells transiently lose their apical-basal polarity and acquire mesenchymal features that promote motility and reorientation to a front-rear polarity (Buckley and St Johnston, 2022). This process, defined as EMT, is associated to repression of E-cadherin and activation of EMT-inducing transcription factors, e.g. Snail, Slug, Twist and Zeb1 and mesenchymal markers such as N-cadherin, vimentin and fibronectin (Lambert and Weinberg, 2021).

In the context of neoplasia, EMT has been linked to cancer progression and the acquisition of a motile and invasive phenotype that enables single cancer cells to detach from the primary tumor, disseminate and colonize distant organs (Hay, 1995). In some solid tumors, such as pancreatic, breast and skin cancer, activation of the EMT program has also been coupled to the generation of stem-cell like cells with enhanced tumor initiating ability and therapy resistance (Eramo et al., 2008; Mani et al., 2008; Kabashima et al., 2009; Zhou et al., 2014; Hollier et al., 2013; Lawson et al., 2015; Latil et al., 2017; Konge et al., 2018). However, cancer cells tracking and functional characterization in mouse models and *in vitro* have led to the identification of “hybrid EMT” or intermediate EMT states that are plastic, reversible, able to initiate new tumors and more metastatic compared to fully mesenchymal cancer cells (Schmidt et al., 2015; Ruscetti et al., 2015; Pastushenko et al., 2018, 2021). This finding supported the idea that in certain carcinomas, cancer stem cells reside in a hybrid and transient EMT state that enables their metastatic dissemination (Lambert and Weinberg, 2021). Hence, plasticity is crucial for metastatic colonization as MET or transition to a

more epithelial state is required to avoid dormancy, initiate proliferation and recapitulate tumor heterogeneity at the metastatic site (Chaffer et al., 2006; Korpai et al., 2011; Tsai et al., 2012; Del Pozo Martin et al., 2015; Jolly et al., 2015; Beerling et al., 2016). Of note, in some carcinomas such as colorectal cancer, osteosarcoma and malignant melanoma, cancer cells, including CSCs, retain their epithelial features and display a limited range of EMT phenotypes, suggesting that the link between hybrid EMT and stemness is specific to tumor types and stage and that acquisition of mesenchymal traits might be uncoupled from stemness (Nieto et al., 2016).

Circulating tumor cells are rare single cells or clusters that are shed from the primary tumor, enter blood vessels through intravasation, and circulate in the blood stream till they eventually extravasate and colonize distant organs. Cell shedding is estimated to be quite high, with as many as 4×10^6 cells per g of tumor tissue shed a day (Butler and Gullino, 1975). Nevertheless, their efficiency is low, with a circulation half-life of the order of minutes (Aceto et al., 2014) and fewer than 0.01% managing to successfully extravasate (Merino et al., 2019; Perea Paizal et al., 2021; Yoshida et al., 1993). Although extremely challenging, isolation and analysis of CTCs can provide important insights on the phenotype of metastatic cancer cells (Eslami-S et al., 2022). Phenotyping CTCs from patients and *in vivo* models led to the identification of a small fraction of cells with stem-like properties, able to form *de novo* tumors and initiate metastasis (Al-Hajj et al., 2003; Giordano et al., 2012; Baccelli et al., 2013; Grillet et al., 2017). These studies also showed high molecular and phenotypic heterogeneity of CTCs, displaying various degrees of epithelial differentiation and EMT (Aceto et al., 2015; Ring et al., 2023). As EMT confers a survival advantage against anoikis, it was proposed as a crucial requirement for survival in the bloodstream. However, the discovery of circulating tumor clusters, with up to a 50-fold increase in the metastatic potential compared to single circulating cells (Aceto et al., 2014; Cheung et al., 2016; Liu et al., 2019), provided an alternative route to the EMT dependent hematogenous dissemination. Tumor cell clustering may confer resistance from anoikis during the transit in the bloodstream and was shown to enhance stemness and promote metastasis and survival (Gkoutela et al., 2019; Liu et al., 2019). Thus, CTCs are characterized by high heterogeneity in terms of molecular phenotype, stem-like properties, and clustering, reflecting on one hand tumor heterogeneity and on the other the adaptive potential required for metastasis.

1.3.4. Mechanical niche and cancer stem cells

Matrix deposition and tissue stiffening, a physical hallmark of cancer, do not occur uniformly throughout the tumor. Instead, the transformed tissue is characterized by mechanical heterogeneity both in the epithelial compartment and in the associated vasculature and stroma (Figure 9) (Lopez et al., 2011; Laklai et al., 2016; Sun et al., 2021). This mechanical variability influences intra-tumor heterogeneity and cancer cell fate.

In breast cancer patients, increased ECM stiffness was associated with chemoresistance, CSC enrichment and poor prognosis (Liu et al., 2023). In another study, stiff and hypoxic microenvironments were shown to promote stemlike properties through modulation of the integrin-linked kinase ILK in breast cancer cells (Pang et al., 2016). Similarly, in a rat model of liver cancer, stroma stiffness correlated with the number of CSCs (Sun et al., 2021). In contrast, in hepatocellular carcinoma (HCC), stemness and chemoresistance were enhanced in cells grown in a soft matrix (Tian et al., 2019). Also in melanoma, culturing tumor repopulating cells in 2D rigid substrates and stiff 3D fibrin matrix inhibits their self-renewal potential and promotes quiescence, suggesting an inhibitory role of stiffness on the stemness of melanoma cells (Tan et al., 2014). Soft fibrin gels, instead, promote selection and growth of a highly tumorigenic melanoma subpopulation, constituting a better selection method than surface markers (Liu et al., 2012). Along these lines, culturing colorectal cancer cells in soft fibrin gels promotes their proliferation while the growth of cancer colonies in stiff gels is inhibited (Chang et al., 2022).

These contrasting findings are likely due to the heterogeneity and plasticity of CSCs and to an arbitrary definition of stiff and soft, without considering the physiological tissue rigidity of the tumor being investigated. Indeed, culturing cancer cell lines in hydrogels of different rigidities revealed that each cell line has an optimal matrix stiffness for the maintenance of cancer stem cells, and it is dependent on the tissue of origin of the cancer cells (Jabbari et al., 2015). Thus, further investigation is required to characterize the mechanical niche supporting CSCs and establish the link between stiffness and cancer cell fate.

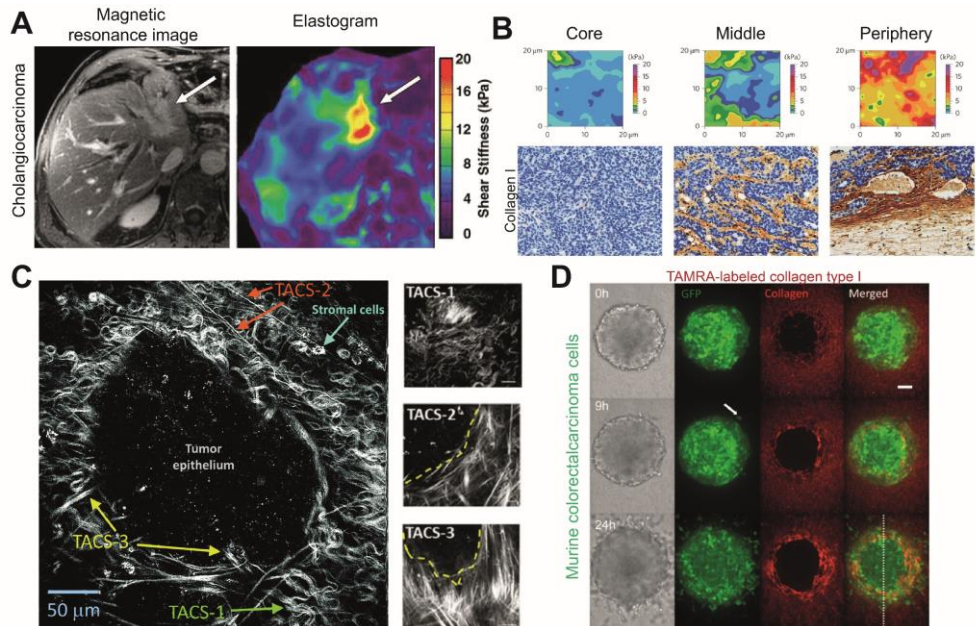


Figure 9: Heterogeneity in mechanical properties of the TME. (A) Heterogeneous stiffness of the TME in cholangiocarcinoma invading the surrounding left lobe of human liver. Adapted from (Venkatesh et al., 2008). (B) Consecutive stiffness maps across invasive ductal carcinoma sample demonstrate mechanical heterogeneity. Adapted from (Cross et al., 2007). (C) Multiphoton image of an isolated ex vivo mouse breast tumor showing different tumor associated collagen signatures (TACS). Adapted from (Conklin and Keely, 2012). (D) Time lapse images of murine colorectal carcinoma CT-26 cells invading collagen matrix. With time the collagen organization changes. Adapted from (Kopanska et al., 2016) Inspired by (Malandrino et al., 2018)

1.3.5. Mechanics of cancer stem cells

Malignant transformation and cancer progression are often associated with softening of cancer cells (Cross et al., 2008; Guck et al., 2005; Lekka et al., 1999; Liu et al., 2020; Suresh et al., 2005; Xu et al., 2012). The relationship between tumor cell mechanics and cancer stemness has been investigated in a few cancers (X. Chen et al., 2022). In a murine model of ovarian cancer, measurements of cell elastic modulus by AFM revealed that CSCs are softer compared to preneoplastic and late-stage counterparts (Babahosseini et al., 2014). Soft cells isolated through a microfluidic approach from different cancer cell lines were able to form new tumors in NOD-SCID or immunocompetent mice, suggesting that cell softness might be a physical signature for tumorigenic

cells (Lv et al., 2021). Highly tumorigenic melanoma cells selected by culture in soft fibrin gels express stem cell markers and are softer than cells cultured in stiff gels (Liu et al., 2012). Another study showed, using cancer cell lines *in vitro*, that liver cancer stem cells selected from sphere culture systems are softer than other hepatoma cells (J. Sun et al., 2016). Although consistent, studies based on CSC selection through culture in soft matrix need to be further corroborated with marker-defined CSCs models, patient samples and *in vivo*.

1.4. COLORECTAL CANCER

1.4.1. Types

Colorectal cancer is the third most diagnosed cancer type and the second leading cause of cancer related deaths (Siegel et al., 2022). CRC can arise sporadically, accounting for about 80% of the cases, or can be associated with a hereditary CRC syndrome, accounting for approximately 15-20% of all patients. Among the hereditary CRC syndromes, the two most common ones are the Lynch syndrome and the familial adenomatous polyposis (Kuipers et al., 2015).

The Lynch syndrome or hereditary nonpolyposis colorectal cancer (HNPCC) is caused by mutations in one of the DNA mismatch repair (MMR) genes, namely *Msh2*, *Msh6*, *Mlh1*, *PMs2*, responsible for correcting DNA mismatches generated during DNA replication (Li, 2008; Lynch and de la Chapelle, 2003). Mutations in one of the MMR genes result in genomic instability and accumulation of mutations, especially in microsatellites, repetitive sequences of 1-6 base pairs (Ellegren, 2004). The onset of HNPCC is at an earlier average age compared to sporadic CRC and is characterized by an accelerated carcinogenesis. Its pathological feature is often poorly differentiated tumors and the presence of infiltrating lymphocytes (Lynch and de la Chapelle, 2003).

Familial adenomatous polyposis arises from germline mutations in the adenomatous polyposis coli (APC) gene, encoding a tumor suppressor protein that regulates the Wnt signaling pathway. The majority of APC mutations lead to a truncated protein, resulting in an increased transcription of Wnt target genes (Noe et al., 2021). Patients with this hereditary syndrome develop adenomas which evolve to carcinomas at a very young age (Kuipers et al., 2015; Lynch and de la Chapelle, 2003).

1.4.2. CRC progression and staging

The malignant transformation of CRC is driven by the accumulation of genetic mutations and epigenetic alterations that lead to the transition from aberrant crypt to early adenoma, which then evolves to advanced adenoma and finally

carcinoma. The transition from adenoma to carcinoma occurs in approximately 10% of the polyps and usually takes 10 to 15 years but can be faster, for example in case of hereditary CRC syndromes (Kuipers et al., 2015; Luo et al., 2014).

Although quite heterogeneous, CRC driver mutations cluster around genes involved in key signaling pathways: Wnt signaling, the mitogen-activated protein kinase (MAPK) signaling, transforming growth factor β (TGF- β) signaling, PI3K-AKT signaling and p53 signaling. The first event in CRC initiation is the constitutive activation of Wnt signaling caused by a mutation in one of the pathway components, the most common one being APC. This leads to the accumulation of β -catenin in the nucleus and the acquisition of a crypt progenitor phenotype by the intestinal epithelial cells (van de Wetering et al., 2002). Deregulation of Wnt signalling often co-occurs with mutations in MAPK signalling, for example in *Kras* or *Braf*, leading to the development of an early adenoma. Inhibition of the tumor suppressor pathway TGF- β further promotes tumor progression and the transition from early adenoma to late adenoma. Mutation of *PIK3CA* activates the PI3K-AKT signaling pathway enhancing CRC stem cell survival and proliferation, leading to treatment resistance (Wang et al., 2018). Loss of function mutations in TP53 further increase genomic instability, unregulated proliferation and cell survival and promote an invasive phenotype, leading to the development of invasive carcinomas (**Figure 10**) (Fearon, 2011; Tauriello et al., 2017).

The standard staging system of CRC is based on the tumor, node, metastasis (TNM) staging system. It assesses the status of primary tumor, regional lymph nodes and the extent of metastatic disease at the time of the diagnosis. In stage I the tumor has invaded the submucosa or the muscularis propria but has not disseminated to the lymph nodes or formed metastasis. In stage IIA the tumor has reached into the subserosa or into the non-peritonealized pericolic or perirectal tissues. In stage IIB the primary tumor has invaded other organs or perforated the visceral peritoneum. In stage III metastasis can be detected in the regional lymph nodes. In stage IV the tumor had spread to distant organs and metastasis can be detected (Compton and Greene, 2004; Vogelstein et al., 2013).

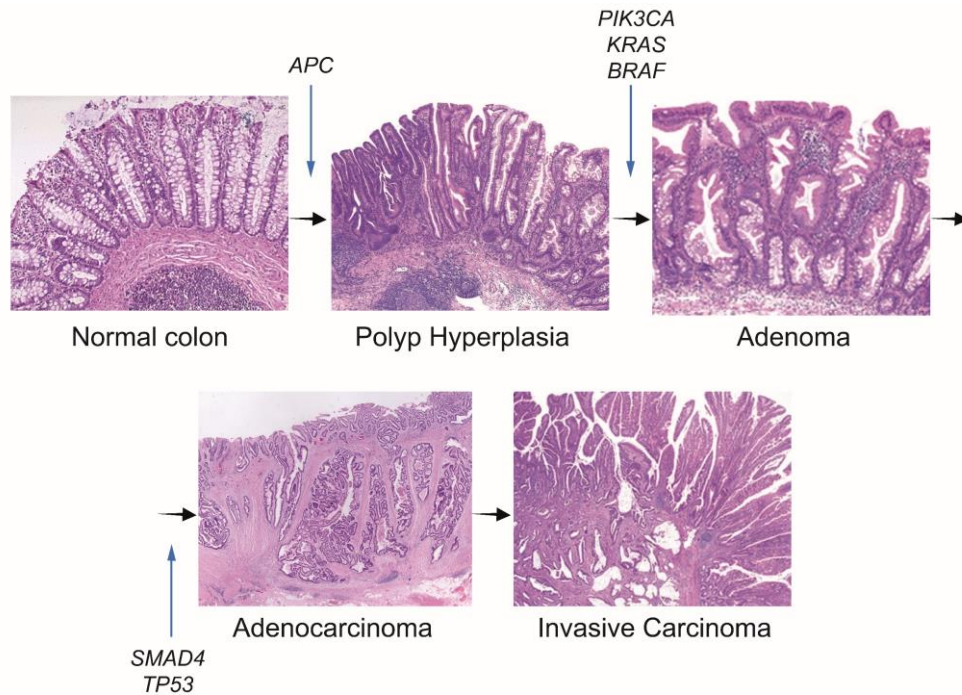


Figure 10: Scheme of progression of colorectal cancer with most common mutations.

1.4.3. Colon cancer stem cells

The intestinal epithelium, the fastest self-renewing tissue in our body, is completely replaced every 5-7 days (Barker, 2014; Gehart and Clevers, 2019). Intestinal stem cells (ISC) fuel this renewal by dividing into transit amplifying cells which in turn differentiate into multiple lineages of short-lived specialized cells (Barker, 2014). In CRC, essential features of this hierarchical structure are maintained, resulting in intratumor heterogeneity².

Among the heterogeneous cell populations composing colorectal adenomas and carcinomas, a subset of cells called cancer stem cells has a high tumor-initiating ability and expresses a genetic signature similar to the ISCs (Batlle and Clevers, 2017; O'Brien et al., 2007; Ricci-Vitiani et al., 2007). Leucine-rich repeat-containing G-protein coupled receptor (LGR5) is a reliable marker for adult ISCs and was proven to mark functional CSCs in CRC (Barker et al., 2009a; Kemper et al., 2012; Schepers et al., 2012; Junttila et al., 2015). Other

commonly associated markers are CD133, CD44/CD166, ALDH1 and high Wnt expression (Kuipers et al., 2015).

In the context of malignant transformation, it is believed that given the high turnover of the intestinal epithelium, ISC are the recipients of mutations inducing tumor initiation and thus are the "cell of origin" (Tomasetti and Vogelstein, 2015; Vermeulen and Snippert, 2014). In a seminal study using a *Lgr5* knockin mouse model, deletion of APC and subsequent activation of Wnt was shown to be sufficient to initiate transformation of stem cells and tumor formation (Barker et al., 2009b). However, following studies showed that hyperactivation of β -Catenin combined with elevated NF- κ B or loss of SMAD4 signaling in non-CSCs can induce dedifferentiation and initiation of tumorigenesis, demonstrating that also more differentiated cells can be recipient of oncogenic mutations and responsible for malignant transformation given the suitable conditions (Perekatt et al., 2018; Schwitalla et al., 2013).

CRC CSCs are also responsible for tumor propagation and growth. Several transplantation studies have identified an undifferentiated sub-population with tumor initiating abilities that is able to give rise to a more differentiated cancer progeny (Dalerba et al., 2011, 2007; Dieter et al., 2011; O'Brien et al., 2007). Nonetheless, these studies have been criticized for not representing the cells native microenvironment and for the results being affected by the degree of immunodeficiency of the recipient mice (Vermeulen and Snippert, 2014). With the advent of lineage tracing and selective cell ablation experiments, the role of CSCs in tumor growth and progression could be studied in their native environment. In 2012, the Hans Clever laboratory implemented lineage tracing to show that LGR5 marks a subpopulation of adenoma cells that are able to differentiate into Paneth cells (Figure 11A, B) (Schepers et al., 2012). A few years later, in an elegant study using *Lgr5* tracing combined with the expression of diphtheria toxin receptor (DTR), de Sousa e Melo et al. investigated the effect of selective elimination of CSCs *in vivo*. The model used was a mouse model recapitulating the clinical progression of CRC with mutations in *Apc*, *Kras*, *Trp53* and *Smad*. Ablation of the LGR5⁺ cells was elicited by administration of diphtheria toxin. These experiments showed that the LGR5⁺ cells possess higher tumor initiating ability compared to LGR5⁻ cells and are able to self-renew and give rise to more differentiated progeny. They also revealed a dual role of CSCs in the primary tumor and metastasis. Selective depletion of LGR5⁺ in primary tumors resulted in growth arrest but not regression, as tumors were

maintained by proliferative LGR5⁺ cells. However, selective CSCs removal in metastatic CRC mouse models led to a substantial reduction of liver metastatic burden revealing a crucial role of CSCs in the formation and maintenance of metastasis (de Sousa e Melo et al., 2017).

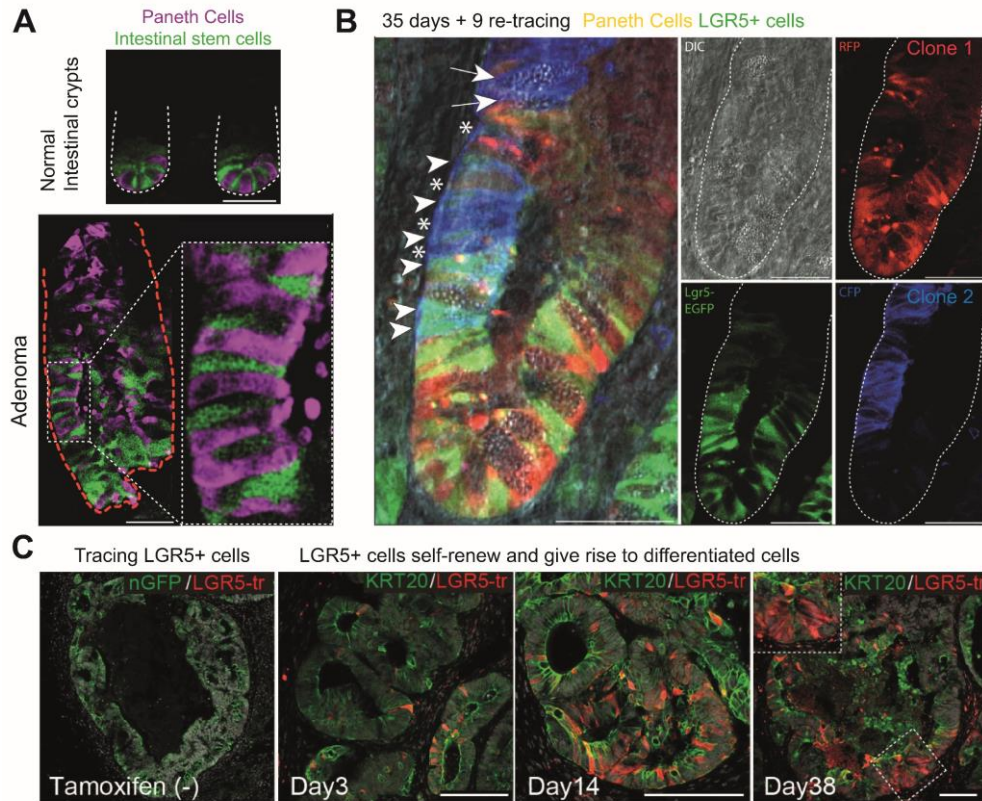


Figure 11: Lineage tracing experiments, LGR5⁺ cells and plasticity. (A) Adenoma are characterized by a similar structure to the normal intestinal crypts, with Paneth cells and LGR5⁺ cells (stem cells) located toward the base of the adenoma segment. (B) Adenoma developed from single APC mutant LGR5⁺ cell. Tracing for 35 days (all cells arising from the cell of origin display the same color) was followed by re-tracing for 9 days. Upon another injection of tamoxifen, some cells switch to a new color so a new progeny can be traced. In the image, cells with red borders all come from one LGR5⁺ cell. Among this progeny we can find Paneth cells, LGR5⁺ cells and other cells, demonstrating the differentiation ability of LGR5⁺. The same happens with the blue progeny, deriving from a different LGR5⁺ cell. Adapted from (Schepers et al., 2012). (C) Tamoxifen treatment elicits expression of the RFP reporter in the LGR5⁺ cells of patient derived organoid xenografts.

Another breakthrough in the understanding of the role of CSCs in CRC derived from the establishment of patient-derived organoid models labelling specific cancer populations such as cells expressing LGR5 or cytokeratin20 (CK20), a marker for intestinal differentiation. This tracing approach further confirmed that LGR5+ cells behave as CSCs in CRC tumors and are crucial for tumor growth (Figure 11C). Nevertheless, it also uncovered cellular plasticity, or the transition between differentiation states, as a way to sustain tumor growth after ablation of LGR5+ cells. Similarly to the findings reported by de Sousa e Melo et al, depletion of LGR5+ cells in their intact microenvironment did not result in tumor regression as tumor growth was maintained by KRT20 cells that converted to an undifferentiated state and fueled proliferation (Cortina et al., 2017; Ganesh et al., 2020; Shimokawa et al., 2017). Together, these studies confirmed the essential role of LGR5+ CSCs in tumor and metastatic growth and highlighted the importance of cellular plasticity as an adaptive mechanism to ensure cancer progression and endure changing microenvironmental pressures (de Sousa e Melo et al., 2017; Fumagalli et al., 2020).

1.4.4. Metastasis in colorectal cancer

Cellular plasticity has been shown to be determinant also in the process of metastasis formation. In a colorectal cancer genetic mouse model, the majority of metastases were found to be seeded by LGR5- cells; only after metastatic colonization, conversion of LGR5- to LGR5+ enabled metastatic growth and the formation of metastatic tumors recapitulating the heterogeneity of the primary tumor (Figure 12) (Fumagalli et al., 2020).

Further reinforcing this model, we recently showed that a subset of LGR5- tumor cells that remain hidden in foreign organs after surgical removal of the primary CRC are responsible for metastatic relapse. These cells express a specific genetic signature that includes 99 genes, most of them associated with poor prognosis. Tracing these high-relapse cells (HRCs) in a metastatic CRC mouse model showed that they are the first tumor cells to reach the liver. Metastatic seeding is then followed by conversion of some HRCs to LGR5+ cells that proliferate and form secondary tumors. Ablation of HRCs prevented formation of the majority of metastasis (Cañellas-Socias et al., 2022).

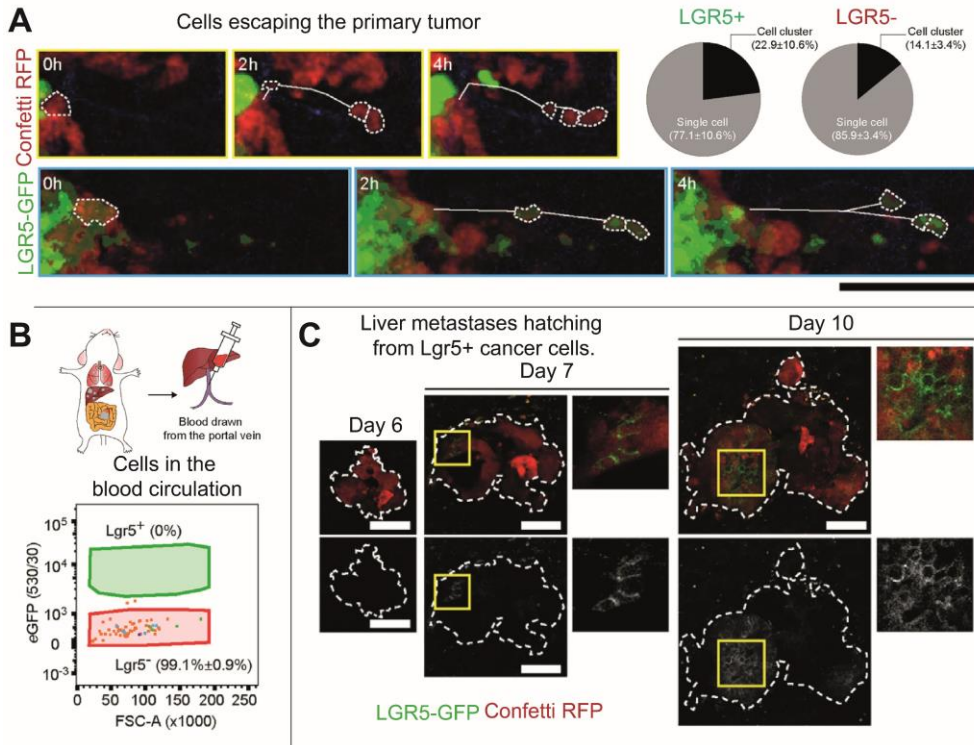


Figure 12: Plasticity of LGR5- cells drives metastasis in CRC. (A) The majority of cells escaping the primary tumor are LGR5- cells. (B) The vast majority of CTCs are LGR5-. (C) Upon arrival to the liver, some LGR5- cells convert to LGR5+ enabling metastatic growth. Adapted from (Fumagalli et al., 2020).

Another study uncovered yet another mechanism involved in CRC metastasis initiation. By using human samples and mouse models, Ganesh et al. showed that the adhesion molecule L1CAM is dispensable for adenoma formation but required for CRC propagation and liver metastasis colonization. Interestingly, high expression of L1CAM is required also for regrowth and healing of the intestine, a condition that, similarly to the process of tumor invasion and metastasis, involves loss of epithelial integrity. Also this study shows plasticity, with some cells being able to acquire the L1CAM^{high} phenotype and enter in a regenerative state following tissue disruption. (Ganesh et al., 2020). Altogether these studies disclose the high cellular heterogeneity involved in metastatic CRC and the crucial role of plasticity.

1.4.5. CRC CSCs and the microenvironment

As previously mentioned, (see Cancer stem cell niche), cancer stemness is not an intrinsic property. Instead stemness is spatiotemporally orchestrated, with functional stem cells being largely defined by the interaction with the microenvironment (Lamprecht et al., 2017; Lenos et al., 2018; Lu et al., 2013; Tsai et al., 2012). One study described functional CSCs that reside at the tumor edge, close to cancer associated fibroblasts that secrete osteopontin, promoting cancer cell growth (Lenos et al., 2018). In another study, poor prognosis was shown to be associated to a mesenchymal gene signature deriving from the tumor-associated stroma and induced by elevated TGF- β . Inhibition of TGF- β hampered disease progression (Calon et al., 2015b). Furthermore, a subset of tumor cells residing adjacent to the stroma was identified as responsible for most of the ribosomal RNA and protein synthesis. Genetic ablation of this population induced tumor growth arrest (Morral et al., 2020). To further add complexity, CAFs can have either an inhibitory or tumor promoting effect on cancer cells, depending on their phenotype and secretome. GREM-1 secreting fibroblasts promote tumorigenesis by inhibition of BMP signaling, which belongs to the TGF- β superfamily, whereas fibroblasts that secrete ISRL, restrain CRC growth (Kobayashi et al., 2021). Moreover, it has been shown that endothelial cells can promote a CSC phenotype in CRC cells by secreting soluble Jagged-1 (Lu et al., 2013). Altogether, these studies highlight the importance of microenvironmental stimuli in shaping CSC functionality in CRC.

2. OBJECTIVES

This thesis work was first aimed at understanding how intra-tumor heterogeneity is linked to cellular mechanical properties in human colorectal carcinoma. Secondly, the goal was to elucidate the functional implications of this link in CRC metastasis. I addressed these questions through a bottom-up approach, performing a mechanical characterization from the single cell level to collective cellular interactions.

Specifically, I focused on the following objectives:

1. To mechanically characterize single cells from colorectal cancer patient-derived organoids based on their stemness.
2. To study the response to confinement of CRC PDO single cells in terms of survival and migration.
3. To study the collective behavior of self-assembled PDO clusters.
4. To analyze the extravasation potential of CRC clusters by assessing their adhesion to an endothelial monolayer and their ability to form transendothelial gaps.
5. To uncover the molecular mechanism explaining the identified mechanical phenotypes.
6. To explore whether the discovered molecular mechanism reflects a general trait of CRC tumors.

3. MATERIALS AND METHODS

3.1. EXPERIMENTAL METHODS

3.1.1. Patient-derived organoids culture

The PDO model used has been previously described and referred to as PDO7 in ref (Cortina et al., 2017). Briefly, the PDO model was engineered by knock-in CRISPR/Cas9- mediated homologous recombination. The IRES-iCasp9-T2A-TdTomato-WPRE-BGHpolyA construct was inserted after the stop codon of the *Lgr5* gene to fluorescently label LGR5+ cells using the LGR5 endogenous promoter as a driver of TdTomato expression. The PDO model carries genetic alterations in four main pathways driving colorectal carcinogenesis, namely WNT pathway (APC loss of function mutation), EGFR signaling (activating KRAS G13D mutation), TGF- β signaling (SMAD4 loss of function) and p53 tumor suppression (mutation in ATM). Tumor cells were grown as organoids embedded in basement membrane extract (Cultrex BME Type 2, AMSbio) using tumor organoid medium composed of Advanced DMEM/F12 (Gibco), 10 mM HEPES (Sigma-Aldrich), 1% GlutaMax; 1 \times B-27, 20 ng ml⁻¹ Human FGF (fibroblast growth factor) basic (all from Gibco); 50 ng ml⁻¹ recombinant human EGF (epidermal growth factor) and recombinant Noggin (100 ng ml⁻¹) (both from Peprotech). The medium was supplemented with 0.2% Normocin (InvivoGen) as an antimicrobial agent. The organoids were split every 6–7 d. For splitting, the organoid-containing drops were enzymatically dissociated by TrypLE (Gibco) for 15 minutes at 37° C and reduced to single cell suspension by pipetting. TrypLE was then diluted with washing medium (Advanced DMEM/F12, 10 mM HEPES (Sigma-Aldrich), 1% GlutaMax) and centrifuged at 100g at RT for 3.5 min. The pellet was resuspended in 1:3 Medium:BME and seeded in 20 μ l drops in 6-wells plates. After incubation for 20 min at 37° C, the drops were covered with tumor organoid medium and maintained at 37° C and 5% CO₂.

3.1.2. Flow cytometry analysis and sorting

For single cell experiments, PDOs were dissociated as described above and resuspended with cold tumor organoid medium at a concentration of 1×10^6 cells ml⁻¹. Single cells suspension was stained with Dapi (Life technologies) for 10 minutes, then analyzed and sorted with FACS Aria flow cytometer (BD Bioscience). The gating strategy defining the LGR5⁺, LGR5^{med} and LGR5⁻ subpopulation is shown in Figure 13. Briefly, cells were selected according to the FSC/SSC parameters. Aggregates were discarded using FSC-width while dead cells were excluded based on Dapi staining. Gating to select the LGR5⁻ cells was set using unlabeled PDO cells. LGR5⁺ and LGR5^{med} were selected to prevent overlapping between the two populations and ensure collection of approximately the same number of cells.

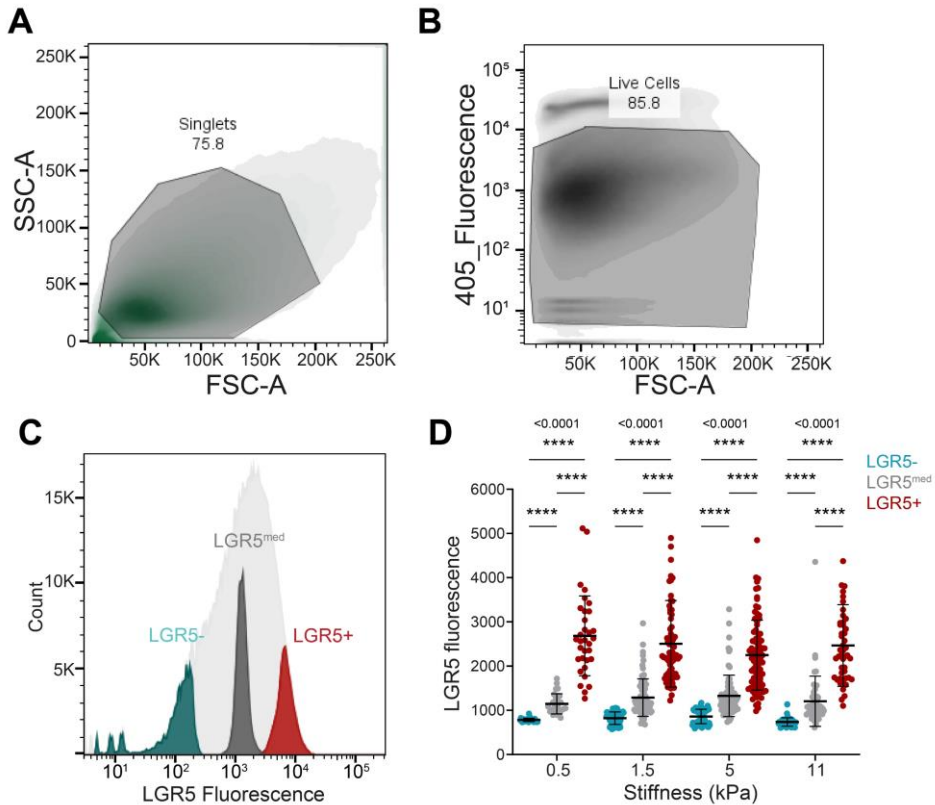


Figure 13: Sorting and measuring TdTomato Fluorescence of LGR5⁻, LGR5^{med} and LGR5⁺ cells. (A-C) Flow cytometric sorting strategy used to obtain LGR5⁻, LGR5^{med} and LGR5⁺ cells from CRC PDOs cultured for 1 week in culture matrix. (A) Side scatter (SSC) and forward scatter (FSC) were used to exclude cell clusters. (B) Cell viability was ensured by excluding cells labelled with Dapi. (C) Tdtomato fluorescence LGR5⁻,

LGR5med and LGR5+ cells as analysed by flow cytometry. (D) Mean Tdtomato fluorescence intensity of sorted LGR5-, LGR5med and LGR5+ cells 24 h after seeding on collagen I coated gels. Quantification from confocal images. Data are represented as the mean \pm s.d. of $n > 73$ cells/condition from four independent experiments. Statistical significance was determined using Shapiro-Wilk normality test, followed by a Kruskal-Wallis multiple-comparison test.

After sorting, cells were centrifuged, resuspended in 50 μ l tumor organoid medium and seeded on gel substrates coated with collagen I. After 3 h incubation to allow the cells to adhere, 1 ml of medium was added in each dish/well. Maintenance of cell identity after dissociation was assessed by measuring LGR5 fluorescence of sorted single cells 24 h after sorting and seeding (Figure 13). All single cell experiments were performed 24 h after seeding and sorting.

3.1.3. Polyacrylamide gel preparation

Polyacrylamide (PAA) gels were used to form substrates with different Young's modulus ranging from 0.5 to 30 kPa. Glass-bottom 35 mm dishes or 6-well glass-bottom (Mattek) were incubated with a solution of Bind-silane (Sigma-Aldrich), acetic acid (Sigma-Aldrich) and absolute ethanol (PanReac) at volume proportions of 1:1:12 for 10 minutes at RT. After 2 washes with absolute ethanol, 20 μ l of PAA solution (Table S1) were placed on the dish glass bottom and covered with 18 mm glass coverslip. For TFM, the gel substrates contained 0.2 μ m green, fluorescent carboxylate-modified beads (FluoSpheres, Thermofisher). After 1 h polymerization at RT, the gels were covered with PBS and the coverslips removed. The gel surface was activated with Sulfo-SANPAH and coated with 150 μ g.ml⁻¹ of Collagen I overnight.

Table 1: Different recipes used for the PAA gel preparation.

Stiffness (kPa)	Acrylamide (BioRad) %	Bis- acrylamide (BioRad) %	Beads** % solids	Ammonium persulphate (Sigma- Aldrich) %	Tetramethyl- ethylenediamine (Sigma-Aldrich) %
0.5	4	0.03	0.03	0.5	0.05
1.5	5	0.04	0.03	0.5	0.05
3	6.16	0.044	0.03	0.5	0.05
5	7.46	0.044	0.03	0.5	0.05
11	7.5	0.1	0.03	0.5	0.05
30	12	0.15	0.03	0.5	0.05

3.1.4. Cell confinement

Cell confinement was achieved using a previously described dynamic cell confiner (Le Berre et al., 2014). Briefly, sorted PDO cells were confined using a microfabricated device consisting of a central PDMS piston that functions as a suction cup and is connected to a system made of a pressure controller (Flow EZ™ LU-FEZ-N800, Fluidigent) and a vacuum pump (LABOPORT N96). The confinement height (4.5 and 7 μm) was controlled using micro-confinement coverslips made of PDMS micropillars of the corresponding heights attached to a glass coverslip, produced as previously described (Figure 14) (Le Berre et al., 2014). All the surfaces of the device were plasma cleaned and coated with 0.5 mg ml^{-1} of PLL-g-PEG to create low attachment conditions. To track confined nuclei and detect dead/dying cells, cells were incubated for 20 min with ReadyProbes Cell Viability Imaging Kit (Blue/Green).

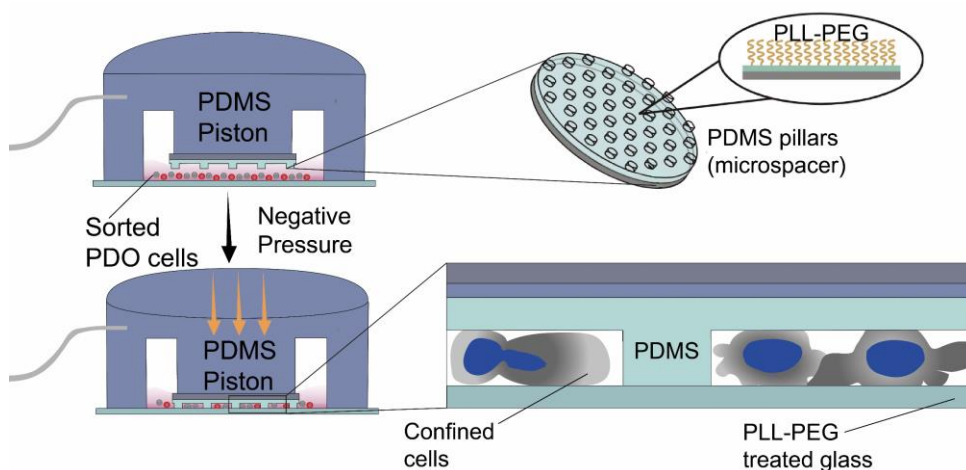


Figure 14: Scheme of dynamic cell confiner. The device acts as a suction cup. When negative pressure is applied, the central PDMS piston holds a glass slide to which PDMS pillars of fixed height (4.5 μm) are attached. Adapted and inspired from (Le Berre et al., 2014).

3.1.5. Mechanical characterization of cells using RT-DC

Real-time deformability cytometry measurements of PDO single cells were performed as previously described (Otto et al., 2015). Briefly, cells grown for 6-7 days in BME or seeded as single cells on PAA gel substrates were harvested using TrypLE and centrifuged at 400 g for 4 min. The pellet was then suspended

in a viscous solution containing 0.5 % methylcellulose with osmolarity of 310-315 mOsm kg⁻¹ and loaded in the RT-DC microfluidic chip using a syringe pump (NemeSys, Cetoni). Cells were flowed through a 300 μm long channel with a square cross-section of 20 × 20 μm at a speed of 0.16 μl s⁻¹ (Figure 15). Deformed cells were imaged at the end of the channel and their cell contours were used to calculate the cell deformation by ShapeIn2 software. Calculation of the apparent elastic modulus was performed using the analysis software Shape-Out version 2.11.5 (Müller Paul, n.d.). Cells with porosity higher than 1.05) or/ and events with size outside the range of 150-350 μm² were discarded to avoid incomplete contours or/ and cell clusters. Measured cells were divided into LGR5-, LGR5^{med} and LGR5+ cells based on Tdtomato fluorescence intensity as shown in Figure 13. Deformation is defined as $1 - (2 * \sqrt{\pi A} / P)$, where A and P are the area and perimeter of the detected cell contour, respectively.

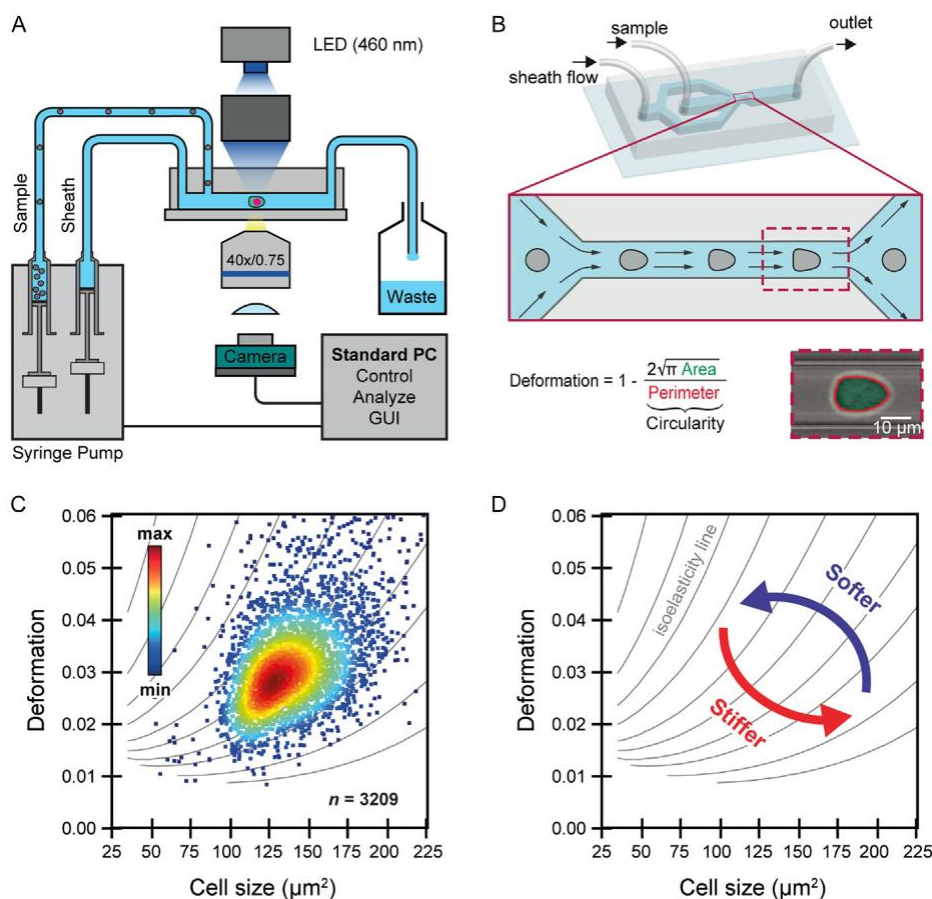


Figure 15: Principle and setup of RT-DC setup. (A) Scheme of the experimental setup consisting of a LED light source, a syringe pump, and a camera installed on an inverted

microscope. **(B)** A 3D representation of the microfluidic device used for RT-DC. Cells suspended in a highly viscous solution are flushed through a 20- μ m-wide microfluidic channel where they are deformed by shear stress and pressure gradients. Deformed cells are imaged in the region of interest (red dashed rectangle) at the back of the chip. Deformation is quantified as the deviation from a circular cross-section. **(C)** Typical RT-DC results of deformation vs. cell size scatter plot. Each dot represents a single cell, the color scale indicates event density. **(D)** Isoelasticity lines derived from numerical simulations enable prediction of cell mechanical properties in the deformation vs. cell size plot. Adapted from (Urbanska et al., 2018).

3.1.6. Cluster Motility assay

PDOs grown in BME for 5 days were extracted from matrix using Dispase I. After neutralization through dilution with 10 ml washing medium, they were centrifuged and resuspended in 1 ml tumor organoid medium. A volume of 70 μ l of the cluster suspension was placed on an 18 mm 3 kPa PAA gel substrates coated with 150 μ g/ml of Collagen I (Fig. 3A). After 3 h incubation at 37° C to allow clusters adhesion, 1 ml medium was added to the dish. 24 h after seeding, clusters were imaged every 60 min, for 42 h.

3.1.7. HUVEC Monolayer Formation and cluster attachment assay

To form a monolayer, HUVEC cells were seeded on 3 kPa PAA gel substrates coated with 150 μ g/ml of Collagen I and cultured for 6 days. EGM-2 endothelial medium was changed every two days. Staining with VE-cadherin confirmed the presence of stable cell-cell junctions after 5-6 days. Once a monolayer was formed, PDO clusters were extracted from BME matrix with Dispase I and seeded on top of the monolayer. The samples were imaged 1 h after seeding every 40 mins for 16 h.

3.1.8. Quantitative PCR (qPCR)

To measure the expression of Ezrin/ Radixin/ Moesin (ERM) proteins in sorted PDO cells, real-time qPCR experiments were performed. RNA was extracted using the Qiagen RNeasy Micro Kit and following the manufacturer's instructions (Qiagen). The concentration of the obtained total mRNA was measured with a

Nanodrop ND- 1000 Spectrophotometer and equal amounts were loaded for reverse transcription. Complementary DNA was produced using the iScript cDNA Synthesis Kit. SYBR Green (Applied Biosystems 4385612) RT-qPCRs were performed in triplicates or duplicates with a StepOnePlus System (Applied Biosystems) under standard settings. The $2^{-\Delta\Delta C_t}$ method was used to calculate relative gene expression. Normalization of all the $\Delta\Delta C_t$ values was carried out to the housekeeping gene GAPDH. Supplementary Table 2 details the primer sequences used.

Table 2: qPCR primer sequences.

Gene	Forward primer	Reverse primer
<i>Lgr5</i>	GCTTCCTGGAGGAGTTACGTC	AACAGCTTGGGGGCACATAG
<i>Krt20</i>	CAGTGGTACGAAACCAACGC	TCCTCTCTCAGTCTCATACTTCA
<i>Itgb1</i>	GCCGCGCGGAAAAGATGAAT	ATCTGGAGGGCAACCCTTCT
<i>Itga1</i>	AAATGAAGAAGGAAAATGGGTGC	CCCACAAGCCAGAAATCCTCC
<i>Itga10</i>	AACTCCCCTTCGTCACTCAC	CTGTACCAGTCCCACCTGTATC
<i>Itga11</i>	CGAGCGGAAAGACAACATGC	TAGGTCTGGCACCTTTGGAG
<i>RhoA</i>	ATTCGTTGCCTGAGCAATGG	TGTGTCCCACAAAGCCAACT
<i>RhoC</i>	GGAGCGGAAGCCTTGAC	GTCCACCTCAATGTCCGCAA
<i>Cdc42</i>	ACGTGAAAGAAAAGTGGGTGC	GCCAGCTTTTCAGCAGTCTC
<i>Rock1</i>	TTCGATTGTTTGCTGGATGG	CCTTCCTGGTGGATTATGCCT
<i>Rac1</i>	CTAGACCCTGCGGATAGGTG	GCTGGACCGAGAGAGTTTCCC
<i>Myh9</i>	AGGTGTCCCATCTCTTGGGT	AACATCCGCTCATAGGTTCGC
<i>Diaph1</i>	CATAGACATGAATGCAGAGGGCG	AAGGTCTCCTCCTCCTCCTCTA
<i>Ezr</i>	CTGCTCTGACTCCAGTTGG	GCCGATAGTCTTTACCACCTGAT
<i>Rdx</i>	GATGAGTTTGAAGCAATGTGGGG	TTAAGGCCCCAGAAAAACCCA
<i>Msn</i>	CCATGCCCAAACGATCAGTG	CAGCCAGGTGGAGAAACCTT

3.1.9. Western blotting

Sorted PDO cells (~100,000) were seeded on 3 kPa PAA gel substrates. After 24 hours, cells were mechanically dissociated from gel substrates using cell scrapers (Biologix) and lysed with RIPA (Radio-Immunoprecipitation Assay) Buffer (Sigma-Aldrich) containing proteases and phosphatases inhibitors (Thermo Fisher). Cell lysates were homogenized, sonicated, and centrifuged at 20000 x g for 20 minutes. Laemli buffer was added to cell lysates and samples were heated at 95°C for 5 minutes. Proteins were separated in 4-20% polyacrylamide gels (Bio-rad) by electrophoresis. Then proteins were transferred to a nitrocellulose membrane (Whatman, GE Healthcare Life Sciences). After transfer, membranes were blocked with 5% dry milk-Tris buffer saline-0.2% Tween and incubated with primary antibodies, p-Ezrin/ Radixin/ Moesin Rabbit (cat. no. 3726, Cell Signaling Technology) and GAPDH antibody (cat. no. 5174S, Cell Signaling) overnight at 4°C. Membranes were incubated with horseradish-peroxidase-coupled secondary antibodies for 2 h at RT. Bands were revealed using LimiLight kit (Roche), visualized with ImageQuant LAS 4000 and quantified using ImageJ/Fiji software.

3.1.10. Generation of stable PDO line expressing inducible iMC-linker

A PiggyBac vector with Neomycin resistance gene and an inducible iMC-linker Halo sequence (JHL9-pPB-tetON-lynlinker-Halo-CH(utr)_optm) was co-nucleofected with a PiggyBac transposase plasmid at volume proportions of 1:2. Nucleofection was performed using Lonza nucleofector kit V (VVCA- 1003) and the Lonza-Amaxall device with program A-32 following manufacturer instructions. 72 h after nucleofection, successfully nucleofected PDO were selected with 400 µg ml⁻¹ neomycin (G418, Invitrogen). Vector expression was induced 16 h before experiments by adding 1 µg ml⁻¹ Doxycycline. iMC-linker was labelled using HaloTag Oregon Green Ligand (Promega). Labelled cells expressing the linker were selected and sorted FACS Aria flow cytometer (BD Bioscience).

3.1.11. Immunostainings

To determine both protein presence and localization we used protein immunostaining. PDO single cells were fixed in 4% paraformaldehyde (PFA; Electron Microscopy Sciences) for 10 min at RT and washed three times with PBS. The samples were permeabilized with 0.1% Triton X-100 (Sigma-Aldrich) for 10 min at RT. After three washes with PBS, the samples were blocked with PBS containing 1% bovine serum albumin (BSA Sigma-Aldrich) for 1 h at RT to prevent any non-specific bonding. Primary antibodies diluted in PBS containing 1% BSA were added and incubated overnight at 4 °C. After three more washes in PBS, secondary antibodies and phalloidin in PBS were added for 2 h at RT. Finally, the samples were washed five times with PBS (5 min each) and imaged. PDO clusters were fixed with 4% paraformaldehyde for 15 min and permeabilized in 0.1% Triton PBS X-100 for 30 min. The other steps were performed as explained above for single cells.

3.1.12. Antibodies

The following is a list of the primary antibodies used and their respective dilutions were as follows: mouse anti-YAP, 1:200 (Santa Cruz, cat. no. sc-271134); mouse anti-CK20, 1:100 (Dako, cat. no. M7019); rabbit anti-VE-cadherin, 1:2,000 (LifeTechnologies, cat. no. PA5-19612). The secondary antibodies used were as follows: goat anti-mouse Alexa Fluor 488 (Thermo Fisher Scientific, cat. no. A-11029); donkey anti-rabbit Alexa Fluor 488 (Thermo Fisher Scientific, cat. no. A-21206), goat anti-rabbit Alexa Fluor 555 (Thermo Fisher Scientific, cat. no. A-21429) and goat anti-mouse Alexa Fluor 405 (Abcam, cat. no. ab175660). All secondary antibodies were used at a dilution of 1:400. To label F-actin, phalloidin Atto 488 (Sigma-Aldrich cat. no. 49409) was used at 1:500 and phalloidin Alexa Fluor-647 (Thermo Fisher Scientific, cat. no. A22287) at 1:400. Hoechst (Thermo Fisher Scientific, cat. no. 33342) was used to label nuclei.

3.2. DATA AND IMAGE ANALYSIS

3.2.1. Image acquisition

For single cells mean traction and morphology measurements the experiments were performed on an automated inverted microscope (Nikon Elipse Ti) using a 20× 0.75 NA objective. To allow higher resolution of traction force distribution, multipole analysis was performed using an inverted Nikon microscope with a spinning disk confocal unit (CSU-WD, Yokogawa) and a Zyla sCMOS camera (Andor, image size 2,048 × 2,048 pixels). The same microscope was used for multidimensional acquisitions of confined sorted PDO single cells, cluster mobility on 2D gel substrates, cluster attachment to an endothelial monolayer. A Nikon ×40 × 0.75 NA air lens objective was used for multipole experiments and clusters experiments. Time-lapses of confined cells were acquired using a ×60 objective (plan apo; NA, 1.2; water immersion). For all the live imaging experiments, a temperature box maintaining 37 °C in the microscope (Life Imaging Services) and a chamber maintaining CO₂ and humidity (Life Imaging services) were used. The open-source Micromanager (Edelstein et al., 2014) was used to carry out multidimensional acquisitions with a custom-made script.

3.2.2. Cell and cluster segmentation

Custom-made MATLAB scripts were used to segment nuclei, cells and clusters. For YAP nuclear to cytoplasmic ratio quantification, fluorescent images of stained nuclei and actin were converted to binary images using level and locally adaptive thresholding. Images were further processed through morphological operations to obtain representative binary masks of detected objects. To obtain binary images of the cytoplasm only, inverted binary images of nuclei were multiplied with masks of segmented cells. For cluster segmentation, confocal phase contrast images from a plane 2 µm above the gel substrates plane were processed similarly. All obtained masks were inspected, and incorrectly segmented cells/ clusters were discarded.

3.2.3. LGR5+ cells Tdtomato fluorescence intensity measurements

Tdtomato fluorescence intensity was quantified using ImageJ/Fiji software or MATLAB scripts. All the values were subtracted with background levels. In the single cell analysis, a mask of the cell borders was either manually drawn using phase-contrast images or obtained using custom-made MATLAB scripts and used to measure the mean fluorescence of Tdtomato. In the cluster analysis, the binary mask obtained from phase-contrast images (see section cell and cluster segmentation) was used to measure the mean grey values of the focal plane located 2 μm above the gel substrate. In the analysis of cluster attachment to an endothelial monolayer, for each cluster, the mean grey value of 4 focal planes at 0, 5, 10, 15 μm from the monolayer, was calculated and reported as Tdtomato fluorescence intensity.

3.2.4. YAP nuclear to cytoplasmic ratio quantification

Segmented images of nuclei and cytoplasm were used to measure the mean fluorescence intensity of YAP. A ratio of the measured intensities was then calculated.

3.2.5. Shape Analysis

Single cells and cluster roundness was measured with the shape descriptor tool in ImageJ/Fiji software.

3.2.6. Cell and clusters tracking

Single cell velocities were obtained as previously described (Trepats et al., 2009). Single cell trajectories from 16 h time-lapses acquired every 20 min were tracked using the Manual Tracking plug-in from ImageJ/Fiji. Quantification of cell velocity calculated as the accumulated distance/total time acquired, was performed and analyzed using the Chemotaxis Tool plug-ins from ImageJ/Fiji. Confined nuclei and cluster velocities were computed using custom-made MATLAB scripts as previously described (Pallarès et al., 2022). In each frame, the centroid position

of segmented nuclei/clusters was detected. Trajectories were built based on proximity and velocity was calculated from the distance between the centroids in each frame. Inconsistent or inaccurate tracks were discarded.

3.2.7. Traction force microscopy

All traction force microscopy experiments were performed using cells seeded on PAA gel substrates of known stiffness, containing fluorescent beads at a concentration of 0.03 w/v. Traction computations and the following analyses of traction forces were carried out with custom-written MATLAB scripts. Fourier transform traction microscopy was used to measure traction forces (Butler et al., 2002; Serra-Picamal et al., 2015; Trepac et al., 2009). The displacement fields of the fluorescence microspheres were obtained using a home-made particle imaging velocimetry (PIV) algorithm using square interrogation windows of side 32 pixels with an overlap of 0.5.

3.2.8. Multipole analysis of tractions

The dipole moment of a cell was calculated as described by Tanimoto and Sano (Tanimoto and Sano, 2014). Cells were manually segmented from the bright field channel, and a binary mask was obtained. This mask was applied to the cell's traction field, to keep only the traction forces generated by the cell and suppress any spurious tractions. Following this, the cell's dipole moment was calculated and diagonalized, yielding eigenvalues corresponding to the major and minor dipole magnitudes. The anisotropy of the cell's mechanical response was quantified as the ratio between the major and minor dipole eigenvalues (Miller and Bishop, 2021).

3.2.9. Patient 10x single-cell analysis

Count matrices were downloaded from ArrayExpress (E-MTAB-8107 for samples EXT001, EXT002, EXT003, EXT009, EXT010, EXT011, EXT012, EXT013, EXT014, EXT018, EXT019, EXT020, EXT021, EXT022, EXT023, EXT024, EXT025, EXT026, EXT027 and EXT028) and GEO (GSE132465 for all

Samsung Medical Center tumor (SMC-T) samples) (Lee et al., 2020). The remaining EXT samples were processed as indicated in E-MTAB-8107 and deposited in ArrayExpress under accession number E-MTAB-9934. Data was processed as detailed in Cañellas-Socias et al. (Cañellas-Socias et al., 2022). Expression was imputed and smoothened using the MAGIC algorithm (Dijk et al., 2018). Signature scores were computed as the mean value of the MAGIC expression per cell for all genes in the signature. The LGR5+ cell population was defined as cells with the LGR5 signature expression (*Bcl11B*, *Axin2*, *Lgr5*, *Ascl2*, *Lrig1*) above the 75th percentile.

3.2.10. Statistical analysis

All the plots were generated in GraphPad Prism 9. All images and videos were processed with the open-source software ImageJ/Fiji. All data are represented as the mean \pm s.d. Sample size (n) and the number of independent repetitions is indicated in the figure captions. Statistical analyses were performed using GraphPad Prism 9. A normality and lognormality test were used to establish the appropriate significance test, followed by a statistical test to compare the mean. For data with more than one variable, analysis of variance tests (ANOVA) or mixed effects analysis followed by multiple comparisons tests were applied.

4. RESULTS

4.1. SINGLE CELL MECHANICAL CHARACTERIZATION

4.1.1. LGR5⁺ and LGR5⁻ cells display differences in morphology and adhesion

Patient-derived Organoids (PDOs) are 3D structures, derived from biopsies, which self-organize and retain essential features of the *in vivo* tumor in terms of architecture, heterogeneity, and gene expression profile (Cortina et al., 2017; de Sousa e Melo et al., 2017; Shimokawa et al., 2017; Tuveson and Clevers, 2019). To mechanically characterize LGR5⁺ and LGR5⁻ cells we used a previously established PDO model engineered by knock-in CRISPR/Cas9-mediated homologous recombination where an IRES-TdTomato-BGHpA cassette was inserted after the stop codon of the *Lgr5* gene, thereby fluorescently labelling the LGR5⁺ cells using the LGR5 endogenous promoter as a driver of TdTomato expression (Cortina et al., 2017).

The organoids differentiated *in vitro* under normal culture conditions, giving rise to heterogeneous populations expressing the stem-cell marker LGR5 and the differentiation marker cytokeratin 20 (CK20) (Figure 16A). We sorted the cells based on LGR5 expression into 3 groups expressing high (LGR5⁺), medium (LGR5^{med}), or low (LGR5⁻) levels of Tdtomato (Figure 16B).

We started the mechanical characterization of the LGR5 subpopulations using single cells dissociated from the organoids and seeded on PAA gels of different stiffness coated with collagen I (Figure 16B). The three groups showed clear differences in cell shape. LGR5⁻ cells were rounder and less adhesive whereas LGR5⁺ spread on the substrate and adopted an elongated morphology (Figure 16C, D). These differences were conserved across the probed stiffness range (Figure 16C, D).

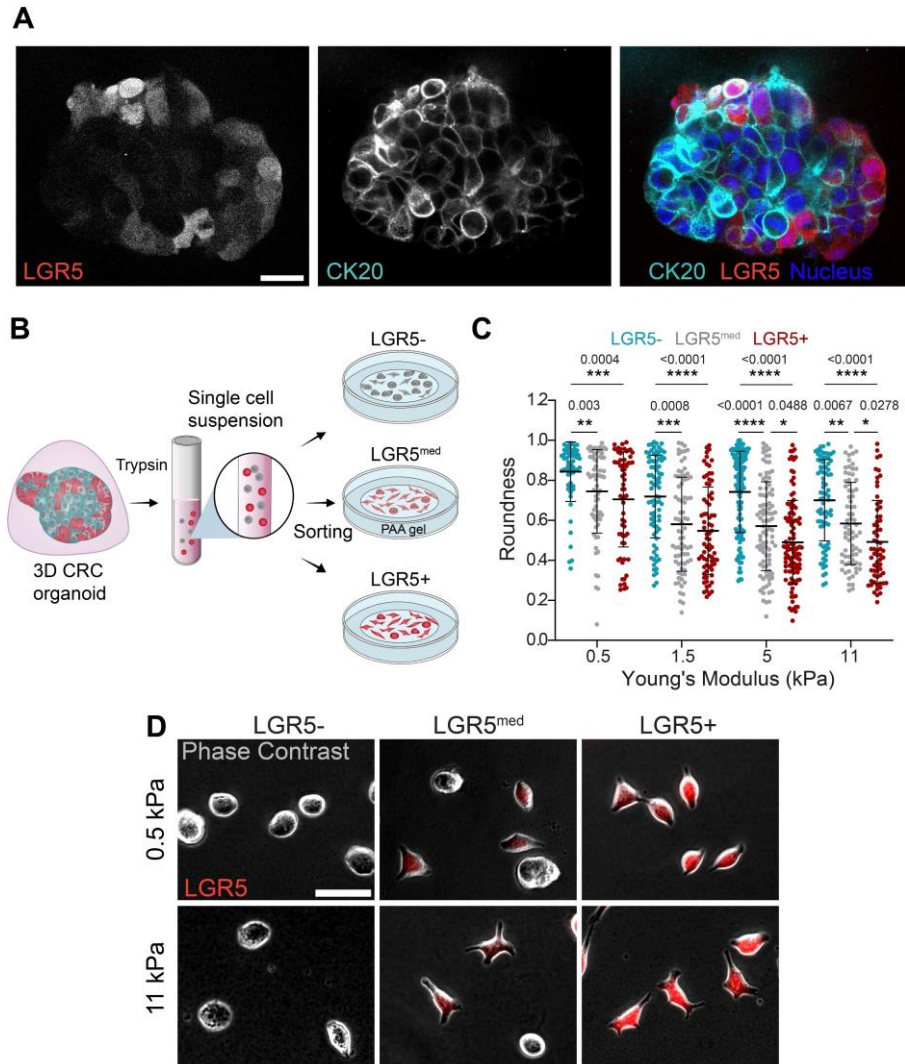


Figure 16: LGR5⁺ and LGR⁻ single cells display differences in morphology and adhesion. (A) CRC PDOs cultured for 1 week in culture matrix gel stained for cytokeratin 20 and nuclei (hoechst). LGR5⁺ cells are labelled with Tdtomato. Scale bar, 20 μ m. (B) Scheme illustrating the preparation of PDOs for single cell analysis on 2D soft substrates. (C) Cell roundness measured for sorted single cells seeded on collagen-I coated gel substrates of 0.5, 3, 5, 11 kPa in stiffness. (D) LGR5⁻, LGR5^{med} and LGR5⁺ cells on 0.5 and 11 kPa gel substrates. Representative images of 4 independent experiments. Scale bar, 50 μ m.

4.1.2. LGR5⁺ and LGR5⁻ cells display differences in YAP localization, but not in mechanosensing

To explore whether differences in roundness were paralleled with changes in mechanotransduction, we stained for the nuclear effector of the Hippo pathway

Yes-associated protein (YAP), which not only regulates intestinal development (Serra et al., 2019), regeneration (Camargo et al., 2007) and tumorigenesis (Camargo et al., 2007; Zanconato et al., 2016), but is also a well-established mechano-sensor (Dupont et al., 2011). Consistent with the trends of cell spreading, YAP nuclear localization was highest in the LGR5⁺ cells, decreased in the intermediate group, and was lowest in the LGR5⁻ cells (Figure 17A, B). This localization pattern was maintained in all tested rigidities from soft (0.5kPa) to stiff (30kPa), revealing a lack of response to stiffness in YAP localization of both LGR5⁺ and LGR5⁻ cells.

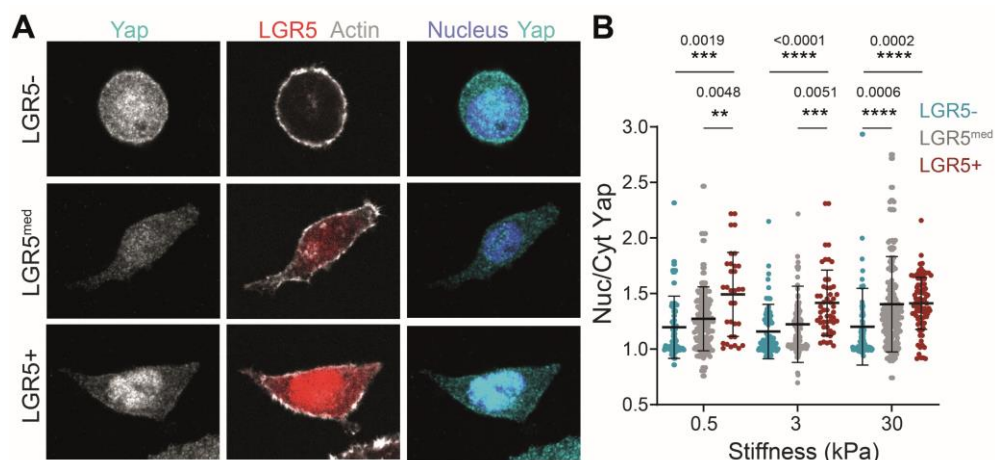


Figure 17: LGR5⁺ and LGR5⁻ single cells display differences in YAP localization but not in mechanosensing. (A) Single PDO cells seeded on 0.5 kPa gel substrates stained for Actin, nuclei and YAP. LGR5⁺ cells are labelled with Tdtomato. Representative images of 4 independent experiments. Scale bar, 10 μ m. (B) Quantification of YAP nuclear/cytoplasmic ratio of LGR5⁻, LGR5^{med} and LGR5⁺ cells seeded on 0.5, 3, 30 kPa gels. Data are represented as the mean \pm s.d. of $n > 60$ cells/condition from 4 independent experiments. Statistical significance was determined using two-way analysis of variance, followed by a Šidák multiple-comparison test.

4.1.3. Cell velocities, mean traction forces and polarization

To determine whether the differences in shape and spreading were coupled to distinct migratory behaviors we tracked the cell movement on the PAA gel substrates. We found no differences in velocities of LGR5⁻ and LGR5⁺ single cells in all tested stiffnesses (Figure 18A). Next, we used TFM to investigate the relation between CRC differentiation states and the ability to generate traction forces. We found no differences in the mean tractions exerted by LGR5⁻,

LGR5^{med} and LGR5⁺ cells (Figure 18B). Nevertheless, the morphological differences observed indicated a possible difference in the force spatial pattern. To explore this possibility, we decomposed the traction stress field into a simpler quantity called the dipole moment. This quantity represents the rotational asymmetry of the stress field and defines the major and minor axis of elongation of the cell (Tanimoto and Sano, 2014). Thus, we used the ratio between the major and minor dipole ($M\delta$) to quantitatively assess the asymmetry of force distribution in the LGR5⁻, LGR5^{med} and LGR5⁺ cells. Compared to the LGR5⁻ cells, the two positive groups displayed higher $M\delta$, indicating a more anisotropic mechanical state (Figure 18C, D).

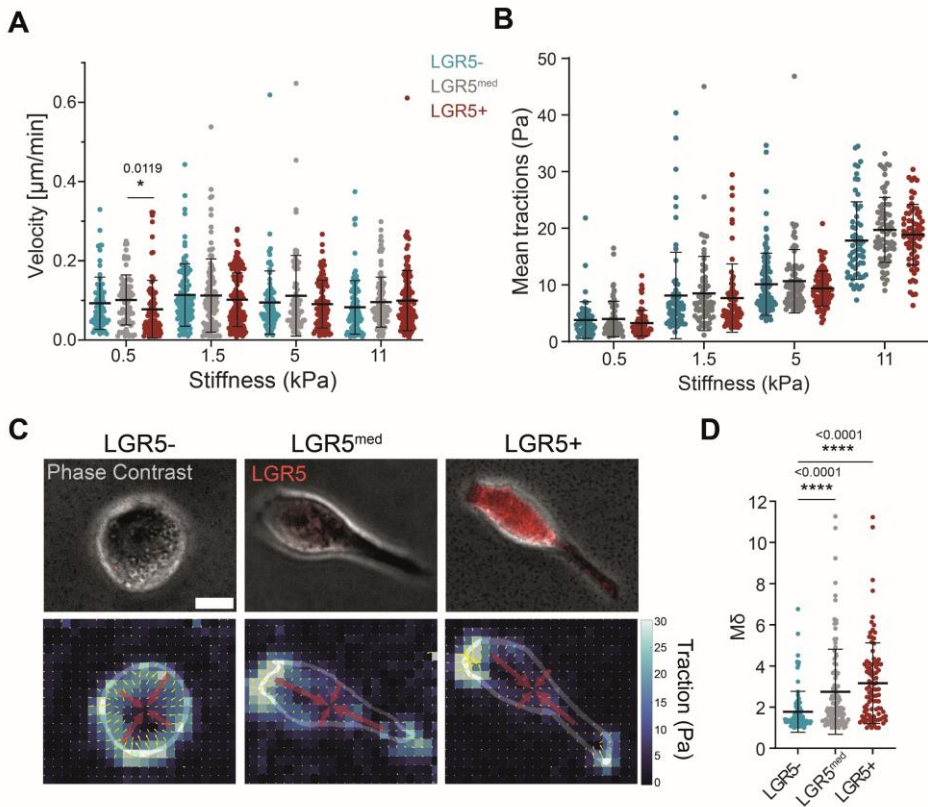


Figure 18: LGR5⁺ and LGR5⁻ cells are equally fast in adhesive conditions and exert similar tractions, but LGR5⁺ are more polarized. (A, B) Quantification of cell velocity (A) and (B) mean tractions exerted by LGR5⁻, LGR5^{med} and LGR5⁺ cells on gels of 0.5, 1.5, 5 and 11 kPa in stiffness. Data are represented as the mean \pm s.d. of $n > 60$ cells/condition from 4 independent experiments. Statistical significance was determined using Shapiro-Wilk normality test, followed by a Kruskal-Wallis multiple-comparison test. (C) LGR5⁻, LGR5^{med} and LGR5⁺ cells seeded on 3 kPa gel substrates and their corresponding traction stress field and force dipole. The traction stress vectors, and their amplitude are represented by the small yellow arrows and colormap, respectively. The

two eigenvectors of the dipole matrix are represented by red arrows. Representative images of 4 independent experiments. Scale bar, 10 μm . **(D)** Quantification of the polarization $M\delta$ of LGR5-, LGR5^{med} and LGR5+ cells. Data are represented as the mean \pm s.d. of $n > 95$ cells/condition from four independent experiments. Statistical significance was determined using Shapiro-Wilk normality test, followed by a Kruskal-Wallis multiple-comparison test.

4.1.4. LGR5+ cells are stiffer

Next, we investigated cell stiffness as a function of their stemness. To do so we used real time deformability cytometry (RT-DC), a high-throughput microfluidic technique where cells suspended in a highly viscous medium are flowed through a narrow channel and deformed by shear stress (Mietke et al., 2015; Otto et al., 2015) (Figure 14 & Figure 19A). With the help of our collaborator from the Guck lab, Catherine Xu, we first validated the RT-DC setup by assessing the cell deformation in the channel constriction compared to the wide part of the device (reservoir) (Figure 19B). We then divided the analyzed cells based on their fluorescence into three groups, namely LGR5⁻, LGR5^{med} and LGR5⁺ (Figure 19C).

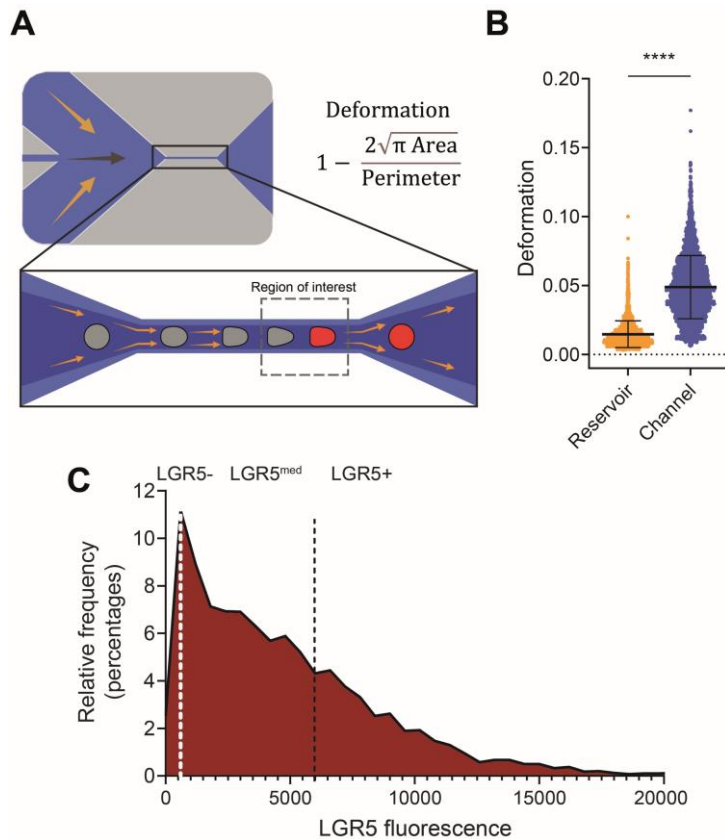


Figure 19: RT-DC experimental setup (A) Scheme of the real time-deformability cytometry (RT-DC) setup. Cells suspended in a highly viscous solution are flushed through a 20- μm -wide microfluidic channel where they are deformed by shear stress and pressure gradients. Deformed cells are imaged in the region of interest (dashed rectangle) at the back of the chip. (B) Cell deformation in the reservoir (wide channel) vs. in the channel constriction. Representative brightfield images of LGR5⁻, LGR5^{med} and

LGR5- analyzed with RT-DC. Scale bar, 5 μm . (**C** and **D**) Cell deformation and derived elastic modulus of LGR5-, LGR5^{med} and LGR5+ cells. Data from one experiment representative of 4 independent ones. $n > 300$ cells/condition. Statistical significance was determined using Shapiro-Wilk normality test, followed by a Kruskal-Wallis multiple-comparison test.

Cell deformability is inversely correlated with cell stiffness and can be used to infer the apparent elastic modulus of cells exposed to shear flow in RT-DC (Mietke et al., 2015). We found that, compared to the LGR5^{med} and LGR5- cells, LGR5+ cells were less deformed upon application of this shear stress, indicative of a higher stiffness (Figure 20A, B). Accordingly, they displayed a higher apparent elastic modulus (Figure 20C).

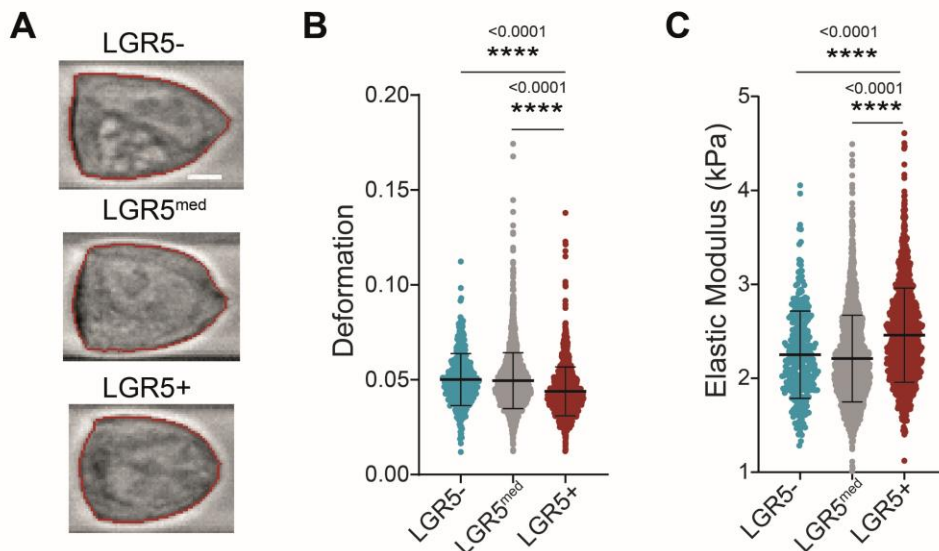


Figure 20: LGR5+ are stiffer. (A) Representative brightfield images of LGR5-, LGR5^{med} and LGR5- analyzed with RT-DC. Scale bar, 5 μm . (B, C) Cell deformation and derived elastic modulus of LGR5-, LGR5^{med} and LGR5+ cells. Data from one experiment representative of 4 independent ones. $n > 300$ cells/condition. Statistical significance was determined using Shapiro-Wilk normality test, followed by a Kruskal-Wallis multiple-comparison test.

4.2. RESPONSE TO CONFINEMENT

4.2.1. LGR5+ cells respond to confinement with higher survival.

Throughout the various steps of the metastatic cascade, cancer cells can encounter confining microenvironments including heterogeneous ECM geometries, 3D longitudinal tracks formed from aligned collagen bundles, porous matrices and narrow inter-endothelial spaces (Paul et al., 2017). Physical confinement and low adhesion have been shown to promote a fast bleb-based amoeboid-like migration in mesenchymal cells and immune cells, as well as in transformed cells (Gabbireddy et al., 2021; Liu et al., 2015; Lomakin et al., 2020; Venturini et al., 2020).

Having observed stemness dependent variations in cell spreading, force generation and stiffness, we hypothesized that LGR5+ cells may respond differently to confinement compared to LGR5- cells. To test this hypothesis, with the help of Valeria Venutrini from the Verena Ruprecht lab, we used a dynamic cell confiner (Le Berre et al., 2014) (Figure 15) where single cells are confined to a precise height between two low-adhesion parallel surfaces. In the absence of confinement and adhesion (suspended cells), the vast majority of PDO cells displayed a round morphology with no blebs and an average diameter of $9.3 \pm 1.2 \mu\text{m}$. As we increased the levels of confinement (7 and $4.5 \mu\text{m}$ pillar height), the fraction of blebbing cells grew and we identified four distinct response categories: no blebbing, round non-polarized blebs, elongated polarized blebs and cell death (Figure 21B).

Analysis of the distribution of the cell responses at $4.5 \mu\text{m}$ confinement revealed that compared to LGR5- cells, LGR5+ cells have a higher tendency to adopt an amoeboid-like blebbing behavior characterized by the appearance of elongated, polarized blebs (Figure 21C, D). Notably, the LGR5- cells showed a substantial increase in cell death in response to confinement (Figure 21C, D).

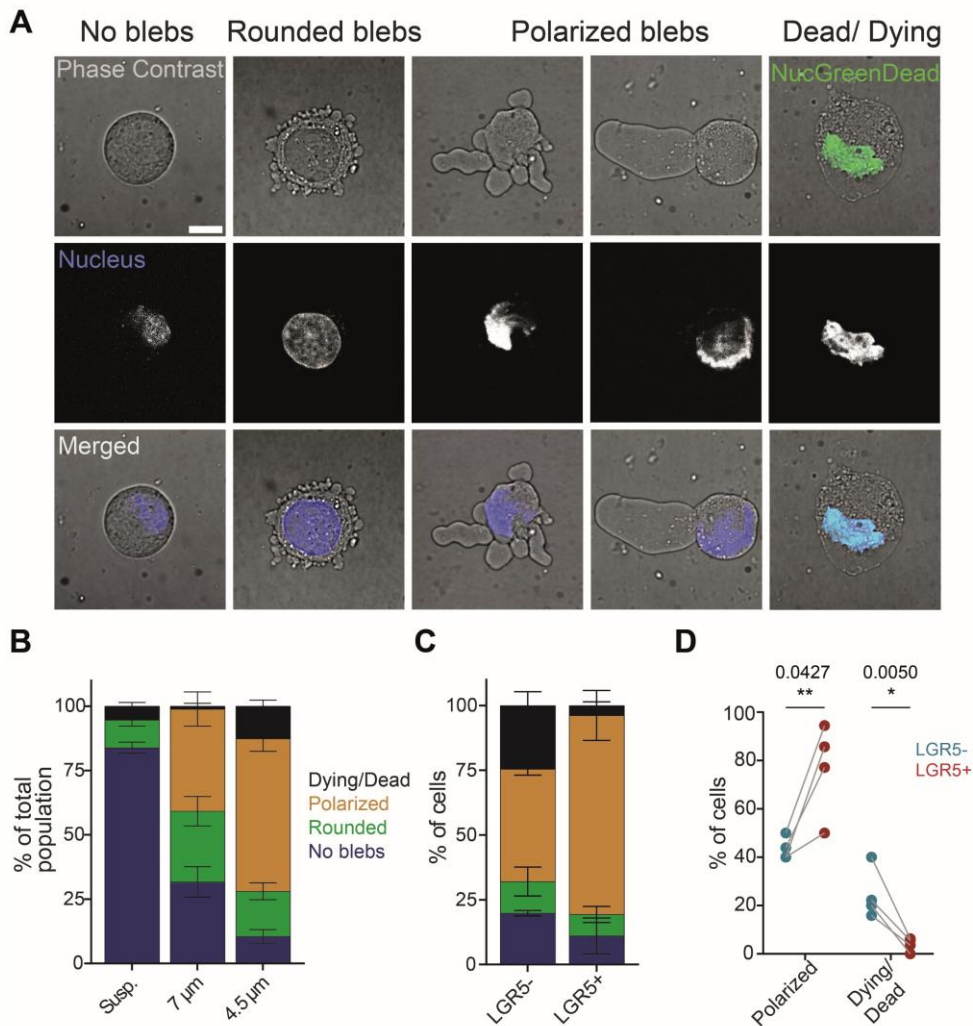


Figure 21: LGR5⁺ cells respond to confinement with a higher survival rate. (A) Representative examples of the four response categories identified in confined LGR5⁻ and LGR5⁺ cells. Scale bar, 10 μ m. (B) Percentage of dying/dead, polarized blebs, rounded blebs, and no blebs in LGR5⁻ and LGR5⁺ cells in suspension or under 7 and 4.5 μ m confinement on a non-adhesive surface. (C) Percentage of dying/dead, polarized blebs, rounded blebs, and no blebs in LGR5⁻ and LGR5⁺ cells in suspension or under 7 and 4.5 μ m confinement. (C, B) Data are represented as the mean \pm s.d. of percentages from four independent experiments. Statistical significance was determined using two-way analysis of variance, followed by a Šidák multiple-comparison test. (D) Percentage of dying/dead and polarized blebs in LGR5⁻ and LGR5⁺ cells under 4.5 μ m confinement on a non-adhesive surface. Data are represented as the mean \pm s.d. of four independent experiments. Statistical significance was determined using two-way analysis of variance, followed by a Šidák multiple-comparison test.

4.2.2. LGR5- cells adopt a faster amoeboid migration

Next, we investigated whether the response to confinement also involved changes in cell migration in each of the four categories. To do so, we tracked the cell nuclei, labelled with Hoechst, and computed their velocities (Figure 22). The total mean velocities of LGR5- and LGR5+ cells showed a very slight difference (Figure 23A). However, analysis of cell velocities in function of confinement response revealed a significant difference in cells displaying polarized blebs with the LGR5- cells moving significantly faster than LGR5+ cells in the same response category, while no significant differences were observed in the migration speed of other categories (Figure 23A, B). These experiments show that LGR5- cells are more fragile under confinement (higher death rate), but those that survive migrate faster.

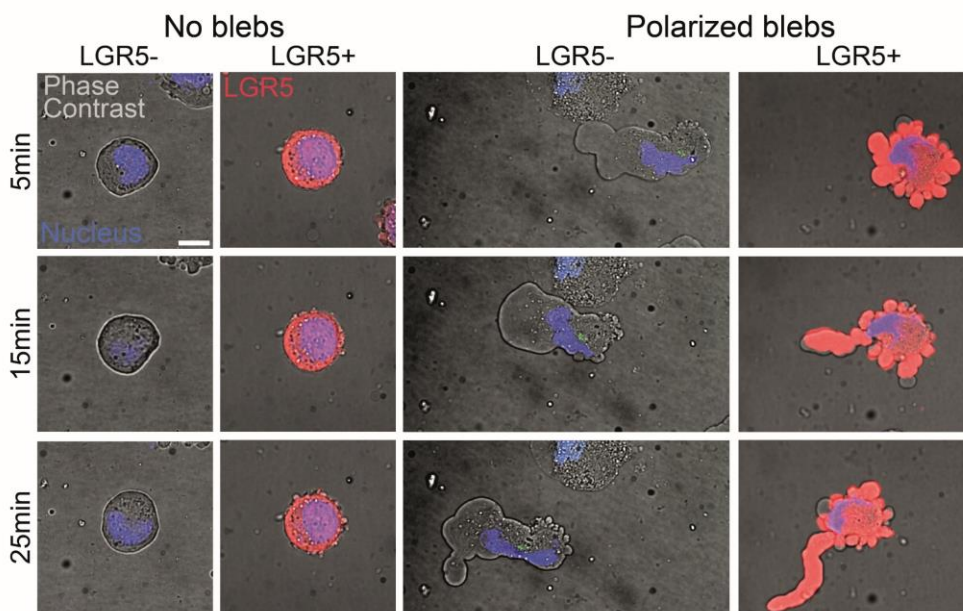


Figure 22: LGR5+ cells respond to confinement with slower amoeboid migration. Representative time lapse images of LGR5- no blebs, LGR5+ and LGR5- polarized blebs. Scale bar, 10 μ m. Images represent four independent experiments, with 303 cells.

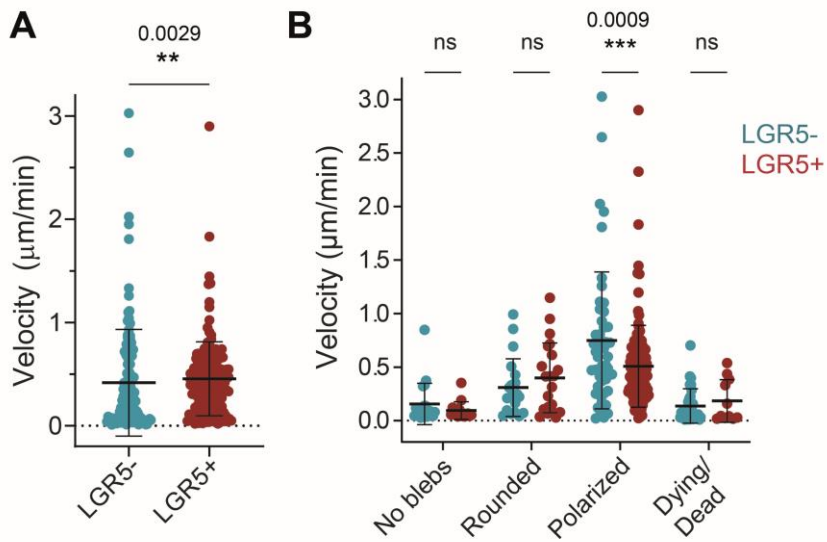


Figure 23: LGR5+ cells respond to confinement with slower amoeboid migration. (A) Migration speed of tracked nuclei of LGR5- and LGR5+ cells. (B) Migration speed of tracked nuclei of LGR5- and LGR5+ cells, divided in categories according to the confinement response. (A, B) Data are represented as the mean \pm s.d. of $n > 303$ cells from 4 independent experiments. Statistical significance was determined using two-way analysis of variance, followed by a Šidák multiple-comparison test.

4.3. COLLECTIVE BEHAVIOUR

4.3.1. LGR5⁻ clusters are rounder, migrate faster and exert less tractions

Metastases can be seeded not only by single cells but also by highly cohesive epithelial cell groups (Aceto et al., 2015; Cheung et al., 2013; Cheung and Ewald, 2016; Fischer et al., 2015; Zajac et al., 2018). Thus, we explored whether multicellular clusters displayed a mechanical phenotype similar to single cells. To study the mechanics of CRC clusters I extracted self-assembled PDOs from 3D matrix gels and seeded them on gel substrates coated with collagen I (Figure 24A).

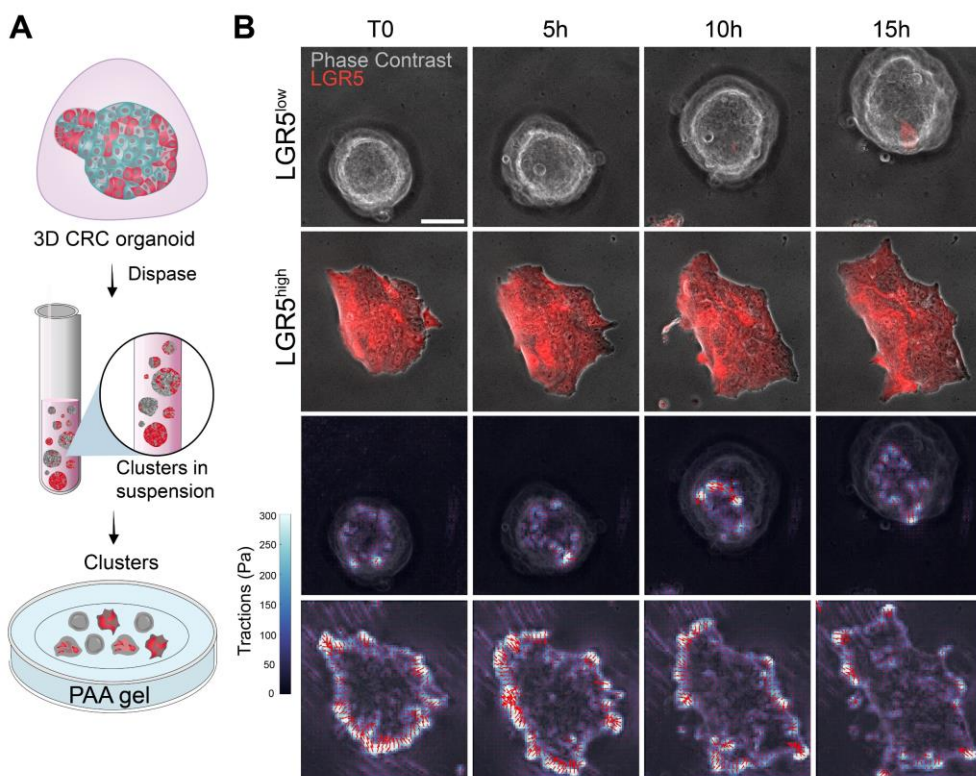


Figure 24: LGR5⁻ clusters are rounder, migrate faster and exert less traction. (A) Scheme of the preparation of PDOs for cluster analysis on 2D soft substrates. **(B)** Time lapse of representative clusters containing low and high amounts of LGR5⁻ and LGR5⁺ cells (first and second rows, respectively). Bottom rows show the time lapse of the

traction stress field of the clusters shown in the top rows. Representative images of four independent experiments. $n = 132$ clusters. Scale bars, $50\ \mu\text{m}$.

We then studied the mechanical properties of cell clusters dividing them into 3 groups based on LGR5 expression (high, medium, and low TdTomato cell clusters), in analogy with the single cell analysis (Figure 24, Figure 25A), tracking their collective migration and measuring the mean traction forces they exert. Similarly to single cells, clusters expressing low levels of LGR5 displayed higher roundness on collagen I substrates while clusters expressing higher LGR5 levels exhibited a more spread, adhesive morphology (Figure 24B, Figure 25B). However, unlike single cells, the migration speed of LGR5^{low} clusters was higher and their mean traction forces were lower (Figure 25C, D). Thus, multicellular clusters retain features of single cell behavior but also display emergent mechanical properties which are absent at the single cell level.

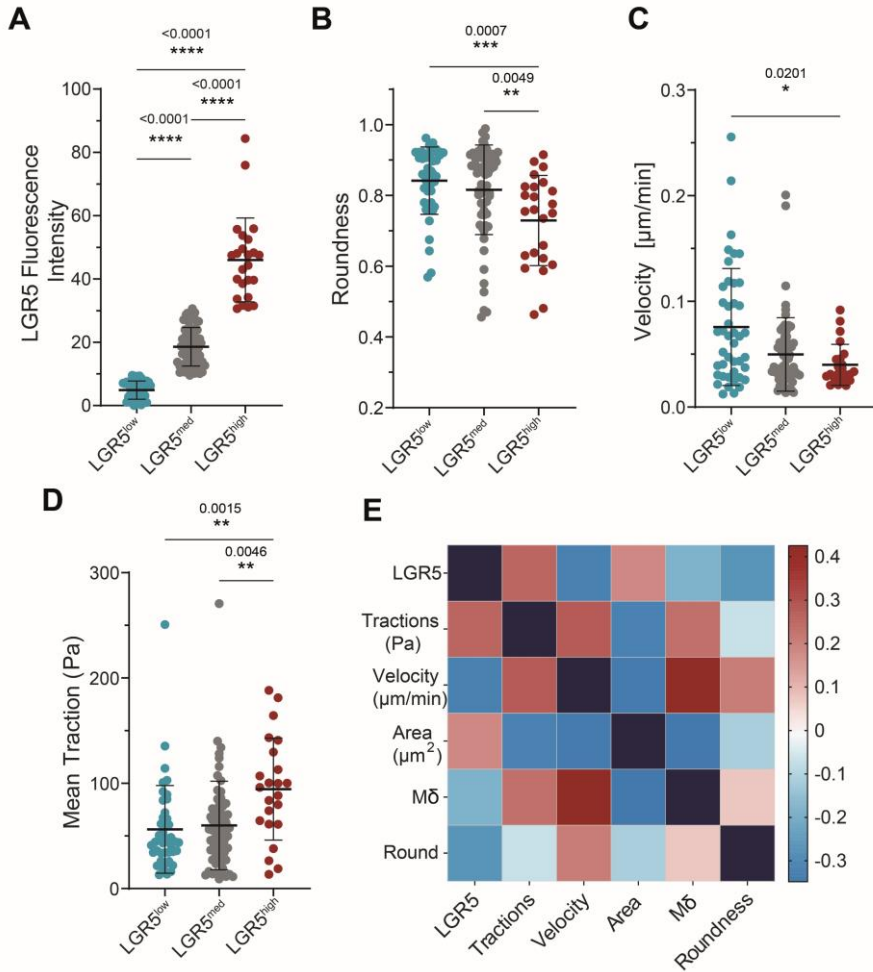


Figure 25: LGR5⁻ clusters are rounder, migrate faster and exert less traction. (A-D) Tdtomato fluorescence intensity (A), cluster roundness (B), migration speed (C), and mean tractions (D). Data are represented as the mean \pm s.d. of $n = 128$ clusters from four independent experiments. Statistical significance was determined using Shapiro-Wilk normality test, followed by a Kruskal-Wallis multiple-comparison test. (E) Correlation matrix of cluster properties including Tdtomato-LGR5 fluorescence, mean traction forces, velocity, area, polarization M δ and roundness. Negative correlation is indicated in blue and positive correlation in red.

4.3.2. LGR5⁺ clusters adhere better to the endothelium and form transendothelial gaps.

One of the fundamental steps in the metastatic cascade is cancer cell extravasation. CTCs are found both as single cells and clusters, the latter being less frequent but with higher metastatic potential (Aceto et al., 2015).

Given the differences in cluster morphology and spreading observed on collagen substrates, we investigated whether clusters with distinct levels of stemness displayed different capacities to adhere to and breach endothelial monolayers. Thus, we grew cohesive human umbilical vein endothelial cells (HUVEC) monolayers on collagen-I substrates and confirmed the presence of stable and mature cell-cell junctions through immunostaining for VE-Cadherin (Figure 26). We then seeded PDOs on top of the monolayer and started imaging one hour after seeding (Figure 26A).

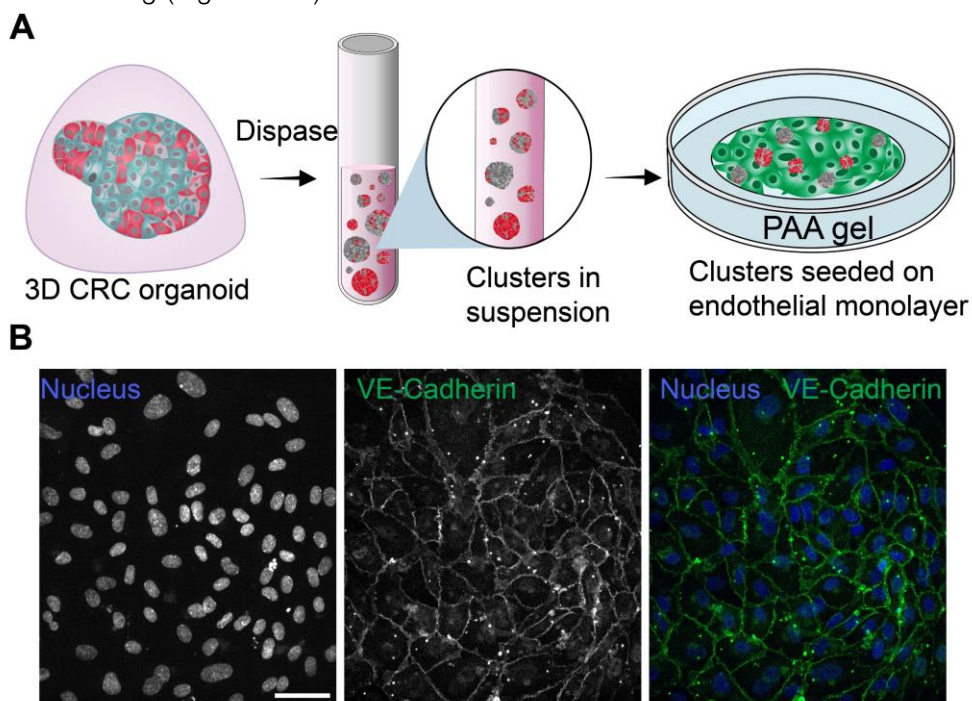


Figure 26. Setup of adhesion to endothelium experiment. (A) Schematic of the preparation of PDOs for adhesion analysis on an endothelial monolayer. (B) HUVEC monolayer grown for 4 days on collagen I coated gels and stained for VE-cadherin and nuclei (hoechst). Scale bar 50 μ m.

We observed that some of the clusters attached to the endothelial cells and created a gap through the monolayer while other clusters detached and floated away from the field of view (Figure 27).

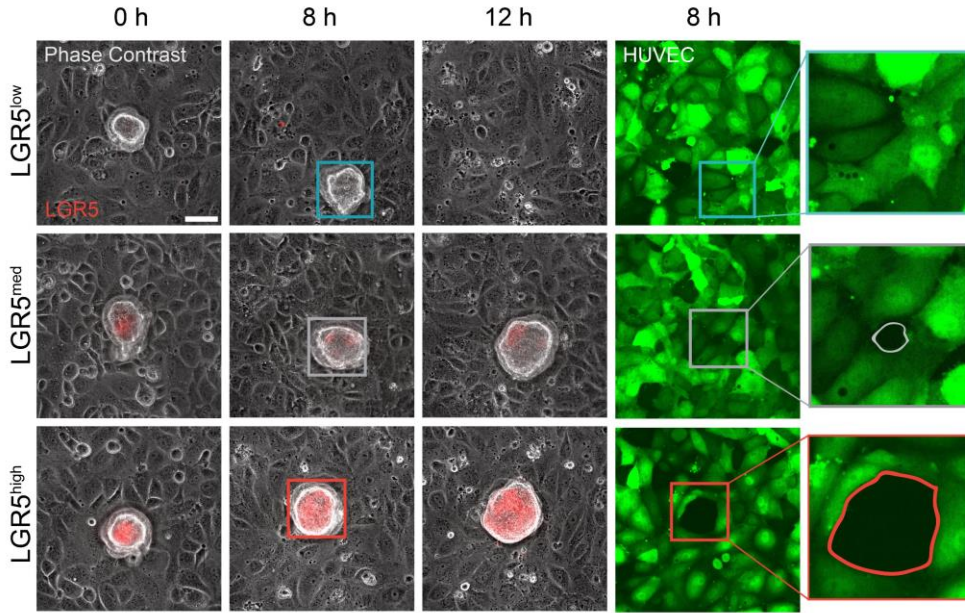


Figure 27. PDO clusters adhering to an endothelial monolayer. PDO clusters seeded on HUVEC monolayers formed on collagen I coated 3 kPa gel. Representative time lapse of LGR5^{low}, LGR5^{med} and LGR5^{high} clusters on a HUVEC monolayer. The last two columns show the fluorescence image of the HUVEC monolayers at 8h including a zoom at the contact point between clusters and monolayers. Scale bars, 50 μ m. Representative images from four independent experiments.

This behavior was independent of the cluster cross-sectional area (Figure 28B). Clusters that remained attached during the whole timelapse exhibited higher mean LGR5 fluorescence compared to clusters that detached (Figure 28A). Furthermore, we quantified the percentage of clusters able to form a gap in the endothelial monolayer as a function of LGR5 expression. Within the three cluster groups (Figure 28C), clusters expressing higher levels of LGR5 were more competent in forming a gap (Figure 28D) as indicated by the higher percentage of gap forming clusters, the shorter time needed for gap formation and the higher gap area (Fig. 28E, F).

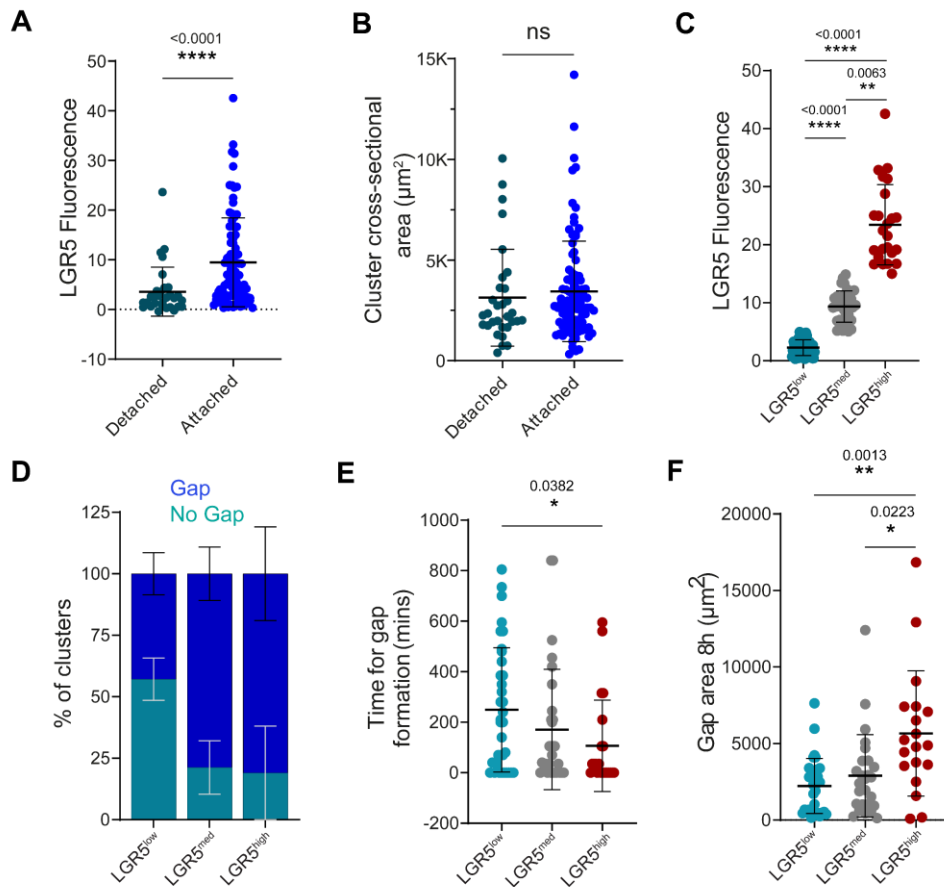


Figure 28: LGR5⁺ clusters adhere better to endothelial monolayers and form transendothelial gaps. (A) Mean Tdtomato fluorescence labelling LGR5⁺ cells in CRC clusters that either remained attached to the monolayer during the whole time-lapse or detached. (B) Cross-sectional area of clusters that remained attached or detached from endothelial monolayer during the 15 h timelapse acquisition. (C) Tdtomato fluorescence intensity of clusters divided into three groups. (A–C) Data are represented as the mean \pm s.d. of $n > 122$ clusters from four independent experiments. Statistical significance was determined using Shapiro-Wilk normality test, followed by a Kruskal-Wallis multiple-comparison test. (D) Percentage of clusters that formed a gap in the endothelial monolayer for LGR5^{low}, LGR5^{med} and LGR5^{high} cell clusters. Data are represented as the mean \pm s.d. of percentages from four independent experiments. Statistical significance was determined using two-way analysis of variance, followed by a Šidák multiple-comparison test. (E) Time for gap formation for LGR5^{low}, LGR5^{med} and LGR5^{high} cell clusters. (F) Gap area measured 8 h after beginning of time lapse acquisition. In (E) and (F) Data are represented as the mean \pm s.d. of $n > 71$ clusters that remained attached during time lapse acquisition from four independent experiments. Statistical significance was determined using Shapiro-Wilk normality test, followed by a Kruskal-Wallis multiple-comparison test.

4.4. MOLECULAR MECHANISM UNDERLYING THE IDENTIFIED PHENOTYPES

4.4.1. Upregulation of ERMs in LGR5- cells

Next, we sought to identify the molecular mechanisms that explain the distinct mechanical phenotypes of LGR5⁺ and LGR5⁻ cells and clusters. To do so we quantified expression levels of several genes associated with adhesion and regulation of the actin cytoskeleton organization (Figure 29). We found that *Itgb11* and *Rock1* expression was increased in the LGR5⁺ cells while *Itga2* and *RhoC* expression was enhanced in the LGR5⁻ cells. These results were not sufficient to explain the uncovered distinct phenotypes of LGR5⁺ and LGR5⁻ cells and thus we continued the quest for molecular candidates.

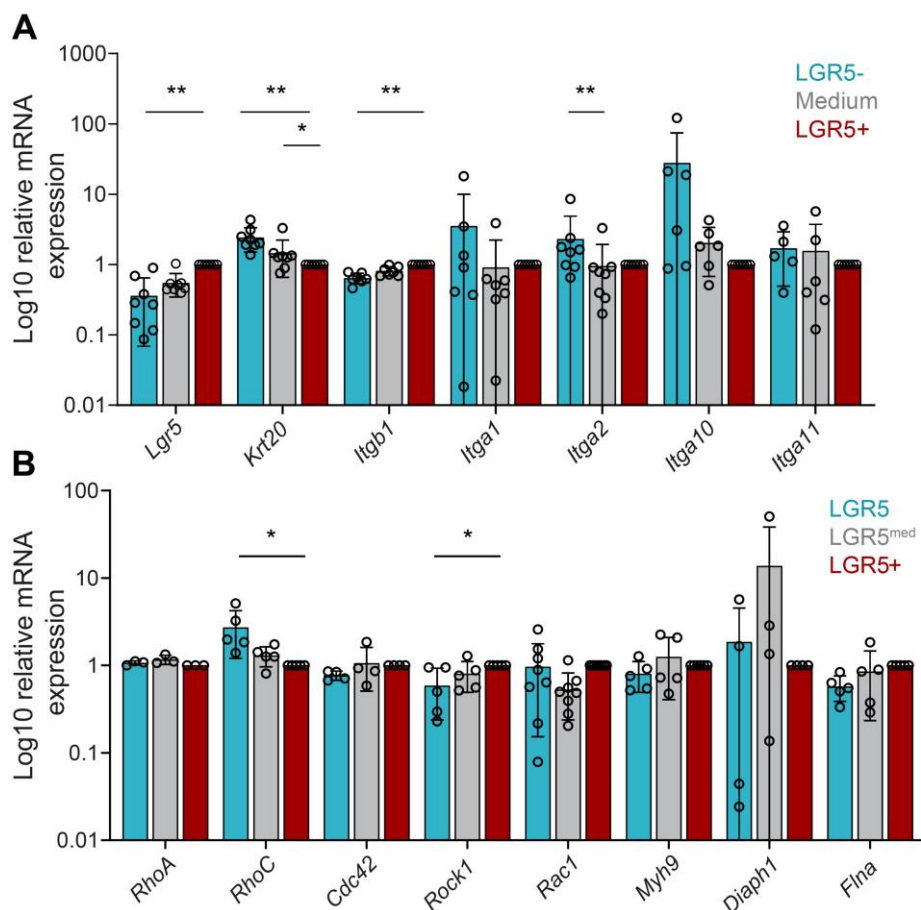


Figure 29: Expression of genes related to adhesion and actin cytoskeleton organization. (A, B) Relative mRNA expression levels of different genes in sorted PDO cells. Data are

represented as the mean \pm s.d. from 4 or more independent experiments. Statistical significance was determined using Shapiro-Wilk normality test, followed by a Kruskal-Wallis multiple-comparison test.

The differences in adhesion and blebbing in response to confinement suggest a role for tethering between the cell membrane and the cytoskeleton, which is mainly governed by Ezrin, Radixin and Moesin, collectively known as ERM proteins (Chishti et al., 1998; Fehon et al., 2010). Indeed, overexpression of these proteins has been shown to induce cellular rounding in adherent single cells (Bergert et al., 2021; De Belly et al., 2021; Tachibana et al., 2015) and to inhibit bleb formation and protrusion (Charras et al., 2006; Diz-Muñoz et al., 2010; Welf et al., 2020). Hence, we investigated whether the identified phenotypes in PDO cells are linked to a differential expression of the ERM proteins. Gene expression analysis with RT-qPCR revealed a substantial upregulation of each of the three ERMs, particularly Moesin and Radixin in LGR5-cells (Figure 30).

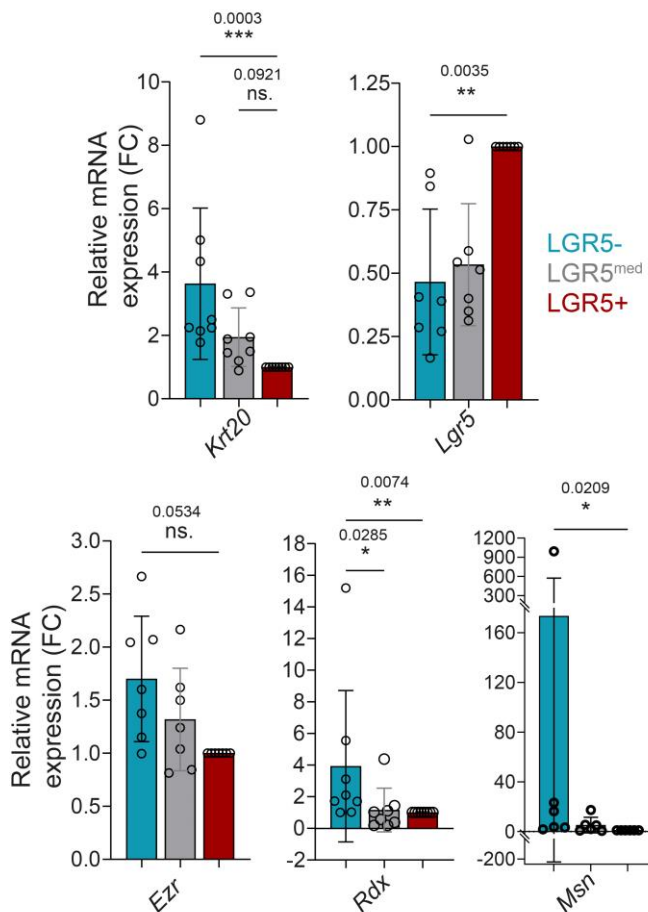


Figure 30: ERM proteins are upregulated in the LGR5- cells. Relative mRNA expression levels of *Lgr5*, *Krt20* and ERM proteins for sorted PDO cells. Data are represented as the mean \pm s.d. from eight independent experiments. Statistical significance was determined using Shapiro-Wilk normality test, followed by a Kruskal-Wallis multiple-comparison test (**Previous page**).

The membrane to cortex attachment (MCA) activity of ERM proteins requires a two-step activation process that involves phosphorylation of a conserved threonine residue present in the F-actin binding site (Arpin et al., 2011; Fehon et al., 2010; Matsui et al., 1998). Measurement of the phosphorylated form of ERM proteins confirmed their increased activity in the LGR5- cells (Figure 31). Moreover, immunostaining of LGR5- and LGR5+ cells showed higher expression of Ezrin in the LGR5- cells (Figure 31).

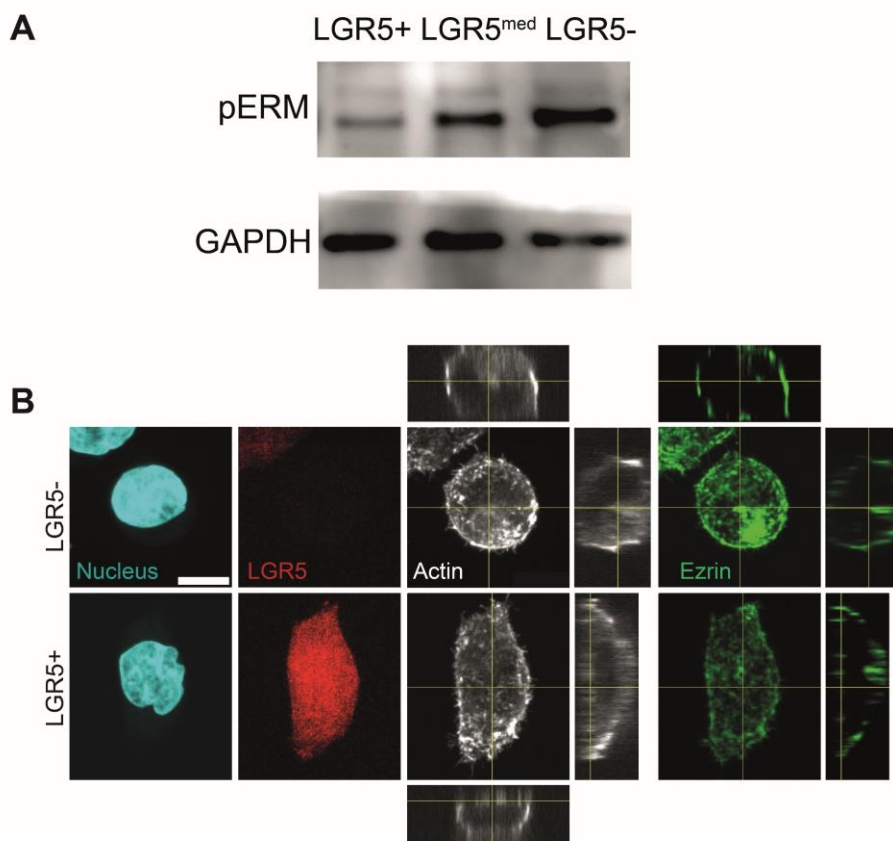


Figure 31: Levels of phosphorylated ERMs and Ezrin expression in sorted LGR5-, LGR5^{med} and LGR5+ cells. (B) Z maximal projection and orthogonal views of nuclei, tdtomato, Actin and Ezrin in LGR5- and LGR5+ cells. Scale bar, 10 μ m.

Increased membrane to cortex attachment (MCA) is responsible for the differences between LGR5⁺ and LGR5⁻ phenotypes

To test whether the increased membrane to cortex attachment (MCA) is indeed responsible for the differences between LGR5⁺ and LGR5⁻ phenotype, we used a previously developed inducible synthetic linker (Bergert et al., 2021) (iMC-linker) that mimics the ERM tethering activity (Figure 32A), without modulating the downstream signaling pathways associated with ERM activation. Induction by doxycycline treatment of the iMC-linker in the LGR5⁺ and LGR5^{med} cells resulted in a marked rounder shape (Figure 32B, C) similar to that observed in LGR5⁻ cells. To determine the link between higher MCA and the rounded phenotype of differentiated clusters, we induced expression of the iMC-linker in self-assembled PDOs. Clusters expressing simultaneously high levels of LGR5 and the iMC-linker presented a rounded non-spread morphology (Figure 32D), thus supporting the involvement of higher MCA in shaping CRC cluster phenotype.

We hypothesized that the higher MCA in the LGR5⁻ cells could account for their lower propensity to adopt a blebbing phenotype under confinement. To test this hypothesis, we induced expression of the iMC-linker in the LGR5⁺ cells and confined them at 4.5 μm . Confinement of LGR5⁺ cells expressing the synthetic iMC-linker resulted in responses remarkably similar to the LGR5⁻ cells, both in terms of amoeboid cell polarization and cell death (Figure 33). These data support that higher MCA in the LGR5⁻ cells reduces their ability to adopt an amoeboid-like behavior upon cell confinement and makes them more susceptible to cell death.

Together, these observations establish the involvement of MCA in defining the mechanical phenotypes of LGR5⁺ and LGR5⁻ cells, both at the single cell and cluster levels.

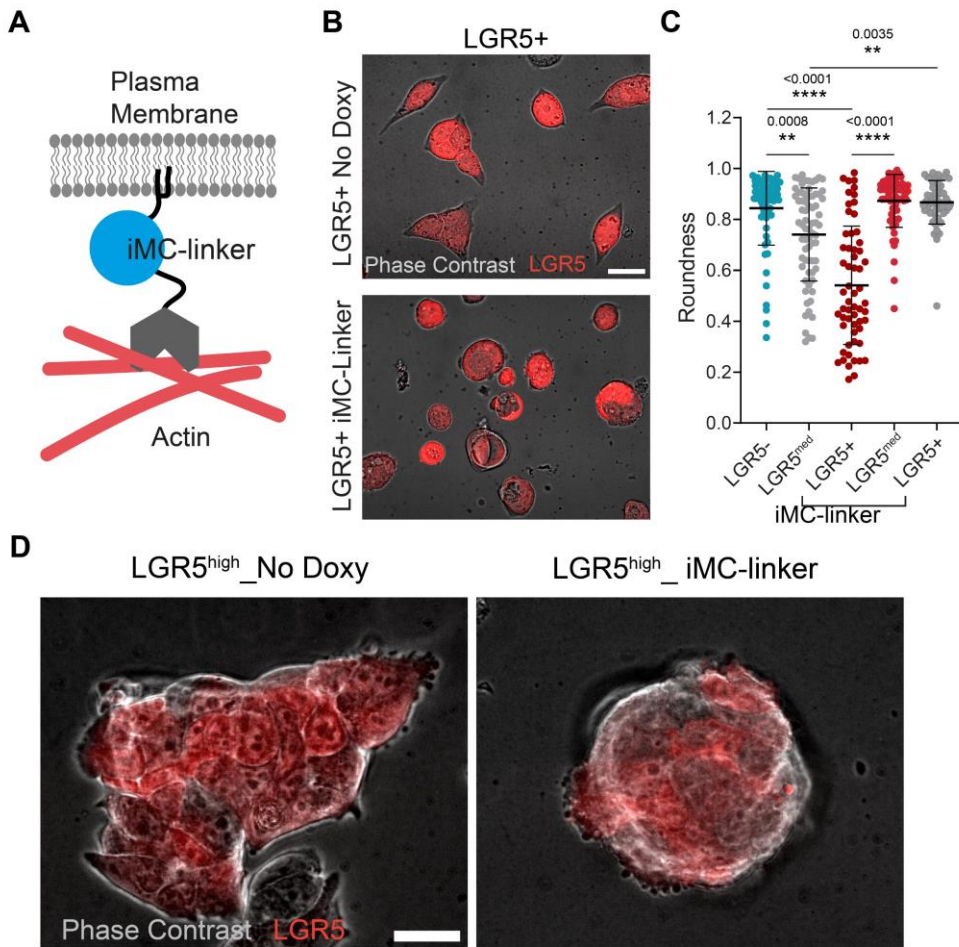


Figure 32: ERM proteins determine the morphological differences between LGR5+ and LGR5- single cells and clusters. (A) Scheme of the iMC-linker. (B) LGR5+ cells treated with doxycycline to induce the iMC-linker expression or untreated (no doxy) on 3 kPa gel substrates. Representative images of 2 independent experiments. Scale bar, 25 μm . (C) Cell roundness calculated for sorted single cells seeded on 3 kPa gel substrates. Data are represented as the mean \pm s.d. of $n > 58$ cells/condition from two independent experiments. Statistical significance was determined using Shapiro-Wilk normality test, followed by a Kruskal-Wallis multiple-comparison test. (D) PDO clusters seeded on Collagen-I coated gel substrates of 3 kPa stiffness. Representative images of two independent experiments. Scale bars, 50 μm .

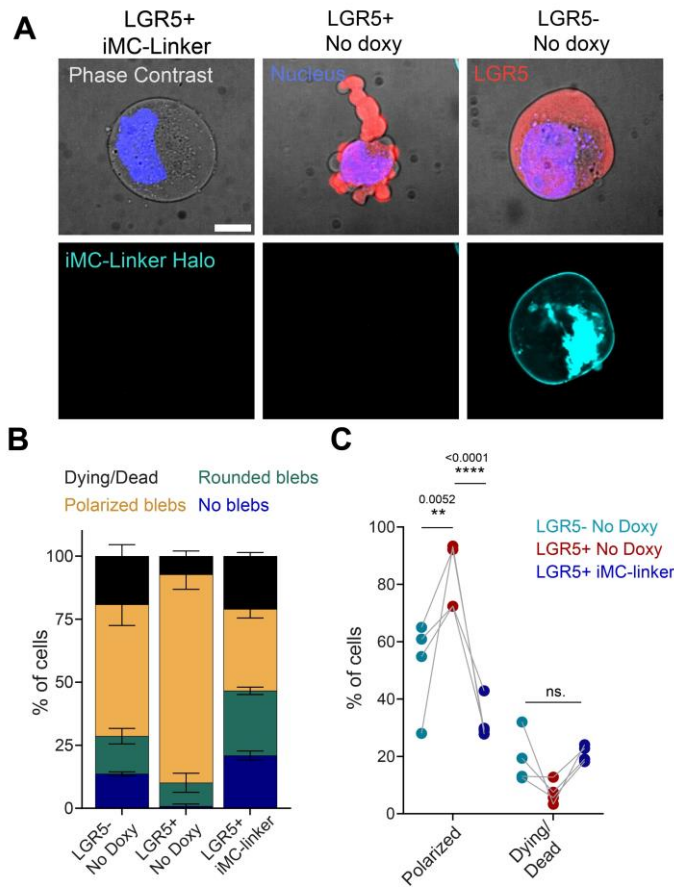


Figure 33: ERM proteins determine the response to confinement in LGR5+ and LGR5- cells. (A) Representative images of LGR5-, LGR5+ and LGR5+ expressing the linker under 4.5 μm confinement on a non-adhesive surface. Scale bar, 10 μm . (B) Percentage of dying/dead, polarized blebs, rounded blebs and no blebs in LGR5-, untreated LGR5+ cells and LGR5+ cells expressing the iMC-linker. (C) Percentage of dying/dead and polarized blebs in LGR5- and LGR5+ cells under 4.5 μm confinement on a non-adhesive surface. (B, C) Data are represented as the mean of four independent experiments ($n = 902$ cells). Statistical significance was determined using two-way analysis of variance, followed by a Šidák multiple-comparison test.

4.5. EXPRESSION OF LGR5 AND EZRIN ARE ANTICORRELATED IN CRC PATIENTS

Finally, to study whether the relationship between LGR5 and ERM protein expression found in our PDO model reflects a general trait of CRC tumors, with the help of Adrià Cañellas-Socias, we analyzed single-cell transcriptomic data from the Samsung Medical Center (SMC) cohort (Lee et al., 2020).

For each patient dataset, cells were divided into two groups based on LGR5 expression and the mean expression of the ERM proteins was calculated. This analysis revealed a significant upregulation of Ezrin in the LGR5⁻ cells (Figure 34A). Although the degree of upregulation showed considerable variability between patients, it was consistent across the cohort (Figure 34B). Interestingly, we only found upregulation of Moesin and Radixin in the LGR5⁻ cells in a subset of the patients (Figure 35), suggesting that the negative correlation between these two proteins and cancer stemness is not as widespread as in the case of Ezrin. Similarly, not in all patients the LGR5⁻ cells displayed upregulation of *Krt20*, suggesting variability in the differentiation levels of CRC tumors (Figure 36C, D). Together, these observations support our conclusion that loss of cancer stemness in colorectal cancer is coupled with an upregulation of the ERM proteins.

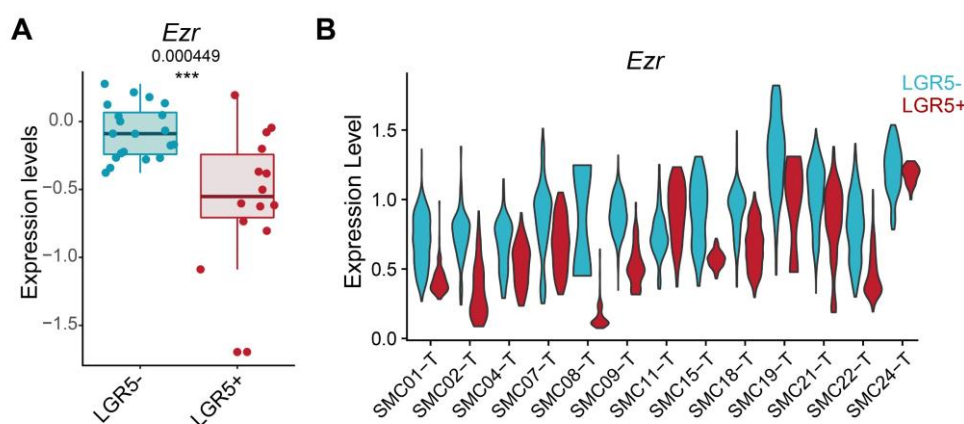


Figure 34: Expression of LGR5 and Ezrin are anticorrelated in transcriptomic data from CRC patients. (A) Gene expression of *Ezr* in epithelial tumor cells from CRC patients in the SMC cohort. Each dot corresponds to the average expression levels of one patient. The box center line represents the median, and the limits represent the first and third quartiles. Whiskers indicate maximum and minimum values. $n = 15$. (B) Violin plots

showing *Ezr* expression levels in single epithelial tumor cells from patients in the SMC cohort. Patient ID is detailed.

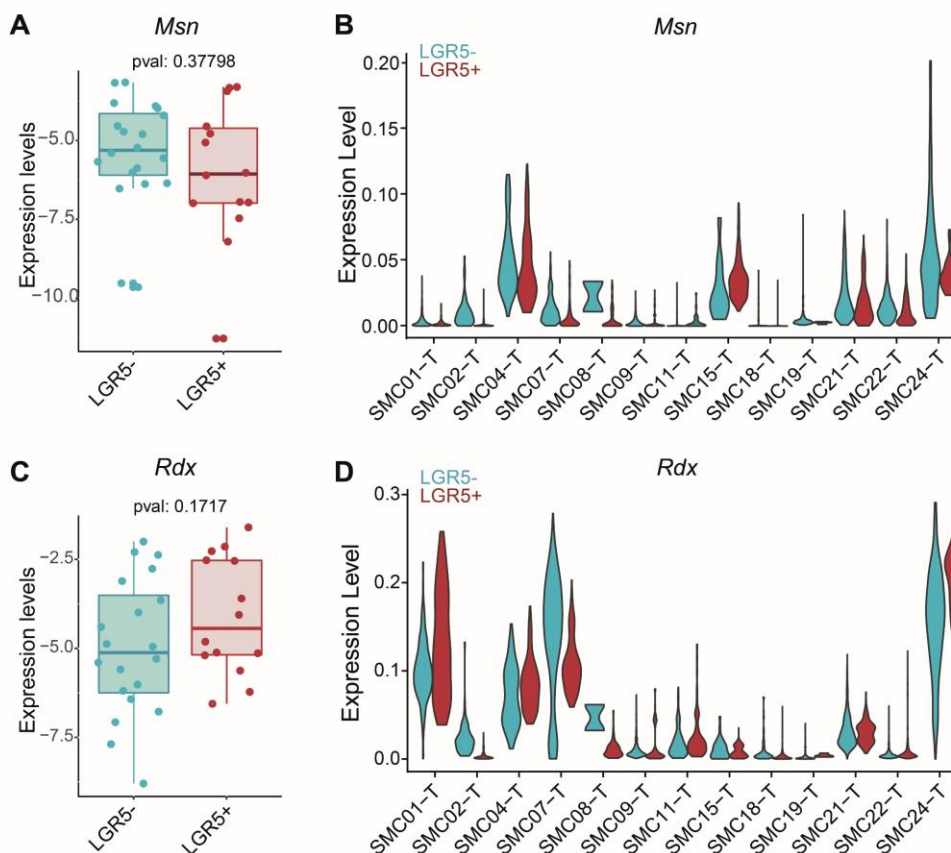


Figure 35. Expression of *Msn* and *Rdx* in CRC patients. (A, C,) Gene expression levels of *Rdx* and *Msn* in epithelial tumor cells from CRC patients in the SMC cohort summarized by patient through the average. Each dot corresponds to the average expression levels of one patient. summarized by patient through the average. The boxes center line represents the median. The box limits represent the first and third quartiles. Whiskers indicate maximum and minimum values. $n = 15$. (B, D,) Violin plots showing expression levels of *Rdx* (B) and *Msn* (D) in epithelial tumor cells from patients in the SMC cohort. Patient ID is detailed.

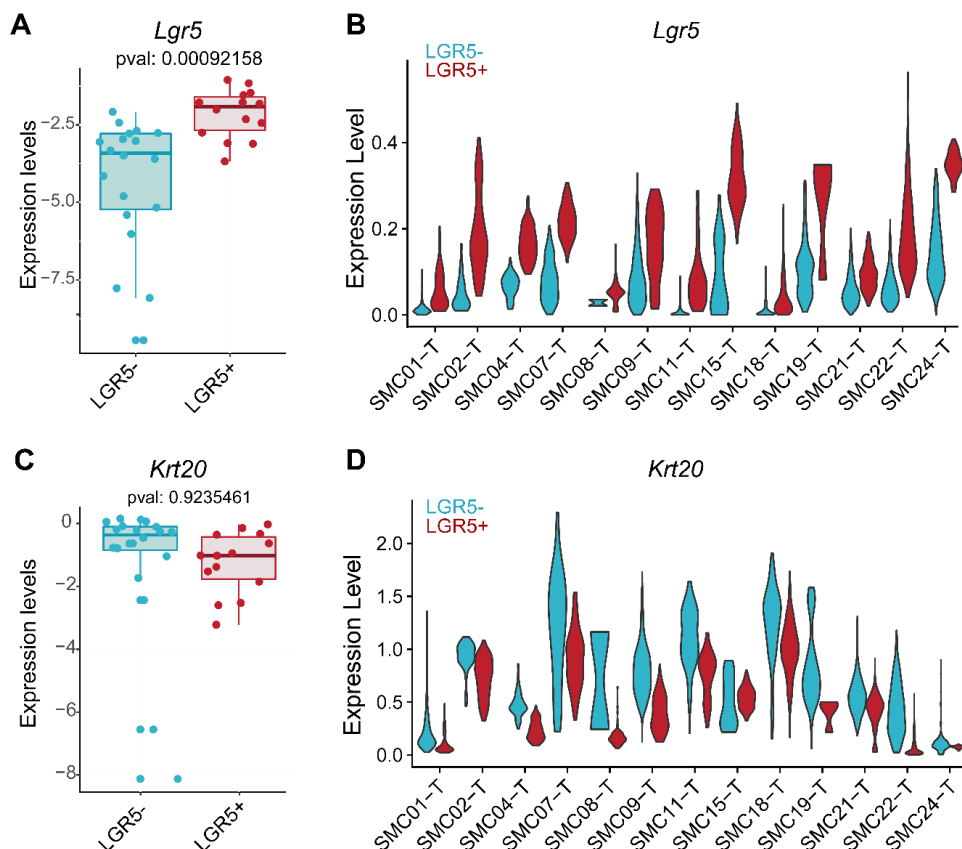


Figure 36. Expression of *Lgr5*, *Krt20* in CRC patients. (A, C) Gene expression levels of *Lgr5* and *Krt20*, in epithelial tumor cells from CRC patients in the SMC cohort summarized by patient through the average. Each dot corresponds to the average expression levels of one patient. summarized by patient through the average. The boxes center line represents the median. The box limits represent the first and third quartiles. Whiskers indicate maximum and minimum values. $n = 15$. (B, D) Violin plots showing expression levels of *Lgr5* (B) and *Krt20* (D) in epithelial tumor cells from patients in the SMC cohort. Patient ID is detailed.

5. DISCUSSION

5.1. DYNAMIC MECHANICAL STATE vs. RESILIENCE

In the present study we establish that expression levels of LGR5 mark distinct mechanical phenotypes in patient-derived colorectal cancer organoids (Figure 37). LGR5⁺ cells are stiffer, adhere better to the ECM, move slower both as single cells and clusters, display nuclear YAP, and show a high survival rate in response to mechanical confinement. These traits together define a phenotype of mechanical stability and resilience. Conversely, LGR5⁻ cells are softer, less adhesive, and faster, thus displaying a mechanical phenotype corresponding to a more dynamic state. These distinct mechanical features may favor different functions for LGR5⁺ and LGR5⁻ in the metastatic cascade. The faster, softer, and less adhesive LGR5⁻ cells likely have an advantage to escape the primary tumor and squeeze through the stroma to reach the vasculature. This can explain observations in mice showing that the majority of disseminating cells are LGR5⁻ and that genetic ablation of a subpopulation of LGR5⁻ cells prevents metastatic disease (Cañellas-Socias et al., 2022; Fumagalli et al., 2020). By contrast, the higher adhesion, stiffness, resilience, and nuclear YAP displayed by LGR5⁺ cells are all suitable mechanobiological features to potentially promote growth at a metastatic site, consistent with studies showing that long term metastatic growth is provided by LGR5⁺ cells (Batlle and Clevers, 2017; de Sousa e Melo et al., 2017; O'Brien et al., 2007; Ricci-Vitiani et al., 2007). We also observed that clusters of LGR5⁺ cells display higher adhesion to the endothelial surface and form transendothelial gaps with higher efficiency than LGR5⁻ cells, suggesting that LGR5⁺ cells have an increase ability to extravasate (Figure 27, 28). This feature of LGR5⁺ cells may explain that when LGR5⁺ and LGR5⁻ are injected in equal amounts into mice, LGR5⁺ cells are more efficient at seeding metastases (Fumagalli et al., 2020).

Cancer stem cells were conceived more than a decade ago as hard-wired, quiescent entities driving tumor growth and progression. More recent reports have shifted this definition to a more niche dependent, plastic phenotype, profoundly influenced by the microenvironment (Batlle and Clevers, 2017). In fact, maintenance of stem cells features requires physical anchorage to the stem

cell niche both in the healthy tissue and in cancer (Sneddon and Werb, 2007). Our study supports a LGR5⁺ mechanical phenotype characterized by lower MCA and higher ability to spread, a feature that might facilitate adhesion to the niche and thus retention of cancer stemness features.

Taken together, our results indicate that differences in mechanical phenotype may provide LGR5⁺ and LGR5⁻ with differential roles in metastasis; the mechanical features of LGR5⁻ cells are suitable for dissemination from the primary tumor, whereas those of LGR5⁺ are suitable for extravasation and growth at secondary sites.

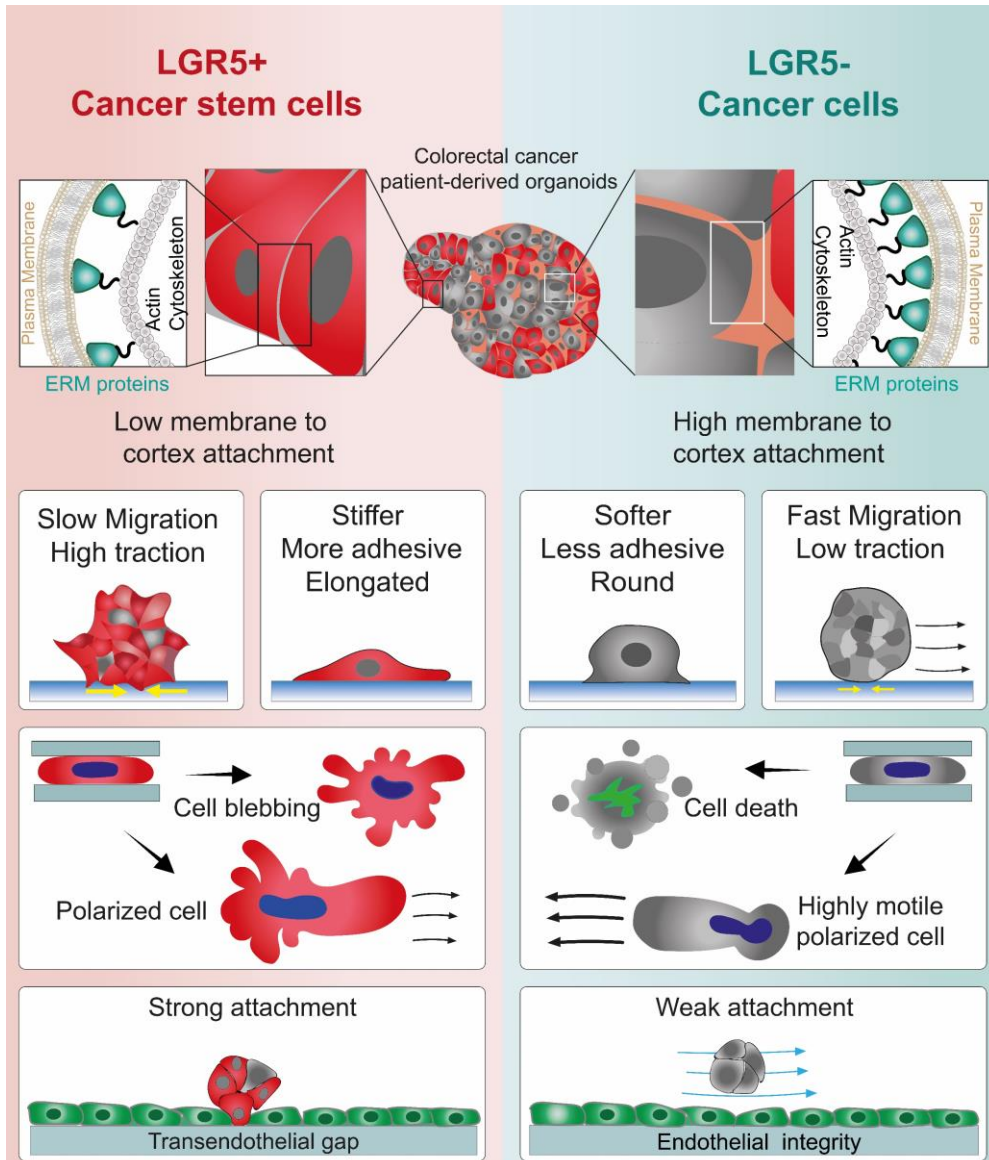


Figure 37: Membrane to cortex attachment determines different mechanical phenotypes in LGR5+ cancer stem cells and LGR5- cancer cells.

5.2. COLLECTIVE BEHAVIOUR AND ACTIVE WETTING

Cancer cell invasion has been attributed to the migration of both individual cells and cell groups (Fumagalli et al., 2020; Cañellas-Socias et al., 2022; Cheung and Ewald, 2016; Aceto et al., 2014; Cheung et al., 2016; Mizukoshi et al., 2020). Here we found that single cells and multicellular clusters share some common mechanical traits dependent on their expression of LGR5. Both single cells and clusters expressing low levels of LGR5 are less adherent to collagen-I substrates and adopt a rounder morphology (Figure 16, 24). However, clusters with different levels of LGR5 expression showed mechanical differences that were absent at the single cell level. Unlike single cells, clusters with lower LGR5 content exerted lower forces on the substrate and moved faster, two features that may provide them with an advantage in invasion.

From a physical perspective, the differences in mechanical phenotypes can be interpreted in terms of the theory of active wetting, proposing that epithelial spreading behaves as the wetting process of an active polar fluid. Based on this model, cellular spreading is due to a decrease in tension which allows the formation of cell-substrate adhesions (Pérez-González et al., 2019). Owing to their lower surface tension, which originates from lower MCA, LGR5+ cells and clusters are able to wet the surfaces such as collagen-I coated substrates or endothelial monolayers. By contrast, LGR5- cells and clusters are close to an intermediate wetting regime, which favors their migration and may render them more sensitive to microenvironmental gradients (Pallarès et al., 2022).

5.3. YAP AND CRC STEMNESS

We show that LGR5+ cells are characterized by higher nuclear YAP while in the medium and LGR5- cells YAP nuclear expression decreases (Figure 17). If we contemplate the idea that CRC tumors partially mirror the intestine hierarchy and physiology, this result is consistent with reports relating YAP expression to a

stem-like signature (Ramalho-Santos et al., 2002) and indicating attenuation of YAP activity as essential for intestinal differentiation and thus heterogeneity (Camargo et al., 2007; Serra et al., 2019). Indeed, overexpression of YAP in mice models was shown to induce expansion of the undifferentiated progenitor compartment and loss of the differentiated cells in the small intestine, thus linking increased expression of YAP to a stem-cell like state in the intestine. (Camargo et al., 2007).

Moreover, YAP activity was associated to a regeneration program in normal intestinal organoids. It has been shown that dissociation of intestinal organoids induces a transient YAP activation, followed by heterogeneous YAP expression among the organoid cells and recreation of a stem cell niche, thus enabling the tissue to repair and return to homeostasis (Serra et al., 2019). We speculate that dissociation of the PDOs to single cells might activate a similar response in the LGR5+ cells, thus enhancing YAP activation in these cells to drive some sort of tissue repair.

Despite being considered oncogenic in several tissues (Yu et al., 2015), YAP role in colorectal cancer remains controversial. A recent study using *in vivo* models, showed that overexpression of YAP reprograms normal intestinal stem cells and colorectal cancer LGR5+ cells to a wound-healing state and hampers the growth of intestinal organoids *in vitro* and CRC tumors *in vivo* (Cheung et al., 2020). These and the previously cited results (Camargo et al., 2007) are confusing as on the one hand they relate YAP overexpression to a progenitor-like state and hyperplasia and on the other they link it to a reduction of CRC tumor growth. We hypothesize that transient YAP activation, followed by attenuation in its activity is necessary for regeneration and tissue repair while constant activation prevents this process and eventually leads to intestinal and CRC growth suppression. In relation to our findings, it would be interesting to explore the dynamics of YAP expression and localization in the LGR5+ cells from the time of PDO dissociation to the formation of new tumor organoids. If this hypothesis is accurate, we would expect a decrease in YAP nuclear expression in the PDO cells that undergo differentiation.

5.4. ERM PROTEINS DETERMINE THE IDENTIFIED MECHANICAL PHENOTYPES

We show that the differences in the mechanical phenotype of LGR5+ and LGR5- cells can be explained by the upregulation of ERM proteins in LGR5- cells. ERMs are highly conserved, homologous proteins that function as linkers between the plasma membrane and the actin cortex. During homeostasis of the healthy intestinal epithelium, Ezrin expression increases as intestinal stem cells differentiate into enterocytes, promoting epithelial polarity and the formation of microvilli (Berryman et al., n.d.; Casaletto et al., 2011; Crawley et al., 2014; Saotome et al., 2004). Our analysis of transcriptomic data from a patient cohort and PDOs showed that the inverse correlation between LGR5 and ERMs expression characteristic of development and homeostasis is retained in tumors, despite the fact that epithelial polarity is generally lost.

The molecular structure of ERMs is composed by four main domains. In the amino terminus they contain the FERM (Four point one, ERM) domain which interacts with cell-surface transmembrane proteins (Chishti et al., 1998). It is followed by a central α -helical domain and a carboxy-terminal domain that binds F-actin and is known as C-ERM association domain (C-ERMAD). In their dormant form, ERM proteins are characterized by an intramolecular masking between the FERM and the C-ERMAD domains (Pearson et al., 2000). To be activated, ERMs are recruited to membrane regions rich in phosphoinositides which render conserved Threonine residues more accessible to phosphorylation and thus weaken the binding between the N and C-tails (Fehon et al., 2010; Pearson et al., 2000). Given this complex activation mechanism, it was crucial to confirm the upregulation of the activated form of ERM proteins in the LGR5- cells (Figure 30 and 31).

To study whether ERMs expression could explain the observed differences in mechanical phenotypes, we expressed a synthetic linker in LGR5+ cells that mimics the ERM tethering activity in LGR5- cells. Upon doing so, LGR5+ and LGR5- became mechanically indistinguishable (Figure 21), indicating that the ERMs are the main responsible for mechanical differences between LGR5+ and LGR5- cells. From a mechanistic perspective, ERMs have been shown to impair protrusion-based spreading by preventing membrane to cortex separation (Chishti et al., 1998; Bergert et al., 2021; Diz-Muñoz et al., 2010; Welf et al.,

2020). Indeed, a local decrease in membrane linkers and subsequent actin-membrane release are a necessary condition for protrusion initiation and thus cell spreading (Welf et al., 2020). Thus, the spread and adhesive phenotype of LGR5+ cells and clusters is explained by higher membrane availability due to decreased membrane to cortex tethering by ERMs.

The prevailing model for bleb-based amoeboid migration divides the process of bleb formation into 3 parts. Bleb initiation is due to actomyosin contractility, which causes an increase in the cytoplasmic hydrostatic pressure and a subsequent breach in the cortex where protrusion of a bleb is initiated. This is followed by bleb expansion, fueled by cytoplasmic flow and influx of calcium ions into the protruding bleb. Finally, a new actin cortex is formed under the bleb membrane, myosin is recruited and the bleb is retracted (Charras and Paluch, 2008). ERM proteins inhibit blebs formation not only by mechanically linking the plasma membrane to the actin cortex and thus preventing membrane detachment and bleb initiation (Charras et al., 2006), but also by preventing calcium entry and thus hindering bleb expansion (Aoki et al., 2021). Hence, a decrease in ERM activated form in the LGR5- cells is responsible for the lower tendency of LGR5- cells to bleb under confinement (Figure 21).

Membrane-cortex tethering has recently been shown to reduce formin activity at the interface of the membrane and the cortex leading to a diminished amount and bundling of actin filaments and decreased cortical thickness. This results in softening of the cortex (Lembo et al., 2023) and therefore can explain the lower cellular stiffness in the LGR5- cells as measured by RT-DC (Figure 20). How ERMs may promote cell death in response to mechanical confinement (Figure 21) is less explored, but we speculate that higher tethering increases membrane tension and favors its fracture in response to large deformations. Our study uncovers a previously unexplored link between colorectal cancer stemness and cell surface mechanics.

ERM protein expression and deregulation have been associated to cancer progression and poor prognosis in various epithelial cancer types including colorectal cancer (Wang et al., 2009; Patara et al., 2011; Jörgren et al., 2012; Leiphakpam et al., 2014; Li et al., 2017; Fathi et al., 2017; Rainey et al., 2020), gastric cancer (Arumugam et al., 2013; Li et al., 2011; Liang et al., 2017), prostate cancer (Valdman et al., 2005; Chuan et al., 2010; Z. Chen et al., 2022) and breast cancer (Elliott et al., 2005; Yu et al., 2019; Hu et al., 2021). In the

breast epithelium Ezrin localization was shown to change with malignant transformation switching from an apical membrane localization in normal epithelial cells to cytoplasmic or the total membrane in breast tumor cells (Sarrió et al., 2006). Ezrin expression was also increased in lymph nodes compared to the breast primary tumor (Ghaffari et al., 2019). Similarly, in CRC, increased expression of phosphorylated ezrin was found in mice and patient metastasis compared to the primary tumor (Leiphrahpam et al., 2014; Li et al., 2017). Although these studies link ERM aberrant signaling with cancer and metastasis, an understanding of the underlying mechanism is still lacking. With this work we disclosed a possible ERM-mediated mechanism that enhances the LGR5⁺ cells migration and decreases their adhesion, thereby supporting a dynamic phenotype suitable for metastasis.

5.5. MECHANICAL ADAPTABILITY

Along the metastatic cascade, cancer cells encounter mechanically heterogeneous microenvironments (Lopez et al., 2011; Laklai et al., 2016; Nia et al., 2020; Sun et al., 2021; Zuela-Sopilniak and Lammerding, 2022). To survive and successfully metastasize, they need to fine-tune their mechanical properties, adapting to the dynamic physical forces they are subjected to. Each one of the mechanical states uncovered by our data, the stable and resilient LGR5⁺ state in contrast to the dynamic and fragile LGR5⁻ state, may offer an advantage in certain steps of the metastatic cascade but may be detrimental in others. As cancer differentiation is plastic and dependent on microenvironmental stimuli, transition between mechanical states may provide an adaptive mechanism to cope with changing microenvironments throughout the metastatic journey. Hence, we propose that mechanical adaptability coupled with cancer cell plasticity may be a crucial mechanism for metastatic progression.

6. CONCLUSIONS

The main conclusions of this thesis are as follow:

1. Cancer stemness is linked to distinct mechanical phenotypes in CRC PDO single cells. Compared to LGR5⁻ cells, LGR5⁺ cancer stem cells tend to display a more adhesive, spread phenotype, higher expression of nuclear YAP and higher stiffness.
2. Cancer stem cells are more resistant to confinement-induced cell death compared to LGR5⁻ cells. They also have a higher tendency to bleb and adopt an amoeboid-like phenotype. Nonetheless, among the cells adopting an amoeboid-like migration, LGR5⁻ cells are faster.
3. Multicellular clusters retain features of single cell behavior but also display emergent mechanical properties which are absent at the single cell level. Clusters expressing high levels of LGR5 are more spread and adhesive, exert more tractions and migrate less.
4. LGR5⁺ clusters are more efficient in adhering to an endothelial monolayer and forming transendothelial gaps. This indicates a higher potential to extravasate.
5. Ezrin/ Radixin/ Moesin are upregulated in the LGR5⁻ cells. This results in higher membrane to cortex tethering and thus lower adhesion, lower protrusive ability and lower tendency to bleb of the LGR5⁻ cells.
6. Loss of cancer stemness is coupled with an upregulation of the ERM proteins in a colorectal cancer patient cohort, suggesting that the uncovered molecular mechanism is a general CRC trait.

7. REFERENCES

- Aceto, N., Bardia, A., Miyamoto, D.T., Donaldson, M.C., Wittner, B.S., Spencer, J.A., Yu, M., Pely, A., Engstrom, A., Zhu, H., Brannigan, B.W., Kapur, R., Stott, S.L., Shioda, T., Ramaswamy, S., Ting, D.T., Lin, C.P., Toner, M., Haber, D.A., Maheswaran, S., 2014. Circulating Tumor Cell Clusters Are Oligoclonal Precursors of Breast Cancer Metastasis. *Cell* 158, 1110–1122. <https://doi.org/10.1016/j.cell.2014.07.013>
- Aceto, N., Toner, M., Maheswaran, S., Haber, D.A., 2015. En Route to Metastasis: Circulating Tumor Cell Clusters and Epithelial-to-Mesenchymal Transition. *Trends Cancer* 1, 44–52. <https://doi.org/10.1016/j.trecan.2015.07.006>
- Adams, S.D., Csere, J., D'angelo, G., Carter, E.P., Romao, M., Arnandis, T., Dodel, M., Kocher, H.M., Grose, R., Raposo, G., Mardakheh, F., Godinho, S.A., 2021. Centrosome amplification mediates small extracellular vesicle secretion via lysosome disruption. *Curr. Biol.* 31, 1403–1416.e7. <https://doi.org/10.1016/j.cub.2021.01.028>
- Alguacil-Núñez, C., Ferrer-Ortiz, I., García-Verdú, E., López- Pirez, P., Llorente-Cortijo, I.M., Sainz, B., 2018. Current perspectives on the crosstalk between lung cancer stem cells and cancer-associated fibroblasts. *Crit. Rev. Oncol. Hematol.* 125, 102–110. <https://doi.org/10.1016/j.critrevonc.2018.02.015>
- Al-Hajj, M., Wicha, M.S., Benito-Hernandez, A., Morrison, S.J., Clarke, M.F., 2003. Prospective identification of tumorigenic breast cancer cells. *Proc. Natl. Acad. Sci.* 100, 3983–3988. <https://doi.org/10.1073/pnas.0530291100>
- Álvarez-Teijeiro, S., García-Inclán, C., Villaronga, M.Á., Casado, P., Hermida-Prado, F., Granda-Díaz, R., Rodrigo, J.P., Calvo, F., Del-Río-Ibáñez, N., Gandarillas, A., Morís, F., Hermesen, M., Cutillas, P., García-Pedrero, J.M., 2018. Factors Secreted by Cancer-Associated Fibroblasts that Sustain Cancer Stem Properties in Head and Neck Squamous Carcinoma Cells as Potential Therapeutic Targets. *Cancers* 10, 334. <https://doi.org/10.3390/cancers10090334>
- Aoki, K., Harada, S., Kawaji, K., Matsuzawa, K., Uchida, S., Ikenouchi, J., 2021. STIM-Orai1 signaling regulates fluidity of cytoplasm during membrane blebbing. *Nat. Commun.* 12, 480. <https://doi.org/10.1038/s41467-020-20826-5>
- Arpin, M., Chirivino, D., Naba, A., Zwaenepoel, I., 2011. Emerging role for ERM proteins in cell adhesion and migration. *Cell Adhes. Migr.* 5, 199–206. <https://doi.org/10.4161/cam.5.2.15081>
- Artegiani, B., van Voorthuisen, L., Lindeboom, R.G.H., Seinstra, D., Heo, I., Tapia, P., López-Iglesias, C., Postrach, D., Dayton, T., Oka, R., Hu, H., van Boxtel, R., van Es, J.H., Offerhaus, J., Peters, P.J., van Rheeën, J., Vermeulen, M., Clevers, H., 2019. Probing the Tumor Suppressor Function of BAP1 in CRISPR-

- Engineered Human Liver Organoids. *Cell Stem Cell* 24, 927-943.e6. <https://doi.org/10.1016/j.stem.2019.04.017>
- Arumugam, P., Partelli, S., Coleman, S.J., Cataldo, I., Beghelli, S., Bassi, C., Wijesuriya, N., Aleong, J.-A.C., Froeling, F.E.M., Scarpa, A., Kocher, H.M., 2013. Ezrin Expression Is an Independent Prognostic Factor in Gastro-intestinal Cancers. *J. Gastrointest. Surg.* 17, 2082–2091. <https://doi.org/10.1007/s11605-013-2384-1>
- Babahosseini, H., Ketene, A.N., Schmelz, E.M., Roberts, P.C., Agah, M., 2014. Biomechanical profile of cancer stem-like/tumor-initiating cells derived from a progressive ovarian cancer model. *Nanomedicine Nanotechnol. Biol. Med.* 10, e1013–e1019. <https://doi.org/10.1016/j.nano.2013.12.009>
- Baccelli, I., Schneeweiss, A., Riethdorf, S., Stenzinger, A., Schillert, A., Vogel, V., Klein, C., Saini, M., Bäuerle, T., Wallwiener, M., Holland-Letz, T., Höfner, T., Sprick, M., Scharpf, M., Marmé, F., Sinn, H.P., Pantel, K., Weichert, W., Trumpp, A., 2013. Identification of a population of blood circulating tumor cells from breast cancer patients that initiates metastasis in a xenograft assay. *Nat. Biotechnol.* 31, 539–544. <https://doi.org/10.1038/nbt.2576>
- Baluk, P., Morikawa, S., Haskell, A., Mancuso, M., McDonald, D.M., 2003. Abnormalities of Basement Membrane on Blood Vessels and Endothelial Sprouts in Tumors. *Am. J. Pathol.* 163, 1801–1815. [https://doi.org/10.1016/S0002-9440\(10\)63540-7](https://doi.org/10.1016/S0002-9440(10)63540-7)
- Barcus, C.E., O’Leary, K.A., Brockman, J.L., Rugowski, D.E., Liu, Y., Garcia, N., Yu, M., Keely, P.J., Eliceiri, K.W., Schuler, L.A., 2017. Elevated collagen-I augments tumor progressive signals, intravasation and metastasis of prolactin-induced estrogen receptor alpha positive mammary tumor cells. *Breast Cancer Res.* 19, 9. <https://doi.org/10.1186/s13058-017-0801-1>
- Barker, N., 2014. Adult intestinal stem cells: critical drivers of epithelial homeostasis and regeneration. *Nat. Rev. Mol. Cell Biol.* 15, 19–33. <https://doi.org/10.1038/nrm3721>
- Barker, N., Ridgway, R.A., van Es, J.H., van de Wetering, M., Begthel, H., van den Born, M., Danenberg, E., Clarke, A.R., Sansom, O.J., Clevers, H., 2009a. Crypt stem cells as the cells-of-origin of intestinal cancer. *Nature* 457, 608–611. <https://doi.org/10.1038/nature07602>
- Barker, N., Ridgway, R.A., van Es, J.H., van de Wetering, M., Begthel, H., van den Born, M., Danenberg, E., Clarke, A.R., Sansom, O.J., Clevers, H., 2009b. Crypt stem cells as the cells-of-origin of intestinal cancer. *Nature* 457, 608–611. <https://doi.org/10.1038/nature07602>
- Bartfeld, S., Bayram, T., van de Wetering, M., Huch, M., Begthel, H., Kujala, P., Vries, R., Peters, P.J., Clevers, H., 2015. In Vitro Expansion of Human Gastric Epithelial Stem Cells and Their Responses to Bacterial Infection. *Gastroenterology* 148, 126-136.e6. <https://doi.org/10.1053/j.gastro.2014.09.042>

- Battle, E., Clevers, H., 2017. Cancer stem cells revisited. *Nat. Med.* 23, 1124–1134. <https://doi.org/10.1038/nm.4409>
- Bauer, J., Emon, M.A.B., Staudacher, J.J., Thomas, A.L., Zessner-Spitzenberg, J., Mancinelli, G., Krett, N., Saif, M.T., Jung, B., 2020. Increased stiffness of the tumor microenvironment in colon cancer stimulates cancer associated fibroblast-mediated prometastatic activin A signaling. *Sci. Rep.* 10, 50. <https://doi.org/10.1038/s41598-019-55687-6>
- Beck, B., Driessens, G., Goossens, S., Youssef, K.K., Kuchnio, A., Caauwe, A., Sotiropoulou, P.A., Loges, S., Lapouge, G., Candi, A., Mascré, G., Drogat, B., Dekoninck, S., Haigh, J.J., Carmeliet, P., Blanpain, C., 2011. A vascular niche and a VEGF–Nrp1 loop regulate the initiation and stemness of skin tumours. *Nature* 478, 399–403. <https://doi.org/10.1038/nature10525>
- Beerling, E., Seinstra, D., de Wit, E., Kester, L., van der Velden, D., Maynard, C., Schäfer, R., van Diest, P., Voest, E., van Oudenaarden, A., Vrisekoop, N., van Rheenen, J., 2016. Plasticity between Epithelial and Mesenchymal States Unlinks EMT from Metastasis-Enhancing Stem Cell Capacity. *Cell Rep.* 14, 2281–2288. <https://doi.org/10.1016/j.celrep.2016.02.034>
- Bergert, M., Lembo, S., Sharma, S., Russo, L., Milovanović, D., Gretarsson, K.H., Börmel, M., Neveu, P.A., Hackett, J.A., Petsalaki, E., Diz-Muñoz, A., 2021. Cell Surface Mechanics Gate Embryonic Stem Cell Differentiation. *Cell Stem Cell* 28, 209–216.e4. <https://doi.org/10.1016/j.stem.2020.10.017>
- Berryman, M., Franck, Z., Bretscher, A., n.d. Ezrin is concentrated in the apical microvilli of a wide variety of epithelial cells whereas moesin is found primarily in endothelial cells.
- Bhagat, M., Palanichamy, J.K., Ramalingam, P., Mudassir, M., Irshad, K., Chosdol, K., Sarkar, C., Seth, P., Goswami, S., Sinha, S., Chattopadhyay, P., 2016. HIF-2 α mediates a marked increase in migration and stemness characteristics in a subset of glioma cells under hypoxia by activating an Oct-4/Sox-2-Mena (INV) axis. *Int. J. Biochem. Cell Biol.* 74, 60–71. <https://doi.org/10.1016/j.biocel.2016.02.017>
- Boj, S.F., Hwang, C.-I., Baker, L.A., Chio, I.I.C., Engle, D.D., Corbo, V., Jager, M., Ponz-Sarvise, M., Tiriach, H., Spector, M.S., Gracanin, A., Oni, T., Yu, K.H., van Boxtel, R., Huch, M., Rivera, K.D., Wilson, J.P., Feigin, M.E., Öhlund, D., Handly-Santana, A., Ardito-Abraham, C.M., Ludwig, M., Elyada, E., Alagesan, B., Biffi, G., Yordanov, G.N., Delcuze, B., Creighton, B., Wright, K., Park, Y., Morsink, F.H.M., Molenaar, I.Q., Borel Rinkes, I.H., Cuppen, E., Hao, Y., Jin, Y., Nijman, I.J., Iacobuzio-Donahue, C., Leach, S.D., Pappin, D.J., Hammell, M., Klimstra, D.S., Basturk, O., Hruban, R.H., Offerhaus, G.J., Vries, R.G.J., Clevers, H., Tuveson, D.A., 2015. Organoid Models of Human and Mouse Ductal Pancreatic Cancer. *Cell* 160, 324–338. <https://doi.org/10.1016/j.cell.2014.12.021>

- Bonnet, D., Dick, J.E., 1997. Human acute myeloid leukemia is organized as a hierarchy that originates from a primitive hematopoietic cell. *Nat. Med.* 3, 730–737. <https://doi.org/10.1038/nm0797-730>
- Brabletz, T., Jung, A., Reu, S., Porzner, M., Hlubek, F., Kunz-Schughart, L.A., Knuechel, R., Kirchner, T., 2001. Variable β -catenin expression in colorectal cancers indicates tumor progression driven by the tumor environment. *Proc. Natl. Acad. Sci.* 98, 10356–10361. <https://doi.org/10.1073/pnas.171610498>
- Buckley, C.E., St Johnston, D., 2022. Apical–basal polarity and the control of epithelial form and function. *Nat. Rev. Mol. Cell Biol.* 23, 559–577. <https://doi.org/10.1038/s41580-022-00465-y>
- Budhwani, K.I., Patel, Z.H., Guenter, R.E., Charania, A.A., 2022. A hitchhiker’s guide to cancer models. *Trends Biotechnol.* 40, 1361–1373. <https://doi.org/10.1016/j.tibtech.2022.04.003>
- Butler, J.P., Tolić-Nørrelykke, I.M., Fabry, B., Fredberg, J.J., 2002. Traction fields, moments, and strain energy that cells exert on their surroundings. *Am. J. Physiol.-Cell Physiol.* 282, C595–C605. <https://doi.org/10.1152/ajpcell.00270.2001>
- Butler, P., Gullino, M., 1975. Quantitation of Cell Shedding into Efferent Blood of Mammary 35.
- Cagnet, S., Faraldo, M.M., Kreft, M., Sonnenberg, A., Raymond, K., Glukhova, M.A., 2014. Signaling events mediated by $\alpha 3 \beta 1$ integrin are essential for mammary tumorigenesis. *Oncogene* 33, 4286–4295. <https://doi.org/10.1038/onc.2013.391>
- Calabrese, C., Poppleton, H., Kocak, M., Hogg, T.L., Fuller, C., Hamner, B., Oh, E.Y., Gaber, M.W., Finklestein, D., Allen, M., Frank, A., Bayazitov, I.T., Zakharenko, S.S., Gajjar, A., Davidoff, A., Gilbertson, R.J., 2007. A Perivascular Niche for Brain Tumor Stem Cells. *Cancer Cell* 11, 69–82. <https://doi.org/10.1016/j.ccr.2006.11.020>
- Callaway, E., 2013. Deal done over HeLa cell line. *Nature* 500, 132–133. <https://doi.org/10.1038/500132a>
- Calon, A., Lonardo, E., Berenguer-Llargo, A., Espinet, E., Hernando-Momblona, X., Iglesias, M., Sevillano, M., Palomo-Ponce, S., Tauriello, D.V.F., Byrom, D., Cortina, C., Morral, C., Barceló, C., Tosi, S., Riera, A., Attolini, C.S.-O., Rossell, D., Sancho, E., Batlle, E., 2015a. Stromal gene expression defines poor-prognosis subtypes in colorectal cancer. *Nat. Genet.* 47, 320–329. <https://doi.org/10.1038/ng.3225>
- Calon, A., Lonardo, E., Berenguer-Llargo, A., Espinet, E., Hernando-Momblona, X., Iglesias, M., Sevillano, M., Palomo-Ponce, S., Tauriello, D.V.F., Byrom, D., Cortina, C., Morral, C., Barceló, C., Tosi, S., Riera, A., Attolini, C.S.-O., Rossell, D., Sancho, E., Batlle, E., 2015b. Stromal gene expression defines poor-prognosis subtypes in colorectal cancer. *Nat. Genet.* 47, 320–329. <https://doi.org/10.1038/ng.3225>

- Camargo, F.D., Gokhale, S., Johnnidis, J.B., Fu, D., Bell, G.W., Jaenisch, R., Brummelkamp, T.R., 2007. YAP1 Increases Organ Size and Expands Undifferentiated Progenitor Cells. *Curr. Biol.* 17, 2054–2060. <https://doi.org/10.1016/j.cub.2007.10.039>
- Cañellas-Socias, A., Cortina, C., Hernando-Momblona, X., Palomo-Ponce, S., Mulholland, E.J., Turon, G., Mateo, L., Conti, S., Roman, O., Sevillano, M., Slebe, F., Stork, D., Caballé-Mestres, A., Berenguer-Llargo, A., Álvarez-Varela, A., Fenderico, N., Novellasdemunt, L., Jiménez-Gracia, L., Sipka, T., Bardia, L., Lorden, P., Colombelli, J., Heyn, H., Trepát, X., Tejpar, S., Sancho, E., Tauriello, D.V.F., Leedham, S., Attolini, C.S.-O., Batlle, E., 2022. Metastatic recurrence in colorectal cancer arises from residual EMP1+ cells. *Nature* 611, 603–613. <https://doi.org/10.1038/s41586-022-05402-9>
- Carcneri de Prati, A., Butturini, E., Rigo, A., Oppici, E., Rossin, M., Boriero, D., Mariotto, S., 2017. Metastatic Breast Cancer Cells Enter Into Dormant State and Express Cancer Stem Cells Phenotype Under Chronic Hypoxia. *J. Cell. Biochem.* 118, 3237–3248. <https://doi.org/10.1002/jcb.25972>
- Casaleto, J.B., Saotome, I., Curto, M., McClatchey, A.I., 2011. Ezrin-mediated apical integrity is required for intestinal homeostasis. *Proc. Natl. Acad. Sci.* 108, 11924–11929. <https://doi.org/10.1073/pnas.1103418108>
- Cerchiari, A.E., Garbe, J.C., Jee, N.Y., Todhunter, M.E., Broaders, K.E., Peehl, D.M., Desai, T.A., LaBarge, M.A., Thomson, M., Gartner, Z.J., 2015. A strategy for tissue self-organization that is robust to cellular heterogeneity and plasticity. *Proc. Natl. Acad. Sci.* 112, 2287–2292. <https://doi.org/10.1073/pnas.1410776112>
- Chaffer, C.L., Brennan, J.P., Slavin, J.L., Blick, T., Thompson, E.W., Williams, E.D., 2006. Mesenchymal-to-Epithelial Transition Facilitates Bladder Cancer Metastasis: Role of Fibroblast Growth Factor Receptor-2. *Cancer Res.* 66, 11271–11278. <https://doi.org/10.1158/0008-5472.CAN-06-2044>
- Chakrabarti, J., Holokai, L., Syu, L., Steele, N., Chang, J., Dlugosz, A., Zavros, Y., 2018. Mouse-Derived Gastric Organoid and Immune Cell Co-culture for the Study of the Tumor Microenvironment. *Methods Mol. Biol. Clifton NJ* 1817, 157–168. https://doi.org/10.1007/978-1-4939-8600-2_16
- Chang, Y., Zhang, J., Huo, X., Qu, X., Xia, C., Huang, K., Xie, F., Wang, N., Wei, X., Jia, Q., 2022. Substrate rigidity dictates colorectal tumorigenic cell stemness and metastasis via CRAD-dependent mechanotransduction. *Cell Rep.* 38. <https://doi.org/10.1016/j.celrep.2022.110390>
- Chao, Y., Wu, Q., Acquafondata, M., Dhir, R., Wells, A., 2012. Partial Mesenchymal to Epithelial Reverting Transition in Breast and Prostate Cancer Metastases. *Cancer Microenviron.* 5, 19–28. <https://doi.org/10.1007/s12307-011-0085-4>
- Chao, Y.L., Shepard, C.R., Wells, A., 2010. Breast carcinoma cells re-express E-cadherin during mesenchymal to epithelial reverting transition. *Mol. Cancer* 9, 179. <https://doi.org/10.1186/1476-4598-9-179>

- Chapman, A., Fernandez del Ama, L., Ferguson, J., Kamarashev, J., Wellbrock, C., Hurlstone, A., 2014. Heterogeneous Tumor Subpopulations Cooperate to Drive Invasion. *Cell Rep.* 8, 688–695. <https://doi.org/10.1016/j.celrep.2014.06.045>
- Charelli, L.E., Ferreira, J.P.D., Naveira-Cotta, C.P., Balbino, T.A., 2021. Engineering mechanobiology through organoids-on-chip: A strategy to boost therapeutics. *J. Tissue Eng. Regen. Med.* 15, 883–899. <https://doi.org/10.1002/term.3234>
- Charras, G., Paluch, E., 2008. Blebs lead the way: how to migrate without lamellipodia. *Nat. Rev. Mol. Cell Biol.* 9, 730–736. <https://doi.org/10.1038/nrm2453>
- Charras, G.T., Hu, C.-K., Coughlin, M., Mitchison, T.J., 2006. Reassembly of contractile actin cortex in cell blebs. *J. Cell Biol.* 175, 477–490. <https://doi.org/10.1083/jcb.200602085>
- Chen, M.B., Lamar, J.M., Li, R., Hynes, R.O., Kamm, R.D., 2016. Elucidation of the Roles of Tumor Integrin $\beta 1$ in the Extravasation Stage of the Metastasis Cascade. *Cancer Res.* 76, 2513–2524. <https://doi.org/10.1158/0008-5472.CAN-15-1325>
- Chen, M.B., Whisler, J.A., Fröse, J., Yu, C., Shin, Y., Kamm, R.D., 2017. On-chip human microvasculature assay for visualization and quantification of tumor cell extravasation dynamics. *Nat. Protoc.* 12, 865–880. <https://doi.org/10.1038/nprot.2017.018>
- Chen, W.-J., Ho, C.-C., Chang, Y.-L., Chen, H.-Y., Lin, C.-A., Ling, T.-Y., Yu, S.-L., Yuan, S.-S., Louisa Chen, Y.-J., Lin, C.-Y., Pan, S.-H., Elizabeth Chou, H.-Y., Chen, Y.-J., Chang, G.-C., Chu, W.-C., Lee, Y.-M., Lee, J.-Y., Lee, P.-J., Li, K.-C., Chen, H.-W., Yang, P.-C., 2014. Cancer-associated fibroblasts regulate the plasticity of lung cancer stemness via paracrine signalling. *Nat. Commun.* 5, 3472. <https://doi.org/10.1038/ncomms4472>
- Chen, X., Tang, K., Li, X., Zhang, C., Xin, Y., Li, K., Tan, Y., 2022. Biomechanics of cancer stem cells. *Essays Biochem.* 66, 359–369. <https://doi.org/10.1042/EBC20220014>
- Chen, Z., Wang, J., Lu, Y., Lai, C., Qu, L., Zhuo, Y., 2022. Ezrin expression in circulating tumor cells is a predictor of prostate cancer metastasis. *Bioengineered* 13, 4076–4084. <https://doi.org/10.1080/21655979.2021.2014710>
- Cheung, K.J., Ewald, A.J., 2016. A collective route to metastasis: Seeding by tumor cell clusters. *Science* 352, 167–169. <https://doi.org/10.1126/science.aaf6546>
- Cheung, K.J., Gabrielson, E., Werb, Z., Ewald, A.J., 2013. Collective Invasion in Breast Cancer Requires a Conserved Basal Epithelial Program. *Cell* 155, 1639–1651. <https://doi.org/10.1016/j.cell.2013.11.029>
- Cheung, K.J., Padmanaban, V., Silvestri, V., Schipper, K., Cohen, J.D., Fairchild, A.N., Gorin, M.A., Verdone, J.E., Pienta, K.J., Bader, J.S., Ewald, A.J., 2016. Polyclonal breast cancer metastases arise from collective dissemination of keratin 14-expressing tumor cell clusters. *Proc. Natl. Acad. Sci.* 113, E854–E863. <https://doi.org/10.1073/pnas.1508541113>

- Cheung, P., Xiol, J., Dill, M.T., Yuan, W.-C., Panero, R., Roper, J., Osorio, F.G., Maglic, D., Li, Q., Gurung, B., Calogero, R.A., Yilmaz, Ö.H., Mao, J., Camargo, F.D., 2020. Regenerative Reprogramming of the Intestinal Stem Cell State via Hippo Signaling Suppresses Metastatic Colorectal Cancer. *Cell Stem Cell* 27, 590–604.e9. <https://doi.org/10.1016/j.stem.2020.07.003>
- Chishti, A.H., Kim, A.C., Marfatia, S.M., Lutchan, M., Hanspal, M., Jindal, H., Liu, S.-C., Low, P.S., Rouleau, G.A., Mohandas, N., Chasis, J.A., Conboy, J.G., Gascard, P., Takakuwa, Y., Huang, S.-C., Jr, E.J.B., Bretscher, A., Fehon, R.G., Gusella, J.F., Ramesh, V., Solomon, F., Marchesi, V.T., Tsukita, Shoichiro, Tsukita, Sachiko, Arpin, M., Louvard, D., Tonks, N.K., Anderson, J.M., Fanning, A.S., Bryant, P.J., Woods, D.F., Hoover, K.B., 1998. The FERM domain: a unique module involved in the linkage of cytoplasmic proteins to the membrane. *Trends Biochem. Sci.* 23, 281–282. [https://doi.org/10.1016/S0968-0004\(98\)01237-7](https://doi.org/10.1016/S0968-0004(98)01237-7)
- Cho, S., Irianto, J., Discher, D.E., 2017. Mechanosensing by the nucleus: From pathways to scaling relationships. *J. Cell Biol.* 216, 305–315. <https://doi.org/10.1083/jcb.201610042>
- Chua, C.W., Shibata, M., Lei, M., Toivanen, R., Barlow, L.J., Bergren, S.K., Badani, K.K., McKiernan, J.M., Benson, M.C., Hibshoosh, H., Shen, M.M., 2014. Single luminal epithelial progenitors can generate prostate organoids in culture. *Nat. Cell Biol.* 16, 951–961. <https://doi.org/10.1038/ncb3047>
- Chuan, Y.-C., Iglesias-Gato, D., Fernandez-Perez, L., Cedazo-Minguez, A., Pang, S.-T., Norstedt, G., Pousette, Å., Flores-Morales, A., 2010. Ezrin mediates c-Myc actions in prostate cancer cell invasion. *Oncogene* 29, 1531–1542. <https://doi.org/10.1038/onc.2009.442>
- Cohnheim, J.F., 1880. *Vorlesungen über allgemeine Pathologie v. 2*, 1880. Hirschwald.
- Collins, A.T., Berry, P.A., Hyde, C., Stower, M.J., Maitland, N.J., 2005. Prospective Identification of Tumorigenic Prostate Cancer Stem Cells. *Cancer Res.* 65, 10946–10951. <https://doi.org/10.1158/0008-5472.CAN-05-2018>
- Compton, C.C., Greene, F.L., 2004. The Staging of Colorectal Cancer: 2004 and Beyond. *CA. Cancer J. Clin.* 54, 295–308. <https://doi.org/10.3322/canjclin.54.6.295>
- Conklin, M.W., Keely, P.J., 2012. Why the stroma matters in breast cancer. *Cell Adhes. Migr.* 6, 249–260. <https://doi.org/10.4161/cam.20567>
- Conti, S., Kato, T., Park, D., Sahai, E., Trepac, X., Labernadie, A., 2021. CAFs and Cancer Cells Co-Migration in 3D Spheroid Invasion Assay, in: Campbell, K., Theveneau, E. (Eds.), *The Epithelial-to Mesenchymal Transition: Methods and Protocols*, Methods in Molecular Biology. Springer US, New York, NY, pp. 243–256. https://doi.org/10.1007/978-1-0716-0779-4_19
- Cooper, M., 2009. Regenerative Pathologies: Stem Cells, Teratomas and Theories of Cancer. *Med. Stud.* 1, 55–66. <https://doi.org/10.1007/s12376-008-0002-4>

- Correa, D., Somoza, R.A., Lin, P., Schiemann, W.P., Caplan, A.I., 2016. Mesenchymal stem cells regulate melanoma cancer cells extravasation to bone and liver at their perivascular niche. *Int. J. Cancer* 138, 417–427. <https://doi.org/10.1002/ijc.29709>
- Cortina, C., Turon, G., Stork, D., Hernando-Momblona, X., Sevillano, M., Aguilera, M., Tosi, S., Merlos-Suárez, A., Stephan-Otto Attolini, C., Sancho, E., Batlle, E., 2017. A genome editing approach to study cancer stem cells in human tumors. *EMBO Mol. Med.* 9, 869–879. <https://doi.org/10.15252/emmm.201707550>
- Cr, B., F, O., Kr, E., Td, D., Sm, D., Cm, H., U, A., F, H., M, K., J, Werner, F, B., N, I., M, S., C, von K., C, S., S, F., B, B., W, W., J, Weitz, H, G., 2017. Succession of transiently active tumor-initiating cell clones in human pancreatic cancer xenografts. *EMBO Mol. Med.* 9. <https://doi.org/10.15252/emmm.201607354>
- Crawley, S.W., Mooseker, M.S., Tyska, M.J., 2014. Shaping the intestinal brush border. *J. Cell Biol.* 207, 441–451. <https://doi.org/10.1083/jcb.201407015>
- Cross, S.E., Jin, Y.-S., Rao, J., Gimzewski, J.K., 2007. Nanomechanical analysis of cells from cancer patients. *Nat. Nanotechnol.* 2, 780–783. <https://doi.org/10.1038/nnano.2007.388>
- Cross, S.E., Jin, Y.-S., Tondre, J., Wong, R., Rao, J., Gimzewski, J.K., 2008. AFM-based analysis of human metastatic cancer cells. *Nanotechnology* 19, 384003. <https://doi.org/10.1088/0957-4484/19/38/384003>
- Curti, B.D., Urba, W.J., Gregory Alvord, W., Janik, J.E., Smith, J.W., II, Madara, K., Longo, D.L., 1993. Interstitial Pressure of Subcutaneous Nodules in Melanoma and Lymphoma Patients: Changes during Treatment¹. *Cancer Res.* 53, 2204–2207.
- Dalerba, P., Dylla, S.J., Park, I.-K., Liu, R., Wang, X., Cho, R.W., Hoey, T., Gurney, A., Huang, E.H., Simeone, D.M., Shelton, A.A., Parmiani, G., Castelli, C., Clarke, M.F., 2007. Phenotypic characterization of human colorectal cancer stem cells. *Proc. Natl. Acad. Sci.* 104, 10158–10163. <https://doi.org/10.1073/pnas.0703478104>
- Dalerba, P., Kalisky, T., Sahoo, D., Rajendran, P.S., Rothenberg, M.E., Leyrat, A.A., Sim, S., Okamoto, J., Johnston, D.M., Qian, D., Zabala, M., Bueno, J., Neff, N.F., Wang, J., Shelton, A.A., Visser, B., Hisamori, S., Shimono, Y., van de Wetering, M., Clevers, H., Clarke, M.F., Quake, S.R., 2011. Single-cell dissection of transcriptional heterogeneity in human colon tumors. *Nat. Biotechnol.* 29, 1120–1127. <https://doi.org/10.1038/nbt.2038>
- Dang, H.X., Krasnick, B.A., White, B.S., Grossman, J.G., Strand, M.S., Zhang, J., Cabanski, C.R., Miller, C.A., Fulton, R.S., Goedegebuure, S.P., Fronick, C.C., Griffith, M., Larson, D.E., Goetz, B.D., Walker, J.R., Hawkins, W.G., Strasberg, S.M., Linehan, D.C., Lim, K.H., Lockhart, A.C., Mardis, E.R., Wilson, R.K., Ley, T.J., Maher, C.A., Fields, R.C., 2020. The clonal evolution of metastatic colorectal cancer. *Sci. Adv.* 6, eaay9691. <https://doi.org/10.1126/sciadv.aay9691>

- Dasgupta, I., McCollum, D., 2019. Control of cellular responses to mechanical cues through YAP/TAZ regulation. *J. Biol. Chem.* 294, 17693–17706. <https://doi.org/10.1074/jbc.REV119.007963>
- De Belly, H., Stubb, A., Yanagida, A., Labouesse, C., Jones, P.H., Paluch, E.K., Chalut, K.J., 2021. Membrane Tension Gates ERK-Mediated Regulation of Pluripotent Cell Fate. *Cell Stem Cell* 28, 273–284.e6. <https://doi.org/10.1016/j.stem.2020.10.018>
- de Sousa e Melo, F., Kurtova, A.V., Harnoss, J.M., Kljavin, N., Hoeck, J.D., Hung, J., Anderson, J.E., Storm, E.E., Modrusan, Z., Koeppen, H., Dijkgraaf, G.J.P., Piskol, R., de Sauvage, F.J., 2017. A distinct role for Lgr5+ stem cells in primary and metastatic colon cancer. *Nature* 543, 676–680. <https://doi.org/10.1038/nature21713>
- Dekkers, J.F., Whittle, J.R., Vaillant, F., Chen, H.-R., Dawson, C., Liu, K., Geurts, M.H., Herold, M.J., Clevers, H., Lindeman, G.J., Visvader, J.E., 2020. Modeling Breast Cancer Using CRISPR-Cas9–Mediated Engineering of Human Breast Organoids. *JNCI J. Natl. Cancer Inst.* 112, 540–544. <https://doi.org/10.1093/jnci/djz196>
- Del Pozo Martin, Y., Park, D., Ramachandran, A., Ombrato, L., Calvo, F., Chakravarty, P., Spencer-Dene, B., Derzsi, S., Hill, C.S., Sahai, E., Malanchi, I., 2015. Mesenchymal Cancer Cell-Stroma Crosstalk Promotes Niche Activation, Epithelial Reversion, and Metastatic Colonization. *Cell Rep.* 13, 2456–2469. <https://doi.org/10.1016/j.celrep.2015.11.025>
- Deng, B., Zhao, Z., Kong, W., Han, C., Shen, X., Zhou, C., 2022. Biological role of matrix stiffness in tumor growth and treatment. *J. Transl. Med.* 20, 540. <https://doi.org/10.1186/s12967-022-03768-y>
- Derksen, P.W.B., Liu, X., Saridin, F., Gulden, H. van der, Zevenhoven, J., Evers, B., Beijnum, J.R. van, Griffioen, A.W., Vink, J., Krimpenfort, P., Peterse, J.L., Cardiff, R.D., Berns, A., Jonkers, J., 2006. Somatic inactivation of E-cadherin and p53 in mice leads to metastatic lobular mammary carcinoma through induction of anoikis resistance and angiogenesis. *Cancer Cell* 10, 437–449. <https://doi.org/10.1016/j.ccr.2006.09.013>
- Desgrosellier, J.S., Barnes, L.A., Shields, D.J., Huang, M., Lau, S.K., Prévost, N., Tarin, D., Shattil, S.J., Cheresch, D.A., 2009. An integrin $\alpha\beta 3$ –c-Src oncogenic unit promotes anchorage-independence and tumor progression. *Nat. Med.* 15, 1163–1169. <https://doi.org/10.1038/nm.2009>
- Dieter, S.M., Ball, C.R., Hoffmann, C.M., Nowrouzi, A., Herbst, F., Zavidij, O., Abel, U., Arens, A., Weichert, W., Brand, K., Koch, M., Weitz, J., Schmidt, M., von Kalle, C., Glimm, H., 2011. Distinct Types of Tumor-Initiating Cells Form Human Colon Cancer Tumors and Metastases. *Cell Stem Cell* 9, 357–365. <https://doi.org/10.1016/j.stem.2011.08.010>
- Dijk, D. van, Sharma, R., Nainys, J., Yim, K., Kathail, P., Carr, A.J., Burdziak, C., Moon, K.R., Chaffer, C.L., Pattabiraman, D., Bierie, B., Mazutis, L., Wolf, G.,

- Krishnaswamy, S., Pe'er, D., 2018. Recovering Gene Interactions from Single-Cell Data Using Data Diffusion. *Cell* 174, 716–729.e27. <https://doi.org/10.1016/j.cell.2018.05.061>
- Diz-Muñoz, A., Krieg, M., Bergert, M., Ibarlucea-Benitez, I., Muller, D.J., Paluch, E., Heisenberg, C.-P., 2010. Control of Directed Cell Migration In Vivo by Membrane-to-Cortex Attachment. *PLOS Biol.* 8, e1000544. <https://doi.org/10.1371/journal.pbio.1000544>
- Donato, C., Kunz, L., Castro-Giner, F., Paasinen-Sohns, A., Strittmatter, K., Szczerba, B.M., Scherrer, R., Maggio, N.D., Heusermann, W., Biehlmaier, O., Beisel, C., Vetter, M., Rochlitz, C., Weber, W.P., Banfi, A., Schroeder, T., Aceto, N., 2020. Hypoxia Triggers the Intravasation of Clustered Circulating Tumor Cells. *Cell Rep.* 32. <https://doi.org/10.1016/j.celrep.2020.108105>
- Driehuis, E., Kretschmar, K., Clevers, H., 2020. Establishment of patient-derived cancer organoids for drug-screening applications. *Nat. Protoc.* 15, 3380–3409. <https://doi.org/10.1038/s41596-020-0379-4>
- Dupont, S., Morsut, L., Aragona, M., Enzo, E., Giulitti, S., Cordenonsi, M., Zanconato, F., Le Digabel, J., Forcato, M., Bicciato, S., Elvassore, N., Piccolo, S., 2011. Role of YAP/TAZ in mechanotransduction. *Nature* 474, 179–183. <https://doi.org/10.1038/nature10137>
- Edelstein, A.D., Tsuchida, M.A., Amodaj, N., Pinkard, H., Vale, R.D., Stuurman, N., 2014. Advanced methods of microscope control using µManager software. *J. Biol. Methods* 1, e10. <https://doi.org/10.14440/jbm.2014.36>
- Eger, A., Aigner, K., Sonderegger, S., Dampier, B., Oehler, S., Schreiber, M., Berx, G., Cano, A., Beug, H., Foisner, R., 2005. DeltaEF1 is a transcriptional repressor of E-cadherin and regulates epithelial plasticity in breast cancer cells. *Oncogene* 24, 2375–2385. <https://doi.org/10.1038/sj.onc.1208429>
- Ellegren, H., 2004. Microsatellites: simple sequences with complex evolution. *Nat. Rev. Genet.* 5, 435–445. <https://doi.org/10.1038/nrg1348>
- Elliott, B.E., Meens, J.A., SenGupta, S.K., Louvard, D., Arpin, M., 2005. The membrane cytoskeletal crosslinker ezrin is required for metastasis of breast carcinoma cells. *Breast Cancer Res.* 7, R365. <https://doi.org/10.1186/bcr1006>
- Eramo, A., Lotti, F., Sette, G., Piloizzi, E., Biffoni, M., Di Virgilio, A., Conticello, C., Ruco, L., Peschle, C., De Maria, R., 2008. Identification and expansion of the tumorigenic lung cancer stem cell population. *Cell Death Differ.* 15, 504–514. <https://doi.org/10.1038/sj.cdd.4402283>
- Erdogan, B., Ao, M., White, L.M., Means, A.L., Brewer, B.M., Yang, L., Washington, M.K., Shi, C., Franco, O.E., Weaver, A.M., Hayward, S.W., Li, D., Webb, D.J., 2017. Cancer-associated fibroblasts promote directional cancer cell migration by aligning fibronectin. *J. Cell Biol.* 216, 3799–3816. <https://doi.org/10.1083/jcb.201704053>
- Eslami-S, Z., Cortés-Hernández, L.E., Thomas, F., Pantel, K., Alix-Panabières, C., 2022. Functional analysis of circulating tumour cells: the KEY to understand the

- biology of the metastatic cascade. *Br. J. Cancer* 127, 800–810. <https://doi.org/10.1038/s41416-022-01819-1>
- Evans, A., Whelehan, P., Thomson, K., Brauer, K., Jordan, L., Purdie, C., McLean, D., Baker, L., Vinnicombe, S., Thompson, A., 2012. Differentiating benign from malignant solid breast masses: value of shear wave elastography according to lesion stiffness combined with greyscale ultrasound according to BI-RADS classification. *Br. J. Cancer* 107, 224–229. <https://doi.org/10.1038/bjc.2012.253>
- Fathi, A., Mosaad, H., Hussein, S., Roshdy, M., Ismail, E.I., 2017. Prognostic significance of CD133 and ezrin expression in colorectal carcinoma. *IUBMB Life* 69, 328–340. <https://doi.org/10.1002/iub.1609>
- Fazilaty, H., Behnam, B., 2014. The perivascular niche governs an autoregulatory network to support breast cancer metastasis. *Cell Biol. Int.* 38, 691–694. <https://doi.org/10.1002/cbin.10261>
- Fearon, E.R., 2011. Molecular Genetics of Colorectal Cancer. *Annu. Rev. Pathol. Mech. Dis.* 6, 479–507. <https://doi.org/10.1146/annurev-pathol-011110-130235>
- Fehon, R.G., McClatchey, A.I., Bretscher, A., 2010. Organizing the cell cortex: the role of ERM proteins. *Nat. Rev. Mol. Cell Biol.* 11, 276–287. <https://doi.org/10.1038/nrm2866>
- Fischer, K.R., Durrans, A., Lee, S., Sheng, J., Li, F., Wong, S.T.C., Choi, H., El Rayes, T., Ryu, S., Troeger, J., Schwabe, R.F., Vahdat, L.T., Altorki, N.K., Mittal, V., Gao, D., 2015. Epithelial-to-mesenchymal transition is not required for lung metastasis but contributes to chemoresistance. *Nature* 527, 472–476. <https://doi.org/10.1038/nature15748>
- Floerchinger, A., Murphy, K.J., Latham, S.L., Warren, S.C., McCulloch, A.T., Lee, Y.-K., Stoehr, J., Méléneć, P., Guaman, C.S., Metcalf, X.L., Lee, V., Zaratzian, A., Da Silva, A., Tayao, M., Rolo, S., Phimmachanh, M., Sultani, G., McDonald, L., Mason, S.M., Ferrari, N., Ooms, L.M., Johnsson, A.-K.E., Spence, H.J., Olson, M.F., Machesky, L.M., Sansom, O.J., Morton, J.P., Mitchell, C.A., Samuel, M.S., Croucher, D.R., Welch, H.C.E., Blyth, K., Caldon, C.E., Herrmann, D., Anderson, K.I., Timpson, P., Nobis, M., 2021. Optimizing metastatic-cascade-dependent Rac1 targeting in breast cancer: Guidance using optical window intravital FRET imaging. *Cell Rep.* 36, 109689. <https://doi.org/10.1016/j.celrep.2021.109689>
- Fujii, M., Shimokawa, M., Date, S., Takano, A., Matano, M., Nanki, K., Ohta, Y., Toshimitsu, K., Nakazato, Y., Kawasaki, K., Uraoka, T., Watanabe, T., Kanai, T., Sato, T., 2016. A Colorectal Tumor Organoid Library Demonstrates Progressive Loss of Niche Factor Requirements during Tumorigenesis. *Cell Stem Cell* 18, 827–838. <https://doi.org/10.1016/j.stem.2016.04.003>
- Fumagalli, A., Oost, K.C., Kester, L., Morgner, J., Bornes, L., Bruens, L., Spaargaren, L., Azkanaz, M., Schelfhorst, T., Beerling, E., Heinz, M.C., Postrach, D., Seinstra, D., Sieuwerts, A.M., Martens, J.W.M., van der Elst, S., van Baalen, M.,

- Bhowmick, D., Vriskoop, N., Ellenbroek, S.I.J., Suijkerbuijk, S.J.E., Snippert, H.J., van Rheenen, J., 2020. Plasticity of Lgr5-Negative Cancer Cells Drives Metastasis in Colorectal Cancer. *Cell Stem Cell* 26, 569-578.e7. <https://doi.org/10.1016/j.stem.2020.02.008>
- Furth, J., Kahn, M.C., Breedis, C., 1937. The Transmission of Leukemia of Mice with a Single Cell. *Am. J. Cancer*.
- Gabbireddy, S.R., Vosatka, K.W., Chung, A.J., Logue, J.S., 2021. Melanoma cells adopt features of both mesenchymal and amoeboid migration within confining channels. *Sci. Rep.* 11, 17804. <https://doi.org/10.1038/s41598-021-97348-7>
- Ganesh, K., Basnet, H., Kaygusuz, Y., Laughney, A.M., He, L., Sharma, R., O'Rourke, K.P., Reuter, V.P., Huang, Y.-H., Turkecul, M., Er, E.E., Masilionis, I., Manova-Todorova, K., Weiser, M.R., Saltz, L.B., Garcia-Aguilar, J., Koche, R., Lowe, S.W., Pe'er, D., Shia, J., Massagué, J., 2020. L1CAM defines the regenerative origin of metastasis-initiating cells in colorectal cancer. *Nat. Cancer* 1, 28–45. <https://doi.org/10.1038/s43018-019-0006-x>
- Gao, D., Vela, I., Sboner, A., Iaquina, P.J., Karthaus, W.R., Gopalan, A., Dowling, C., Wanjala, J.N., Undvall, E.A., Arora, V.K., Wongvipat, J., Kossai, M., Ramazanoglu, S., Barboza, L.P., Di, W., Cao, Z., Zhang, Q.F., Sirota, I., Ran, L., MacDonald, T.Y., Beltran, H., Mosquera, J.-M., Touijer, K.A., Scardino, P.T., Laudone, V.P., Curtis, K.R., Rathkopf, D.E., Morris, M.J., Danila, D.C., Slovin, S.F., Solomon, S.B., Eastham, J.A., Chi, P., Carver, B., Rubin, M.A., Scher, H.I., Clevers, H., Sawyers, C.L., Chen, Y., 2014. Organoid Cultures Derived from Patients with Advanced Prostate Cancer. *Cell* 159, 176–187. <https://doi.org/10.1016/j.cell.2014.08.016>
- Garcia, K.E., Wang, X., Kroenke, C.D., 2021. A model of tension-induced fiber growth predicts white matter organization during brain folding. *Nat. Commun.* 12, 6681. <https://doi.org/10.1038/s41467-021-26971-9>
- Gehart, H., Clevers, H., 2019. Tales from the crypt: new insights into intestinal stem cells. *Nat. Rev. Gastroenterol. Hepatol.* 16, 19–34. <https://doi.org/10.1038/s41575-018-0081-y>
- Gensbittel, V., Kräter, M., Harlepp, S., Busnelli, I., Guck, J., Goetz, J.G., 2021. Mechanical Adaptability of Tumor Cells in Metastasis. *Dev. Cell* 56, 164–179. <https://doi.org/10.1016/j.devcel.2020.10.011>
- Ghaffari, A., Hoskin, V., Turashvili, G., Varma, S., Mewburn, J., Mullins, G., Greer, P.A., Kiefer, F., Day, A.G., Madarnas, Y., SenGupta, S., Elliott, B.E., 2019. Intravital imaging reveals systemic ezrin inhibition impedes cancer cell migration and lymph node metastasis in breast cancer. *Breast Cancer Res.* 21, 12. <https://doi.org/10.1186/s13058-018-1079-7>
- Giordano, A., Gao, H., Anfossi, S., Cohen, E., Mego, M., Lee, B.-N., Tin, S., De Laurentiis, M., Parker, C.A., Alvarez, R.H., Valero, V., Ueno, N.T., De Placido, S., Mani, S.A., Esteva, F.J., Cristofanilli, M., Reuben, J.M., 2012. Epithelial-Mesenchymal Transition and Stem Cell Markers in Patients with HER2-Positive

- Metastatic Breast Cancer. *Mol. Cancer Ther.* 11, 2526–2534. <https://doi.org/10.1158/1535-7163.MCT-12-0460>
- Gkountela, S., Castro-Giner, F., Szczerba, B.M., Vetter, M., Landin, J., Scherrer, R., Krol, I., Scheidmann, M.C., Beisel, C., Stirnimann, C.U., Kurzeder, C., Heinzelmann-Schwarz, V., Rochlitz, C., Weber, W.P., Aceto, N., 2019. Circulating Tumor Cell Clustering Shapes DNA Methylation to Enable Metastasis Seeding. *Cell* 176, 98–112.e14. <https://doi.org/10.1016/j.cell.2018.11.046>
- Gómez-González, M., Latorre, E., Arroyo, M., Trepát, X., 2020. Measuring mechanical stress in living tissues. *Nat. Rev. Phys.* 2, 300–317. <https://doi.org/10.1038/s42254-020-0184-6>
- González-Callejo, P., Gener, P., Díaz-Riascos, Z.V., Conti, S., Cámara-Sánchez, P., Riera, R., Mancilla, S., García-Gabilondo, M., Peg, V., Arango, D., Rosell, A., Labernadie, A., Trepát, X., Albertazzi, L., Schwartz Jr, S., Seras-Franzoso, J., Abasolo, I., 2023. Extracellular vesicles secreted by triple-negative breast cancer stem cells trigger premetastatic niche remodeling and metastatic growth in the lungs. *Int. J. Cancer* 152, 2153–2165. <https://doi.org/10.1002/ijc.34447>
- Grillet, F., Bayet, E., Villeronce, O., Zappia, L., Lagerqvist, E.L., Lunke, S., Charafe-Jauffret, E., Pham, K., Molck, C., Rolland, N., Bourgaux, J.F., Prudhomme, M., Philippe, C., Bravo, S., Boyer, J.C., Canterel-Thouennon, L., Taylor, G.R., Hsu, A., Pascussi, J.M., Hollande, F., Pannequin, J., 2017. Circulating tumour cells from patients with colorectal cancer have cancer stem cell hallmarks in ex vivo culture. *Gut* 66, 1802–1810. <https://doi.org/10.1136/gutjnl-2016-311447>
- Guck, J., Schinkinger, S., Lincoln, B., Wottawah, F., Ebert, S., Romeyke, M., Lenz, D., Erickson, H.M., Ananthakrishnan, R., Mitchell, D., Käs, J., Ulvick, S., Bilby, C., 2005. Optical Deformability as an Inherent Cell Marker for Testing Malignant Transformation and Metastatic Competence. *Biophys. J.* 88, 3689–3698. <https://doi.org/10.1529/biophysj.104.045476>
- Guilak, F., Tedrow, J.R., Burgkart, R., 2000. Viscoelastic Properties of the Cell Nucleus. *Biochem. Biophys. Res. Commun.* 269, 781–786. <https://doi.org/10.1006/bbrc.2000.2360>
- Gundem, G., Van Loo, P., Kremeyer, B., Alexandrov, L.B., Tubio, J.M.C., Papaemmanuil, E., Brewer, D.S., Kallio, H.M.L., Högnäs, G., Annala, M., Kivinummi, K., Goody, V., Latimer, C., O'Meara, S., Dawson, K.J., Isaacs, W., Emmert-Buck, M.R., Nykter, M., Foster, C., Kote-Jarai, Z., Easton, D., Whitaker, H.C., Neal, D.E., Cooper, C.S., Eeles, R.A., Visakorpi, T., Campbell, P.J., McDermott, U., Wedge, D.C., Bova, G.S., 2015. The evolutionary history of lethal metastatic prostate cancer. *Nature* 520, 353–357. <https://doi.org/10.1038/nature14347>
- Gupta, P.B., Fillmore, C.M., Jiang, G., Shapira, S.D., Tao, K., Kuperwasser, C., Lander, E.S., 2011. Stochastic State Transitions Give Rise to Phenotypic Equilibrium in

- Populations of Cancer Cells. *Cell* 146, 633–644. <https://doi.org/10.1016/j.cell.2011.07.026>
- Gutmann, R., Leunig, M., Feyh, J., Goetz, A.E., Messmer, K., Kastenbauer, E., Jain, R.K., 1992. Interstitial Hypertension in Head and Neck Tumors in Patients: Correlation with Tumor Size. *Cancer Res.* 52, 1993–1995.
- Hamidi, H., Ivaska, J., 2018. Every step of the way: integrins in cancer progression and metastasis. *Nat. Rev. Cancer* 18, 533–548. <https://doi.org/10.1038/s41568-018-0038-z>
- Han, Y.L., Pegoraro, A.F., Li, H., Li, K., Yuan, Y., Xu, G., Gu, Z., Sun, J., Hao, Y., Gupta, S.K., Li, Y., Tang, W., Kang, H., Teng, L., Fredberg, J.J., Guo, M., 2020. Cell swelling, softening and invasion in a three-dimensional breast cancer model. *Nat. Phys.* 16, 101–108. <https://doi.org/10.1038/s41567-019-0680-8>
- Han, Y.L., Ronceray, P., Xu, G., Malandrino, A., Kamm, R.D., Lenz, M., Broedersz, C.P., Guo, M., 2018. Cell contraction induces long-ranged stress stiffening in the extracellular matrix. *Proc. Natl. Acad. Sci.* 115, 4075–4080. <https://doi.org/10.1073/pnas.1722619115>
- Hassell, B.A., Goyal, G., Lee, E., Sontheimer-Phelps, A., Levy, O., Chen, C.S., Ingber, D.E., 2017. Human Organ Chip Models Recapitulate Orthotopic Lung Cancer Growth, Therapeutic Responses, and Tumor Dormancy In Vitro. *Cell Rep.* 21, 508–516. <https://doi.org/10.1016/j.celrep.2017.09.043>
- Hay, E.D., 1995. An Overview of Epithelio-Mesenchymal Transformation. *Cells Tissues Organs* 154, 8–20. <https://doi.org/10.1159/000147748>
- Hayward, M.-K., Muncie, J.M., Weaver, V.M., 2021. Tissue mechanics in stem cell fate, development, and cancer. *Dev. Cell* 56, 1833–1847. <https://doi.org/10.1016/j.devcel.2021.05.011>
- Heldin, C.-H., Rubin, K., Pietras, K., Östman, A., 2004. High interstitial fluid pressure — an obstacle in cancer therapy. *Nat. Rev. Cancer* 4, 806–813. <https://doi.org/10.1038/nrc1456>
- Hofer, M., Lutolf, M.P., 2021. Engineering organoids. *Nat. Rev. Mater.* 6, 402–420. <https://doi.org/10.1038/s41578-021-00279-y>
- Holcomb, M.C., Gao, G.-J.J., Servati, M., Schneider, D., McNeely, P.K., Thomas, J.H., Blawdziewicz, J., 2021. Mechanical feedback and robustness of apical constrictions in *Drosophila* embryo ventral furrow formation. *PLOS Comput. Biol.* 17, e1009173. <https://doi.org/10.1371/journal.pcbi.1009173>
- Hollier, B.G., Tinnirello, A.A., Werden, S.J., Evans, K.W., Taube, J.H., Sarkar, T.R., Sphyris, N., Shariati, M., Kumar, S.V., Battula, V.L., Herschkowitz, J.I., Guerra, R., Chang, J.T., Miura, N., Rosen, J.M., Mani, S.A., 2013. FOXC2 Expression Links Epithelial–Mesenchymal Transition and Stem Cell Properties in Breast Cancer. *Cancer Res.* 73, 1981–1992. <https://doi.org/10.1158/0008-5472.CAN-12-2962>
- Hu, X., Liu, Y., Bing, Z., Ye, Q., Li, C., 2021. High Moesin Expression Is a Predictor of Poor Prognosis of Breast Cancer: Evidence From a Systematic Review With

- Meta-Analysis. *Front. Oncol.* 11, 650488. <https://doi.org/10.3389/fonc.2021.650488>
- Ishihara, S., Haga, H., 2022. Matrix Stiffness Contributes to Cancer Progression by Regulating Transcription Factors. *Cancers* 14, 1049. <https://doi.org/10.3390/cancers14041049>
- Jabbari, E., Sarvestani, S.K., Daneshian, L., Moeinzadeh, S., 2015. Optimum 3D Matrix Stiffness for Maintenance of Cancer Stem Cells Is Dependent on Tissue Origin of Cancer Cells. *PLOS ONE* 10, e0132377. <https://doi.org/10.1371/journal.pone.0132377>
- Janiszewska, M., Primi, M.C., Izard, T., 2020. Cell adhesion in cancer: Beyond the migration of single cells. *J. Biol. Chem.* 295, 2495–2505. <https://doi.org/10.1074/jbc.REV119.007759>
- Jehanno, C., Vulin, M., Richina, V., Richina, F., Bentires-Alj, M., 2022. Phenotypic plasticity during metastatic colonization. *Trends Cell Biol.* 32, 854–867. <https://doi.org/10.1016/j.tcb.2022.03.007>
- Jeon, J.S., Bersini, S., Gilardi, M., Dubini, G., Charest, J.L., Moretti, M., Kamm, R.D., 2015. Human 3D vascularized organotypic microfluidic assays to study breast cancer cell extravasation. *Proc. Natl. Acad. Sci.* 112, 214–219. <https://doi.org/10.1073/pnas.1417115112>
- Jinushi, M., Chiba, S., Yoshiyama, H., Masutomi, K., Kinoshita, I., Dosaka-Akita, H., Yagita, H., Takaoka, A., Tahara, H., 2011. Tumor-associated macrophages regulate tumorigenicity and anticancer drug responses of cancer stem/initiating cells. *Proc. Natl. Acad. Sci.* 108, 12425–12430. <https://doi.org/10.1073/pnas.1106645108>
- Jolly, M.K., Jia, D., Boareto, M., Mani, S.A., Pienta, K.J., Ben-Jacob, E., Levine, H., 2015. Coupling the modules of EMT and stemness: A tunable ‘stemness window’ model. *Oncotarget* 6, 25161–25174. <https://doi.org/10.18632/oncotarget.4629>
- Jörgren, F., Nilbert, M., Rambeck, E., Bendahl, P.-O., Lindmark, G., 2012. Ezrin expression in rectal cancer predicts time to development of local recurrence. *Int. J. Colorectal Dis.* 27, 893–899. <https://doi.org/10.1007/s00384-011-1397-z>
- Junttila, M.R., Mao, W., Wang, X., Wang, B.-E., Pham, T., Flygare, J., Yu, S.-F., Yee, S., Goldenberg, D., Fields, C., Eastham-Anderson, J., Singh, M., Vij, R., Hongo, J.-A., Firestein, R., Schutten, M., Flagella, K., Polakis, P., Polson, A.G., 2015. Targeting LGR5+ cells with an antibody-drug conjugate for the treatment of colon cancer. *Sci. Transl. Med.* 7, 314ra186-314ra186. <https://doi.org/10.1126/scitranslmed.aac7433>
- Kabashima, A., Higuchi, H., Takaishi, H., Matsuzaki, Y., Suzuki, S., Izumiya, M., Iizuka, H., Sakai, G., Hozawa, S., Azuma, T., Hibi, T., 2009. Side population of pancreatic cancer cells predominates in TGF- β -mediated epithelial to

- mesenchymal transition and invasion. *Int. J. Cancer* 124, 2771–2779. <https://doi.org/10.1002/ijc.24349>
- Kang, W., Ferruzzi, J., Spatarelu, C.-P., Han, Y.L., Sharma, Y., Koehler, S.A., Mitchel, J.A., Khan, A., Butler, J.P., Roblyer, D., Zaman, M.H., Park, J.-A., Guo, M., Chen, Z., Pegoraro, A.F., Fredberg, J.J., 2021. A novel jamming phase diagram links tumor invasion to non-equilibrium phase separation. *iScience* 24, 103252. <https://doi.org/10.1016/j.isci.2021.103252>
- Karami, D., Richbourg, N., Sikavitsas, V., 2019. Dynamic in vitro models for tumor tissue engineering. *Cancer Lett.* 449, 178–185. <https://doi.org/10.1016/j.canlet.2019.01.043>
- Kemper, K., Prasetyanti, P.R., De Lau, W., Rodermond, H., Clevers, H., Medema, J.P., 2012. Monoclonal Antibodies Against Lgr5 Identify Human Colorectal Cancer Stem Cells. *Stem Cells* 30, 2378–2386. <https://doi.org/10.1002/stem.1233>
- Kienast, Y., von Baumgarten, L., Fuhrmann, M., Klinkert, W.E.F., Goldbrunner, R., Herms, J., Winkler, F., 2010. Real-time imaging reveals the single steps of brain metastasis formation. *Nat. Med.* 16, 116–122. <https://doi.org/10.1038/nm.2072>
- Kim, H., Lin, Q., Glazer, P.M., Yun, Z., 2018. The hypoxic tumor microenvironment in vivo selects the cancer stem cell fate of breast cancer cells. *Breast Cancer Res.* 20, 16. <https://doi.org/10.1186/s13058-018-0944-8>
- Kinugasa, Y., Matsui, T., Takakura, N., 2014. CD44 Expressed on Cancer-Associated Fibroblasts Is a Functional Molecule Supporting the Stemness and Drug Resistance of Malignant Cancer Cells in the Tumor Microenvironment. *Stem Cells* 32, 145–156. <https://doi.org/10.1002/stem.1556>
- Kirby, T.J., Lammerding, J., 2018. Emerging views of the nucleus as a cellular mechanosensor. *Nat. Cell Biol.* 20, 373–381. <https://doi.org/10.1038/s41556-018-0038-y>
- Kleinsmith, L.J., Pierce, G.B., Jr., 1964. Multipotentiality of Single Embryonal Carcinoma Cells*. *Cancer Res.* 24, 1544–1551.
- Kobayashi, H., Gieniec, K.A., Wright, J.A., Wang, T., Asai, N., Mizutani, Y., Lida, T., Ando, R., Suzuki, N., Lannagan, T.R.M., Ng, J.Q., Hara, A., Shiraki, Y., Mii, S., Ichinose, M., Vrbanc, L., Lawrence, M.J., Sammour, T., Uehara, K., Davies, G., Lisowski, L., Alexander, I.E., Hayakawa, Y., Butler, L.M., Zannettino, A.C.W., Din, M.O., Hasty, J., Burt, A.D., Leedham, S.J., Rustgi, A.K., Mukherjee, S., Wang, T.C., Enomoto, A., Takahashi, M., Worthley, D.L., Woods, S.L., 2021. The Balance of Stromal BMP Signaling Mediated by GREM1 and ISLR Drives Colorectal Carcinogenesis. *Gastroenterology* 160, 1224-1239.e30. <https://doi.org/10.1053/j.gastro.2020.11.011>
- Kok, S.Y., Oshima, H., Takahashi, K., Nakayama, M., Murakami, K., Ueda, H.R., Miyazono, K., Oshima, M., 2021. Malignant subclone drives metastasis of genetically and phenotypically heterogeneous cell clusters through fibrotic niche generation. *Nat. Commun.* 12, 863. <https://doi.org/10.1038/s41467-021-21160-0>

- Konge, J., Leteurtre, F., Goislard, M., Biard, D., Morel-Altmeier, S., Vaurijoux, A., Gruel, G., Chevillard, S., Lebeau, J., 2018. Breast cancer stem cell-like cells generated during TGF β -induced EMT are radioresistant. *Oncotarget* 9, 23519–23531. <https://doi.org/10.18632/oncotarget.25240>
- Kopanska, K.S., Alcheikh, Y., Staneva, R., Vignjevic, D., Betz, T., 2016. Tensile Forces Originating from Cancer Spheroids Facilitate Tumor Invasion. *PLOS ONE* 11, e0156442. <https://doi.org/10.1371/journal.pone.0156442>
- Kopper, O., de Witte, C.J., Löhmussaar, K., Valle-Inclan, J.E., Hami, N., Kester, L., Balgobind, A.V., Korving, J., Proost, N., Begthel, H., van Wijk, L.M., Revilla, S.A., Theeuwssen, R., van de Ven, M., van Roosmalen, M.J., Ponsioen, B., Ho, V.W.H., Neel, B.G., Bosse, T., Gaarenstroom, K.N., Vrieling, H., Vreeswijk, M.P.G., van Diest, P.J., Witteveen, P.O., Jonges, T., Bos, J.L., van Oudenaarden, A., Zweemer, R.P., Snippert, H.J.G., Kloosterman, W.P., Clevers, H., 2019. An organoid platform for ovarian cancer captures intra- and interpatient heterogeneity. *Nat. Med.* 25, 838–849. <https://doi.org/10.1038/s41591-019-0422-6>
- Korpal, M., Ell, B.J., Buffa, F.M., Ibrahim, T., Blanco, M.A., Celià-Terrassa, T., Mercatali, L., Khan, Z., Goodarzi, H., Hua, Y., Wei, Y., Hu, G., Garcia, B.A., Ragoussis, J., Amadori, D., Harris, A.L., Kang, Y., 2011. Direct targeting of Sec23a by miR-200s influences cancer cell secretome and promotes metastatic colonization. *Nat. Med.* 17, 1101–1108. <https://doi.org/10.1038/nm.2401>
- Kowalski, P.J., Rubin, M.A., Kleer, C.G., 2003. E-cadherin expression in primary carcinomas of the breast and its distant metastases. *Breast Cancer Res.* 5, R217. <https://doi.org/10.1186/bcr651>
- Kreso, A., Dick, J.E., 2014. Evolution of the Cancer Stem Cell Model. *Cell Stem Cell* 14, 275–291. <https://doi.org/10.1016/j.stem.2014.02.006>
- Kretschmar, K., Watt, F.M., 2012. Lineage Tracing. *Cell* 148, 33–45. <https://doi.org/10.1016/j.cell.2012.01.002>
- Krndija, D., El Marjou, F., Guirao, B., Richon, S., Leroy, O., Bellaiche, Y., Hannezo, E., Matic Vignjevic, D., 2019. Active cell migration is critical for steady-state epithelial turnover in the gut. *Science* 365, 705–710. <https://doi.org/10.1126/science.aau3429>
- Kuipers, E.J., Grady, W.M., Lieberman, D., Seufferlein, T., Sung, J.J., Boelens, P.G., van de Velde, C.J.H., Watanabe, T., 2015. Colorectal cancer. *Nat. Rev. Dis. Primer* 1, 1–25. <https://doi.org/10.1038/nrdp.2015.65>
- Labernadie, A., Kato, T., Brugués, A., Serra-Picamal, X., Derzsi, S., Arwert, E., Weston, A., González-Tarragó, V., Elosegui-Artola, A., Albertazzi, L., Alcaraz, J., Roca-Cusachs, P., Sahai, E., Trepac, X., 2017. A mechanically active heterotypic E-cadherin/N-cadherin adhesion enables fibroblasts to drive cancer cell invasion. *Nat. Cell Biol.* 19, 224–237. <https://doi.org/10.1038/ncb3478>
- Laklai, H., Miroshnikova, Y.A., Pickup, M.W., Collisson, E.A., Kim, G.E., Barrett, A.S., Hill, R.C., Lakins, J.N., Schlaepfer, D.D., Mouw, J.K., LeBleu, V.S., Roy, N.,

- Novitskiy, S.V., Johansen, J.S., Poli, V., Kalluri, R., Iacobuzio-Donahue, C.A., Wood, L.D., Hebrok, M., Hansen, K., Moses, H.L., Weaver, V.M., 2016. Genotype tunes pancreatic ductal adenocarcinoma tissue tension to induce matricellular fibrosis and tumor progression. *Nat. Med.* 22, 497–505. <https://doi.org/10.1038/nm.4082>
- Lambert, A.W., Pattabiraman, D.R., Weinberg, R.A., 2017. Emerging Biological Principles of Metastasis. *Cell* 168, 670–691. <https://doi.org/10.1016/j.cell.2016.11.037>
- Lambert, A.W., Weinberg, R.A., 2021. Linking EMT programmes to normal and neoplastic epithelial stem cells. *Nat. Rev. Cancer* 21, 325–338. <https://doi.org/10.1038/s41568-021-00332-6>
- Lamprecht, S., Schmidt, E.M., Blaj, C., Hermeking, H., Jung, A., Kirchner, T., Horst, D., 2017. Multicolor lineage tracing reveals clonal architecture and dynamics in colon cancer. *Nat. Commun.* 8, 1406. <https://doi.org/10.1038/s41467-017-00976-9>
- Lapidot, T., Sirard, C., Vormoor, J., Murdoch, B., Hoang, T., Caceres-Cortes, J., Minden, M., Paterson, B., Caligiuri, M.A., Dick, J.E., 1994. A cell initiating human acute myeloid leukaemia after transplantation into SCID mice. *Nature* 367, 645–648. <https://doi.org/10.1038/367645a0>
- Latil, M., Nassar, D., Beck, B., Boumahdi, S., Wang, L., Brisebarre, A., Dubois, C., Nkusi, E., Lenglez, S., Checinska, A., Vercauteren Drubbel, A., Devos, M., Declercq, W., Yi, R., Blanpain, C., 2017. Cell-Type-Specific Chromatin States Differentially Prime Squamous Cell Carcinoma Tumor-Initiating Cells for Epithelial to Mesenchymal Transition. *Cell Stem Cell* 20, 191–204.e5. <https://doi.org/10.1016/j.stem.2016.10.018>
- Lawson, D.A., Bhakta, N.R., Kessenbrock, K., Prummel, K.D., Yu, Y., Takai, K., Zhou, A., Eyob, H., Balakrishnan, S., Wang, C.-Y., Yaswen, P., Goga, A., Werb, Z., 2015. Single-cell analysis reveals a stem-cell program in human metastatic breast cancer cells. *Nature* 526, 131–135. <https://doi.org/10.1038/nature15260>
- Le Berre, M., Zlotek-Zlotkiewicz, E., Bonazzi, D., Lautenschlaeger, F., Piel, M., 2014. Methods for Two-Dimensional Cell Confinement, in: *Methods in Cell Biology*. Elsevier, pp. 213–229. <https://doi.org/10.1016/B978-0-12-800281-0.00014-2>
- Lee, H.-O., Hong, Y., Etioglu, H.E., Cho, Y.B., Pomella, V., Van den Bosch, B., Vanhecke, J., Verbandt, S., Hong, H., Min, J.-W., Kim, N., Eum, H.H., Qian, J., Boeckx, B., Lambrechts, D., Tsantoulis, P., De Hertogh, G., Chung, W., Lee, T., An, M., Shin, H.-T., Joung, J.-G., Jung, M.-H., Ko, G., Wirapati, P., Kim, S.H., Kim, H.C., Yun, S.H., Tan, I.B.H., Ranjan, B., Lee, W.Y., Kim, T.-Y., Choi, J.K., Kim, Y.-J., Prabhakar, S., Tejpar, S., Park, W.-Y., 2020. Lineage-dependent gene expression programs influence the immune landscape of colorectal cancer. *Nat. Genet.* 52, 594–603. <https://doi.org/10.1038/s41588-020-0636-z>

- Lee, S., Kim, S., Koo, D.-J., Yu, J., Cho, H., Lee, H., Song, J.M., Kim, S.-Y., Min, D.-H., Jeon, N.L., 2021. 3D Microfluidic Platform and Tumor Vascular Mapping for Evaluating Anti-Angiogenic RNAi-Based Nanomedicine. *ACS Nano* 15, 338–350. <https://doi.org/10.1021/acsnano.0c05110>
- Leiphrahpam, P.D., Rajput, A., Mathiesen, M., Agarwal, E., Lazenby, A.J., Are, C., Brattain, M.G., Chowdhury, S., 2014. Ezrin expression and cell survival regulation in colorectal cancer. *Cell. Signal.* 26, 868–879. <https://doi.org/10.1016/j.cellsig.2014.01.014>
- Lekka, M., Laidler, P., Gil, D., Lekki, J., Stachura, Z., Hryniewicz, A.Z., 1999. Elasticity of normal and cancerous human bladder cells studied by scanning force microscopy. *Eur. Biophys. J.* 28, 312–316. <https://doi.org/10.1007/s002490050213>
- Lembo, S., Strauss, L., Cheng, W.C.D., Vermeil, J., Siggel, M., Toro-Nahuelpan, M., Chan, C.J., Kosinski, J., Piel, M., Roure, O.D., Heuvingh, J., Mahamid, J., Diz-Muñoz, A., 2023. The distance between the plasma membrane and the actomyosin cortex acts as a nanogate to control cell surface mechanics. <https://doi.org/10.1101/2023.01.31.526409>
- Lenos, K.J., Miedema, D.M., Lodestijn, S.C., Nijman, L.E., van den Bosch, T., Romero Ros, X., Lourenço, F.C., Lecca, M.C., van der Heijden, M., van Neerven, S.M., van Oort, A., Leveille, N., Adam, R.S., de Sousa E Melo, F., Otten, J., Veerman, P., Hypolite, G., Koens, L., Lyons, S.K., Stassi, G., Winton, D.J., Medema, J.P., Morrissey, E., Bijlsma, M.F., Vermeulen, L., 2018. Stem cell functionality is microenvironmentally defined during tumour expansion and therapy response in colon cancer. *Nat. Cell Biol.* 20, 1193–1202. <https://doi.org/10.1038/s41556-018-0179-z>
- LeSavage, B.L., Suhar, R.A., Broguiere, N., Lutolf, M.P., Heilshorn, S.C., 2022. Next-generation cancer organoids. *Nat. Mater.* 21, 143–159. <https://doi.org/10.1038/s41563-021-01057-5>
- Less, J.R., Posner, M.C., Boucher, Y., Borochoviz, D., Wolmark, N., Jain, R.K., 1992. Interstitial Hypertension in Human Breast and Colorectal Tumors¹. *Cancer Res.* 52, 6371–6374.
- Leu, A.J., Berk, D.A., Lymboussaki, A., Alitalo, K., Jain, R.K., 2000. Absence of Functional Lymphatics within a Murine Sarcoma: A Molecular and Functional Evaluation¹. *Cancer Res.* 60, 4324–4327.
- Levayer, R., 2020. Solid stress, competition for space and cancer: The opposing roles of mechanical cell competition in tumour initiation and growth. *Semin. Cancer Biol.*, Emerging role of cell competition in cancer 63, 69–80. <https://doi.org/10.1016/j.semcancer.2019.05.004>
- Li, C., Heidt, D.G., Dalerba, P., Burant, C.F., Zhang, L., Adsay, V., Wicha, M., Clarke, M.F., Simeone, D.M., 2007. Identification of Pancreatic Cancer Stem Cells. *Cancer Res.* 67, 1030–1037. <https://doi.org/10.1158/0008-5472.CAN-06-2030>

- Li, G.-M., 2008. Mechanisms and functions of DNA mismatch repair. *Cell Res.* 18, 85–98. <https://doi.org/10.1038/cr.2007.115>
- Li, L., Wang, Y.-Y., Zhao, Z.-S., Ma, J., 2011. Ezrin is Associated with Gastric Cancer Progression and Prognosis. *Pathol. Oncol. Res.* 17, 909–915. <https://doi.org/10.1007/s12253-011-9402-y>
- Li, P., Zhou, C., Xu, L., Xiao, H., 2013. Hypoxia Enhances Stemness of Cancer Stem Cells in Glioblastoma: An In Vitro Study. *Int. J. Med. Sci.* 10, 399–407. <https://doi.org/10.7150/ijms.5407>
- Li, X., Nadauld, L., Ootani, A., Corney, D.C., Pai, R.K., Gevaert, O., Cantrell, M.A., Rack, P.G., Neal, J.T., Chan, C.W.-M., Yeung, T., Gong, X., Yuan, J., Wilhelmy, J., Robine, S., Attardi, L.D., Plevritis, S.K., Hung, K.E., Chen, C.-Z., Ji, H.P., Kuo, C.J., 2014. Oncogenic transformation of diverse gastrointestinal tissues in primary organoid culture. *Nat. Med.* 20, 769–777. <https://doi.org/10.1038/nm.3585>
- Li, Y., Lin, Z., Chen, B., Chen, S., Jiang, Z., Zhou, T., Hou, Z., Wang, Y., 2017. Ezrin/NF- κ B activation regulates epithelial- mesenchymal transition induced by EGF and promotes metastasis of colorectal cancer. *Biomed. Pharmacother.* 92, 140–148. <https://doi.org/10.1016/j.biopha.2017.05.058>
- Liang, F., Wang, Y., Shi, L., Zhang, J., 2017. Association of Ezrin expression with the progression and prognosis of gastrointestinal cancer: a meta-analysis. *Oncotarget* 8, 93186–93195. <https://doi.org/10.18632/oncotarget.21473>
- Liu, J., Tan, Y., Zhang, H., Zhang, Y., Xu, P., Chen, J., Poh, Y.-C., Tang, K., Wang, N., Huang, B., 2012. Soft fibrin gels promote selection and growth of tumorigenic cells. *Nat. Mater.* 11, 734–741. <https://doi.org/10.1038/nmat3361>
- Liu, X., Taftaf, R., Kawaguchi, M., Chang, Y.-F., Chen, W., Entenberg, D., Zhang, Y., Gerratana, L., Huang, S., Patel, D.B., Tsui, E., Adorno-Cruz, V., Chirieleison, S.M., Cao, Y., Harney, A.S., Patel, S., Patsialou, A., Shen, Y., Avril, S., Gilmore, H.L., Lathia, J.D., Abbott, D.W., Cristofanilli, M., Condeelis, J.S., Liu, H., 2019. Homophilic CD44 Interactions Mediate Tumor Cell Aggregation and Polyclonal Metastasis in Patient-Derived Breast Cancer Models. *Cancer Discov.* 9, 96–113. <https://doi.org/10.1158/2159-8290.CD-18-0065>
- Liu, X., Ye, Y., Zhu, L., Xiao, X., Zhou, B., Gu, Y., Si, H., Liang, H., Liu, M., Li, Jiaqian, Jiang, Q., Li, Jiang, Yu, S., Ma, R., Su, S., Liao, J.-Y., Zhao, Q., 2023. Niche stiffness sustains cancer stemness via TAZ and NANOG phase separation. *Nat. Commun.* 14, 238. <https://doi.org/10.1038/s41467-023-35856-y>
- Liu, Y.-J., Le Berre, M., Lautenschlaeger, F., Maiuri, P., Callan-Jones, A., Heuzé, M., Takaki, T., Voituriez, R., Piel, M., 2015. Confinement and Low Adhesion Induce Fast Amoeboid Migration of Slow Mesenchymal Cells. *Cell* 160, 659–672. <https://doi.org/10.1016/j.cell.2015.01.007>
- Liu, Z., Lee, S.J., Park, S., Konstantopoulos, K., Glunde, K., Chen, Y., Barman, I., 2020. Cancer cells display increased migration and deformability in pace with

- metastatic progression. *FASEB J.* 34, 9307–9315. <https://doi.org/10.1096/fj.202000101RR>
- Lomakin, A.J., Cattin, C.J., Cuvelier, D., Alraies, Z., Molina, M., Nader, G.P.F., Srivastava, N., Sáez, P.J., Garcia-Arcos, J.M., Zhitnyak, I.Y., Bhargava, A., Driscoll, M.K., Welf, E.S., Fiolka, R., Petrie, R.J., De Silva, N.S., González-Granado, J.M., Manel, N., Lennon-Duménil, A.M., Müller, D.J., Piel, M., 2020. The nucleus acts as a ruler tailoring cell responses to spatial constraints. *Science* 370, eaba2894. <https://doi.org/10.1126/science.aba2894>
- Lopez, J.I., Kang, I., You, W.-K., McDonald, D.M., Weaver, V.M., 2011. In situ force mapping of mammary gland transformation. *Integr. Biol.* 3, 910–921. <https://doi.org/10.1039/c1ib00043h>
- Lu, H., Lyu, Y., Tran, L., Lan, J., Xie, Y., Yang, Y., Murugan, N.L., Wang, Y.J., Semenza, G.L., 2021. HIF-1 recruits NANOG as a coactivator for TERT gene transcription in hypoxic breast cancer stem cells. *Cell Rep.* 36. <https://doi.org/10.1016/j.celrep.2021.109757>
- Lu, J., Ye, X., Fan, F., Xia, L., Bhattacharya, R., Bellister, S., Tozzi, F., Sceusi, E., Zhou, Y., Tachibana, I., Maru, D.M., Hawke, D.H., Rak, J., Mani, S.A., Zweidler-McKay, P., Ellis, L.M., 2013. Endothelial Cells Promote the Colorectal Cancer Stem Cell Phenotype through a Soluble Form of Jagged-1. *Cancer Cell* 23, 171–185. <https://doi.org/10.1016/j.ccr.2012.12.021>
- Luo, Y., Wong, C.-J., Kaz, A.M., Dzieciatkowski, S., Carter, K.T., Morris, S.M., Wang, J., Willis, J.E., Makar, K.W., Ulrich, C.M., Lutterbaugh, J.D., Shrubsole, M.J., Zheng, W., Markowitz, S.D., Grady, W.M., 2014. Differences in DNA Methylation Signatures Reveal Multiple Pathways of Progression From Adenoma to Colorectal Cancer. *Gastroenterology* 147, 418–429.e8. <https://doi.org/10.1053/j.gastro.2014.04.039>
- Lv, J., Liu, Yaoping, Cheng, F., Li, J., Zhou, Y., Zhang, T., Zhou, N., Li, C., Wang, Z., Ma, L., Liu, M., Zhu, Q., Liu, X., Tang, K., Ma, J., Zhang, Huafeng, Xie, J., Fang, Y., Zhang, Haizeng, Wang, N., Liu, Yuying, Huang, B., 2021. Cell softness regulates tumorigenicity and stemness of cancer cells. *EMBO J.* 40, e106123. <https://doi.org/10.15252/embj.2020106123>
- Lynch, H.T., de la Chapelle, A., 2003. Hereditary Colorectal Cancer. *N. Engl. J. Med.* 348, 919–932. <https://doi.org/10.1056/NEJMra012242>
- Mabry, K.M., Payne, S.Z., Anseth, K.S., 2016. Microarray analyses to quantify advantages of 2D and 3D hydrogel culture systems in maintaining the native valvular interstitial cell phenotype. *Biomaterials* 74, 31–41. <https://doi.org/10.1016/j.biomaterials.2015.09.035>
- Malandrino, A., Mak, M., Kamm, R.D., Moeendarbary, E., 2018. Complex mechanics of the heterogeneous extracellular matrix in cancer. *Extreme Mech. Lett.* 21, 25–34. <https://doi.org/10.1016/j.eml.2018.02.003>
- Mani, S.A., Guo, W., Liao, M.-J., Eaton, E.Ng., Ayyanan, A., Zhou, A.Y., Brooks, M., Reinhard, F., Zhang, C.C., Shipitsin, M., Campbell, L.L., Polyak, K., Briskin, C.,

- Yang, J., Weinberg, R.A., 2008. The Epithelial-Mesenchymal Transition Generates Cells with Properties of Stem Cells. *Cell* 133, 704–715. <https://doi.org/10.1016/j.cell.2008.03.027>
- Matano, M., Date, S., Shimokawa, M., Takano, A., Fujii, M., Ohta, Y., Watanabe, T., Kanai, T., Sato, T., 2015. Modeling colorectal cancer using CRISPR-Cas9-mediated engineering of human intestinal organoids. *Nat. Med.* 21, 256–262. <https://doi.org/10.1038/nm.3802>
- Matsui, T., Maeda, M., Doi, Y., Yonemura, S., Amano, M., Kaibuchi, K., Tsukita, Sachiko, Tsukita, Shoichiro, 1998. Rho-Kinase Phosphorylates COOH-terminal Threonines of Ezrin/Radixin/Moesin (ERM) Proteins and Regulates Their Head-to-Tail Association. *J. Cell Biol.* 140, 647–657. <https://doi.org/10.1083/jcb.140.3.647>
- Melissaridou, S., Wiechec, E., Magan, M., Jain, M.V., Chung, M.K., Farnebo, L., Roberg, K., 2019. The effect of 2D and 3D cell cultures on treatment response, EMT profile and stem cell features in head and neck cancer. *Cancer Cell Int.* 19. <https://doi.org/10.1186/s12935-019-0733-1>
- Merino, D., Weber, T.S., Serrano, A., Vaillant, F., Liu, K., Pal, B., Di Stefano, L., Schreuder, J., Lin, D., Chen, Y., Asselin-Labat, M.L., Schumacher, T.N., Cameron, D., Smyth, G.K., Papenfuss, A.T., Lindeman, G.J., Visvader, J.E., Naik, S.H., 2019. Barcoding reveals complex clonal behavior in patient-derived xenografts of metastatic triple negative breast cancer. *Nat. Commun.* 10, 766. <https://doi.org/10.1038/s41467-019-08595-2>
- Mietke, A., Otto, O., Girardo, S., Rosendahl, P., Taubenberger, A., Golfier, S., Ulbricht, E., Aland, S., Guck, J., Fischer-Friedrich, E., 2015. Extracting Cell Stiffness from Real-Time Deformability Cytometry: Theory and Experiment. *Biophys. J.* 109, 2023–2036. <https://doi.org/10.1016/j.bpj.2015.09.006>
- Miller, H.E., Bishop, A.J.R., 2021. Correlation AnalyzeR: functional predictions from gene co-expression correlations. *BMC Bioinformatics* 22, 206. <https://doi.org/10.1186/s12859-021-04130-7>
- Mizukoshi, K., Okazawa, Y., Haeno, H., Koyama, Y., Sulidan, K., Komiyama, H., Saeki, H., Ohtsui, N., Ito, Y., Kojima, Y., Goto, M., Habu, S., Hino, O., Sakamoto, K., Orimo, A., 2020. Metastatic seeding of human colon cancer cell clusters expressing the hybrid epithelial/mesenchymal state. *Int. J. Cancer* 146, 2547–2562. <https://doi.org/10.1002/ijc.32672>
- Montanez-Sauri, S.I., Sung, K.E., Berthier, E., Beebe, D.J., 2013. Enabling Screening in 3D Microenvironments: Probing Matrix and Stromal Effects on the Morphology and Proliferation of T47D Breast Carcinoma Cells. *Integr. Biol. Quant. Biosci. Nano Macro* 5, 631–640. <https://doi.org/10.1039/c3ib20225a>
- Moose, D.L., Krog, B.L., Kim, T.-H., Zhao, L., Williams-Perez, S., Burke, G., Rhodes, L., Vanneste, M., Breheny, P., Milhem, M., Stipp, C.S., Rowat, A.C., Henry, M.D., 2020. Cancer Cells Resist Mechanical Destruction in Circulation via

- RhoA/Actomyosin-Dependent Mechano-Adaptation. *Cell Rep.* 30, 3864-3874.e6. <https://doi.org/10.1016/j.celrep.2020.02.080>
- Morral, C., Stanisavljevic, J., Hernando-Momblona, X., Mereu, E., Álvarez-Varela, A., Cortina, C., Stork, D., Slebe, F., Turon, G., Whissell, G., Sevillano, M., Merlos-Suárez, A., Casanova-Martí, À., Moutinho, C., Lowe, S.W., Dow, L.E., Villanueva, A., Sancho, E., Heyn, H., Batlle, E., 2020. Zonation of Ribosomal DNA Transcription Defines a Stem Cell Hierarchy in Colorectal Cancer. *Cell Stem Cell* 26, 845-861.e12. <https://doi.org/10.1016/j.stem.2020.04.012>
- Muciño-Olmos, E.A., Vázquez-Jiménez, A., Avila-Ponce de León, U., Matadamas-Guzman, M., Maldonado, V., López-Santaella, T., Hernández-Hernández, A., Resendis-Antonio, O., 2020. Unveiling functional heterogeneity in breast cancer multicellular tumor spheroids through single-cell RNA-seq. *Sci. Rep.* 10, 12728. <https://doi.org/10.1038/s41598-020-69026-7>
- Müller Paul, n.d. Analysis software for real-time deformability cytometry [Software]. Available at <https://github.com/ZELLMECHANIK-DRESDEN/ShapeOut2>.
- Murthy, S.E., Dubin, A.E., Patapoutian, A., 2017. Piezos thrive under pressure: mechanically activated ion channels in health and disease. *Nat. Rev. Mol. Cell Biol.* 18, 771–783. <https://doi.org/10.1038/nrm.2017.92>
- Nair, N., Calle, A.S., Zahra, M.H., Prieto-Vila, M., Oo, A.K.K., Hurley, L., Vaidyanath, A., Seno, A., Masuda, J., Iwasaki, Y., Tanaka, H., Kasai, T., Seno, M., 2017. A cancer stem cell model as the point of origin of cancer-associated fibroblasts in tumor microenvironment. *Sci. Rep.* 7, 6838. <https://doi.org/10.1038/s41598-017-07144-5>
- Nguyen, A.K., Kilian, K.A., 2020. Physicochemical Tools for Visualizing and Quantifying Cell-Generated Forces. *ACS Chem. Biol.* 15, 1731–1746. <https://doi.org/10.1021/acscchembio.0c00304>
- Nia, H.T., Liu, H., Seano, G., Datta, M., Jones, D., Rahbari, N., Incio, J., Chauhan, V.P., Jung, K., Martin, J.D., Askoxylakis, V., Padera, T.P., Fukumura, D., Boucher, Y., Hornicek, F.J., Grodzinsky, A.J., Baish, J.W., Munn, L.L., Jain, R.K., 2016. Solid stress and elastic energy as measures of tumour mechanopathology. *Nat. Biomed. Eng.* 1, 1–11. <https://doi.org/10.1038/s41551-016-0004>
- Nia, H.T., Munn, L.L., Jain, R.K., 2020. Physical traits of cancer. *Science* 370, eaaz0868. <https://doi.org/10.1126/science.aaz0868>
- Nieto, M.A., Huang, R.Y.-J., Jackson, R.A., Thiery, J.P., 2016. EMT: 2016. *Cell* 166, 21–45. <https://doi.org/10.1016/j.cell.2016.06.028>
- Noe, O., Filipiak, L., Royfman, R., Campbell, A., Lin, L., Hamouda, D., Stanbery, L., Nemunaitis, J., 2021. Adenomatous polyposis coli in cancer and therapeutic implications. *Oncol. Rev.* 15, 534. <https://doi.org/10.4081/oncol.2021.534>
- O'Brien, C.A., Pollett, A., Gallinger, S., Dick, J.E., 2007. A human colon cancer cell capable of initiating tumour growth in immunodeficient mice. *Nature* 445, 106–110. <https://doi.org/10.1038/nature05372>

- Öhlund, D., Handly-Santana, A., Biffi, G., Elyada, E., Almeida, A.S., Ponz-Sarvisé, M., Corbo, V., Oni, T.E., Hearn, S.A., Lee, E.J., Chio, I.I.C., Hwang, C.-I., Tiriác, H., Baker, L.A., Engle, D.D., Feig, C., Kultti, A., Egeblad, M., Fearon, D.T., Crawford, J.M., Clevers, H., Park, Y., Tuveson, D.A., 2017. Distinct populations of inflammatory fibroblasts and myofibroblasts in pancreatic cancer. *J. Exp. Med.* 214, 579–596. <https://doi.org/10.1084/jem.20162024>
- Osmani, N., Follain, G., García León, M.J., Lefebvre, O., Busnelli, I., Larnicol, A., Harlepp, S., Goetz, J.G., 2019. Metastatic Tumor Cells Exploit Their Adhesion Repertoire to Counteract Shear Forces during Intravascular Arrest. *Cell Rep.* 28, 2491–2500.e5. <https://doi.org/10.1016/j.celrep.2019.07.102>
- Otto, O., Rosendahl, P., Mietke, A., Golfier, S., Herold, C., Klaue, D., Girardo, S., Pagliara, S., Ekpenyong, A., Jacobi, A., Wobus, M., Töpfner, N., Keyser, U.F., Mansfeld, J., Fischer-Friedrich, E., Guck, J., 2015. Real-time deformability cytometry: on-the-fly cell mechanical phenotyping. *Nat. Methods* 12, 199–202. <https://doi.org/10.1038/nmeth.3281>
- Padera, T.P., Kadambi, A., di Tomaso, E., Carreira, C.M., Brown, E.B., Boucher, Y., Choi, N.C., Mathisen, D., Wain, J., Mark, E.J., Munn, L.L., Jain, R.K., 2002. Lymphatic Metastasis in the Absence of Functional Intratumor Lymphatics. *Science* 296, 1883–1886. <https://doi.org/10.1126/science.1071420>
- Pallarès, M.E., Pi-Jaumà, I., Fortunato, I.C., Grazu, V., Gómez-González, M., Roca-Cusachs, P., de la Fuente, J.M., Alert, R., Sunyer, R., Casademunt, J., Trepát, X., 2022. Stiffness-dependent active wetting enables optimal collective cell durotaxis. *Nat. Phys.* 1–11. <https://doi.org/10.1038/s41567-022-01835-1>
- Pang, M.-F., Siedlik, M.J., Han, S., Stallings-Mann, M., Radisky, D.C., Nelson, C.M., 2016. Tissue stiffness and hypoxia modulate the integrin-linked kinase ilk to control breast cancer stem-like cells. *Cancer Res.* 76, 5277–5287. <https://doi.org/10.1158/0008-5472.CAN-16-0579>
- Pasch, C.A., Favreau, P.F., Yueh, A.E., Babiarz, C.P., Gillette, A.A., Sharick, J.T., Karim, M.R., Nickel, K.P., DeZeeuw, A.K., Sprackling, C.M., Emmerich, P.B., DeStefanis, R.A., Pitera, R.T., Payne, S.N., Korkos, D.P., Clipson, L., Walsh, C.M., Miller, D., Carchman, E.H., Burkard, M.E., Lemmon, K.K., Matkowskyj, K.A., Newton, M.A., Ong, I.M., Bassetti, M.F., Kimple, R.J., Skala, M.C., Deming, D.A., 2019. Patient-Derived Cancer Organoid Cultures to Predict Sensitivity to Chemotherapy and Radiation. *Clin. Cancer Res.* 25, 5376–5387. <https://doi.org/10.1158/1078-0432.CCR-18-3590>
- Pastushenko, I., Brisebarre, A., Sifrim, A., Fioramonti, M., Revenco, T., Boumahdi, S., Van Keymeulen, A., Brown, D., Moers, V., Lemaire, S., De Clercq, S., Minguijón, E., Balsat, C., Sokolow, Y., Dubois, C., De Cock, F., Scozzaro, S., Sopena, F., Lanas, A., D'Haene, N., Salmon, I., Marine, J.-C., Voet, T., Sotiropoulou, P.A., Blanpain, C., 2018. Identification of the tumour transition states occurring during EMT. *Nature* 556, 463–468. <https://doi.org/10.1038/s41586-018-0040-3>

- Pastushenko, I., Mauri, F., Song, Y., de Cock, F., Meeusen, B., Swedlund, B., Impens, F., Van Haver, D., Opitz, M., Thery, M., Bareche, Y., Lapouge, G., Vermeersch, M., Van Eycke, Y.-R., Balsat, C., Decaestecker, C., Sokolow, Y., Hassid, S., Perez-Bustillo, A., Agreda-Moreno, B., Rios-Buceta, L., Jaen, P., Redondo, P., Sieira-Gil, R., Millan-Cayetano, J.F., Sanmatrin, O., D'Haene, N., Moers, V., Rozzi, M., Blondeau, J., Lemaire, S., Scozzaro, S., Janssens, V., De Troya, M., Dubois, C., Pérez-Morga, D., Salmon, I., Sotiriou, C., Helmbacher, F., Blanpain, C., 2021. Fat1 deletion promotes hybrid EMT state, tumour stemness and metastasis. *Nature* 589, 448–455. <https://doi.org/10.1038/s41586-020-03046-1>
- Patara, M., Santos, E.M.M., Coudry, R. de A., Soares, F.A., Ferreira, F.O., Rossi, B.M., 2011. Ezrin Expression as a Prognostic Marker in Colorectal Adenocarcinoma. *Pathol. Oncol. Res.* 17, 827–833. <https://doi.org/10.1007/s12253-011-9389-4>
- Paul, C.D., Mistriotis, P., Konstantopoulos, K., 2017. Cancer cell motility: lessons from migration in confined spaces. *Nat. Rev. Cancer* 17, 131–140. <https://doi.org/10.1038/nrc.2016.123>
- Pearson, M.A., Reczek, D., Bretscher, A., Karplus, P.A., 2000. Structure of the ERM Protein Moesin Reveals the FERM Domain Fold Masked by an Extended Actin Binding Tail Domain. *Cell* 101, 259–270. [https://doi.org/10.1016/S0092-8674\(00\)80836-3](https://doi.org/10.1016/S0092-8674(00)80836-3)
- Pećina-Šlaus, N., 2003. Tumor suppressor gene E-cadherin and its role in normal and malignant cells. *Cancer Cell Int.* 3, 17. <https://doi.org/10.1186/1475-2867-3-17>
- Pedersen, K.B., Nesland, J.M., Fodstad, Ø., Mælandsmo, G.M., 2002. Expression of S100A4, E-cadherin, α - and β -catenin in breast cancer biopsies. *Br. J. Cancer* 87, 1281–1286. <https://doi.org/10.1038/sj.bjc.6600624>
- Perea Paizal, J., Au, S.H., Bakal, C., 2021. Squeezing through the microcirculation: survival adaptations of circulating tumour cells to seed metastasis. *Br. J. Cancer* 124, 58–65. <https://doi.org/10.1038/s41416-020-01176-x>
- Perekatt, A.O., Shah, P.P., Cheung, S., Jariwala, N., Wu, A., Gandhi, V., Kumar, N., Feng, Q., Patel, N., Chen, L., Joshi, S., Zhou, A., Taketo, M.M., Xing, J., White, E., Gao, N., Gatz, M.L., Verzi, M.P., 2018. SMAD4 Suppresses WNT-Driven Dedifferentiation and Oncogenesis in the Differentiated Gut Epithelium. *Cancer Res.* 78, 4878–4890. <https://doi.org/10.1158/0008-5472.CAN-18-0043>
- Pérez-González, C., Alert, R., Blanch-Mercader, C., Gómez-González, M., Kolodziej, T., Bazellieres, E., Casademunt, J., Trepas, X., 2019. Active wetting of epithelial tissues. *Nat. Phys.* 15, 79–88. <https://doi.org/10.1038/s41567-018-0279-5>
- Pérez-González, C., Ceada, G., Greco, F., Matejčić, M., Gómez-González, M., Castro, N., Menendez, A., Kale, S., Krndija, D., Clark, A.G., Gannavarapu, V.R., Álvarez-Varela, A., Roca-Cusachs, P., Batlle, E., Vignjevic, D.M., Arroyo, M., Trepas, X., 2021. Mechanical compartmentalization of the intestinal organoid enables crypt folding and collective cell migration. *Nat. Cell Biol.* 23, 745–757. <https://doi.org/10.1038/s41556-021-00699-6>

- Perrin, L., Belova, E., Bayarmagnai, B., Tüzel, E., Gligorijevic, B., 2022. Invadopodia enable cooperative invasion and metastasis of breast cancer cells. *Commun. Biol.* 5, 1–14. <https://doi.org/10.1038/s42003-022-03642-z>
- Pierce, G.B., Speers, W.C., 1988. Tumors as caricatures of the process of tissue renewal: prospects for therapy by directing differentiation. *Cancer Res.* 48, 1996–2004.
- Prager, B.C., Xie, Q., Bao, S., Rich, J.N., 2019. Cancer Stem Cells: The Architects of the Tumor Ecosystem. *Cell Stem Cell* 24, 41–53. <https://doi.org/10.1016/j.stem.2018.12.009>
- Prevedel, R., Diz-Muñoz, A., Ruocco, G., Antonacci, G., 2019. Brillouin microscopy: an emerging tool for mechanobiology. *Nat. Methods* 16, 969–977. <https://doi.org/10.1038/s41592-019-0543-3>
- Puram, S.V., Tirosh, I., Parikh, A.S., Patel, A.P., Yizhak, K., Gillespie, S., Rodman, C., Luo, C.L., Mroz, E.A., Emerick, K.S., Deschler, D.G., Varvares, M.A., Mylvaganam, R., Rozenblatt-Rosen, O., Rocco, J.W., Faquin, W.C., Lin, D.T., Regev, A., Bernstein, B.E., 2017. Single-Cell Transcriptomic Analysis of Primary and Metastatic Tumor Ecosystems in Head and Neck Cancer. *Cell* 171, 1611–1624.e24. <https://doi.org/10.1016/j.cell.2017.10.044>
- Quintana, E., Shackleton, M., Sabel, M.S., Fullen, D.R., Johnson, T.M., Morrison, S.J., 2008. Efficient tumour formation by single human melanoma cells. *Nature* 456, 593–598. <https://doi.org/10.1038/nature07567>
- Rainey, L., Deevi, R.K., McClements, J., Khawaja, H., Watson, C.J., Roudier, M., Van Schaeybroeck, S., Campbell, F.C., 2020. Fundamental control of grade-specific colorectal cancer morphology by Src regulation of ezrin-centrosome engagement. *J. Pathol.* 251, 310–322. <https://doi.org/10.1002/path.5452>
- Ramalho-Santos, M., Yoon, S., Matsuzaki, Y., Mulligan, R.C., Melton, D.A., 2002. “Stemness”: Transcriptional Profiling of Embryonic and Adult Stem Cells. *Science* 298, 597–600. <https://doi.org/10.1126/science.1072530>
- Reymond, N., d’Água, B.B., Ridley, A.J., 2013. Crossing the endothelial barrier during metastasis. *Nat. Rev. Cancer* 13, 858–870. <https://doi.org/10.1038/nrc3628>
- Ricci-Vitiani, L., Lombardi, D.G., Pilozzi, E., Biffoni, M., Todaro, M., Peschle, C., De Maria, R., 2007. Identification and expansion of human colon-cancer-initiating cells. *Nature* 445, 111–115. <https://doi.org/10.1038/nature05384>
- Ring, A., Nguyen-Sträuli, B.D., Wicki, A., Aceto, N., 2023. Biology, vulnerabilities and clinical applications of circulating tumour cells. *Nat. Rev. Cancer* 23, 95–111. <https://doi.org/10.1038/s41568-022-00536-4>
- Roca-Cusachs, P., Conte, V., Trepats, X., 2017. Quantifying forces in cell biology. *Nat. Cell Biol.* 19, 742–751. <https://doi.org/10.1038/ncb3564>
- Rodrigues, J., Heinrich, M.A., Teixeira, L.M., Prakash, J., 2021. 3D In Vitro Model (R)evolution: Unveiling Tumor–Stroma Interactions. *Trends Cancer* 7, 249–264. <https://doi.org/10.1016/j.trecan.2020.10.009>

- Roesch, A., Fukunaga-Kalabis, M., Schmidt, E.C., Zabierowski, S.E., Brafford, P.A., Vultur, A., Basu, D., Gimotty, P., Vogt, T., Herlyn, M., 2010. A Temporarily Distinct Subpopulation of Slow-Cycling Melanoma Cells Is Required for Continuous Tumor Growth. *Cell* 141, 583–594. <https://doi.org/10.1016/j.cell.2010.04.020>
- Rouvière, O., Melodelima, C., Hoang Dinh, A., Bratan, F., Pagnoux, G., Sanzalone, T., Crouzet, S., Colombel, M., Mège-Lechevallier, F., Souchon, R., 2017. Stiffness of benign and malignant prostate tissue measured by shear-wave elastography: a preliminary study. *Eur. Radiol.* 27, 1858–1866. <https://doi.org/10.1007/s00330-016-4534-9>
- Ruscetti, M., Quach, B., Dadashian, E.L., Mulholland, D.J., Wu, H., 2015. Tracking and Functional Characterization of Epithelial-Mesenchymal Transition and Mesenchymal Tumor Cells During Prostate Cancer Metastasis. *Cancer Res.* 75, 2749–2759. <https://doi.org/10.1158/0008-5472.CAN-14-3476>
- Sachs, N., de Ligt, J., Kopper, O., Gogola, E., Bounova, G., Weeber, F., Balgobind, A.V., Wind, K., Gracanin, A., Begthel, H., Korving, J., van Boxtel, R., Duarte, A.A., Lelieveld, D., van Hoeck, A., Ernst, R.F., Blokzijl, F., Nijman, I.J., Hoogstraat, M., van de Ven, M., Egan, D.A., Zinzalla, V., Moll, J., Boj, S.F., Voest, E.E., Wessels, L., van Diest, P.J., Rottenberg, S., Vries, R.G.J., Cuppen, E., Clevers, H., 2018. A Living Biobank of Breast Cancer Organoids Captures Disease Heterogeneity. *Cell* 172, 373–386.e10. <https://doi.org/10.1016/j.cell.2017.11.010>
- Saha, B., Chaiwun, B., Imam, S.S., Tsao-Wei, D.D., Groshen, S., Naritoku, W.Y., Imam, S.A., 2007. Overexpression of E-cadherin Protein in Metastatic Breast Cancer Cells in Bone. *Anticancer Res.* 27, 3903–3908.
- Sahai, E., Astsurov, I., Cukierman, E., DeNardo, D.G., Egeblad, M., Evans, R.M., Fearon, D., Gretchen, F.R., Hingorani, S.R., Hunter, T., Hynes, R.O., Jain, R.K., Janowitz, T., Jorgensen, C., Kimmelman, A.C., Kolonin, M.G., Maki, R.G., Powers, R.S., Puré, E., Ramirez, D.C., Scherz-Shouval, R., Sherman, M.H., Stewart, S., Tlsty, T.D., Tuveson, D.A., Watt, F.M., Weaver, V., Weeraratna, A.T., Werb, Z., 2020. A framework for advancing our understanding of cancer-associated fibroblasts. *Nat. Rev. Cancer* 20, 174–186. <https://doi.org/10.1038/s41568-019-0238-1>
- Samuel, M.S., Lopez, J.I., McGhee, E.J., Croft, D.R., Strachan, D., Timpson, P., Munro, J., Schröder, E., Zhou, J., Brunton, V.G., Barker, N., Clevers, H., Sansom, O.J., Anderson, K.I., Weaver, V.M., Olson, M.F., 2011. Actomyosin-Mediated Cellular Tension Drives Increased Tissue Stiffness and β -Catenin Activation to Induce Epidermal Hyperplasia and Tumor Growth. *Cancer Cell* 19, 776–791. <https://doi.org/10.1016/j.ccr.2011.05.008>
- Saotome, I., Curto, M., McClatchey, A.I., 2004. Ezrin Is Essential for Epithelial Organization and Villus Morphogenesis in the Developing Intestine. *Dev. Cell* 6, 855–864. <https://doi.org/10.1016/j.devcel.2004.05.007>

- Sarrió, D., Rodríguez-Pinilla, S.M., Dotor, A., Calero, F., Hardisson, D., Palacios, J., 2006. Abnormal ezrin localization is associated with clinicopathological features in invasive breast carcinomas. *Breast Cancer Res. Treat.* 98, 71–79. <https://doi.org/10.1007/s10549-005-9133-4>
- Sato, T., Stange, D.E., Ferrante, M., Vries, R.G.J., van Es, J.H., van den Brink, S., van Houdt, W.J., Pronk, A., van Gorp, J., Siersema, P.D., Clevers, H., 2011. Long-term Expansion of Epithelial Organoids From Human Colon, Adenoma, Adenocarcinoma, and Barrett's Epithelium. *Gastroenterology* 141, 1762–1772. <https://doi.org/10.1053/j.gastro.2011.07.050>
- Scarcelli, G., Yun, S.H., 2008. Confocal Brillouin microscopy for three-dimensional mechanical imaging. *Nat. Photonics* 2, 39–43. <https://doi.org/10.1038/nphoton.2007.250>
- Scheel, C., Eaton, E.N., Li, S.H.-J., Chaffer, C.L., Reinhardt, F., Kah, K.-J., Bell, G., Guo, W., Rubin, J., Richardson, A.L., Weinberg, R.A., 2011. Paracrine and autocrine signals induce and maintain mesenchymal and stem cell states in the breast. *Cell* 145, 926–940. <https://doi.org/10.1016/j.cell.2011.04.029>
- Schepers, A.G., Snippert, H.J., Stange, D.E., van den Born, M., van Es, J.H., van de Wetering, M., Clevers, H., 2012. Lineage Tracing Reveals Lgr5+ Stem Cell Activity in Mouse Intestinal Adenomas. *Science* 337, 730–735. <https://doi.org/10.1126/science.1224676>
- Schmidt, J.M., Panzilius, E., Bartsch, H.S., Irmeler, M., Beckers, J., Kari, V., Linnemann, J.R., Dragoi, D., Hirschi, B., Kloos, U.J., Sass, S., Theis, F., Kahlert, S., Johnsen, S.A., Sotlar, K., Scheel, C.H., 2015. Stem-Cell-like Properties and Epithelial Plasticity Arise as Stable Traits after Transient Twist1 Activation. *Cell Rep.* 10, 131–139. <https://doi.org/10.1016/j.celrep.2014.12.032>
- Schnalzgger, T.E., de Groot, M.H., Zhang, C., Mosa, M.H., Michels, B.E., Röder, J., Darvishi, T., Wels, W.S., Farin, H.F., 2019. 3D model for CAR-mediated cytotoxicity using patient-derived colorectal cancer organoids. *EMBO J.* 38, e100928. <https://doi.org/10.15252/embj.2018100928>
- Schwitalla, S., Fingerle, A.A., Cammareri, P., Nebelsiek, T., Göktuna, S.I., Ziegler, P.K., Canli, O., Heijmans, J., Huels, D.J., Moreaux, G., Rupec, R.A., Gerhard, M., Schmid, R., Barker, N., Clevers, H., Lang, R., Neumann, J., Kirchner, T., Taketo, M.M., van den Brink, G.R., Sansom, O.J., Arkan, M.C., Greten, F.R., 2013. Intestinal Tumorigenesis Initiated by Dedifferentiation and Acquisition of Stem-Cell-like Properties. *Cell* 152, 25–38. <https://doi.org/10.1016/j.cell.2012.12.012>
- Scognamiglio, G., De Chiara, A., Parafioriti, A., Armiraglio, E., Fazioli, F., Gallo, M., Aversa, L., Camerlingo, R., Cacciatore, F., Colella, G., Pili, R., de Nigris, F., 2019. Patient-derived organoids as a potential model to predict response to PD-1/PD-L1 checkpoint inhibitors. *Br. J. Cancer* 121, 979–982. <https://doi.org/10.1038/s41416-019-0616-1>
- Seino, T., Kawasaki, S., Shimokawa, M., Tamagawa, H., Toshimitsu, K., Fujii, M., Ohta, Y., Matano, M., Nanki, K., Kawasaki, K., Takahashi, S., Sugimoto, S., Iwasaki,

- E., Takagi, J., Itoi, T., Kitago, M., Kitagawa, Y., Kanai, T., Sato, T., 2018. Human Pancreatic Tumor Organoids Reveal Loss of Stem Cell Niche Factor Dependence during Disease Progression. *Cell Stem Cell* 22, 454–467.e6. <https://doi.org/10.1016/j.stem.2017.12.009>
- Serra, D., Mayr, U., Boni, A., Lukonin, I., Rempfler, M., Challet Meylan, L., Stadler, M.B., Strnad, P., Papasaikas, P., Vischi, D., Waldt, A., Roma, G., Liberali, P., 2019. Self-organization and symmetry breaking in intestinal organoid development. *Nature* 569, 66–72. <https://doi.org/10.1038/s41586-019-1146-y>
- Serra-Picamal, X., Conte, V., Sunyer, R., Muñoz, J.J., Trepát, X., 2015. Chapter 17 - Mapping forces and kinematics during collective cell migration, in: Paluch, E.K. (Ed.), *Methods in Cell Biology, Biophysical Methods in Cell Biology*. Academic Press, pp. 309–330. <https://doi.org/10.1016/bs.mcb.2014.11.003>
- Shahryari, M., Tzschätzsch, H., Guo, J., Marticorena Garcia, S.R., Böning, G., Fehrenbach, U., Stencel, L., Asbach, P., Hamm, B., Käs, J.A., Braun, J., Denecke, T., Sack, I., 2019. Tomoelastography Distinguishes Noninvasively between Benign and Malignant Liver Lesions. *Cancer Res.* 79, 5704–5710. <https://doi.org/10.1158/0008-5472.CAN-19-2150>
- Shimokawa, M., Ohta, Y., Nishikori, S., Matano, M., Takano, A., Fujii, M., Date, S., Sugimoto, S., Kanai, T., Sato, T., 2017. Visualization and targeting of LGR5+ human colon cancer stem cells. *Nature* 545, 187–192. <https://doi.org/10.1038/nature22081>
- Siegel, R.L., Miller, K.D., Fuchs, H.E., Jemal, A., 2022. Cancer statistics, 2022. *CA. Cancer J. Clin.* 72, 7–33. <https://doi.org/10.3322/caac.21708>
- Singh, S.K., Hawkins, C., Clarke, I.D., Squire, J.A., Bayani, J., Hide, T., Henkelman, R.M., Cusimano, M.D., Dirks, P.B., 2004. Identification of human brain tumour initiating cells. *Nature* 432, 396–401. <https://doi.org/10.1038/nature03128>
- Sneddon, J.B., Werb, Z., 2007. Location, Location, Location: The Cancer Stem Cell Niche. *Cell Stem Cell* 1, 607–611. <https://doi.org/10.1016/j.stem.2007.11.009>
- Sontheimer-Phelps, A., Hassell, B.A., Ingber, D.E., 2019. Modelling cancer in microfluidic human organs-on-chips. *Nat. Rev. Cancer* 19, 65–81. <https://doi.org/10.1038/s41568-018-0104-6>
- Stevens, L.C., 1970. The development of transplantable teratocarcinomas from intratesticular grafts of pre- and postimplantation mouse embryos. *Dev. Biol.* 21, 364–382. [https://doi.org/10.1016/0012-1606\(70\)90130-2](https://doi.org/10.1016/0012-1606(70)90130-2)
- Stevens, L.C., 1960. Embryonic potency of embryoid bodies derived from a transplantable testicular teratoma of the mouse. *Dev. Biol.* 2, 285–297. [https://doi.org/10.1016/0012-1606\(60\)90010-5](https://doi.org/10.1016/0012-1606(60)90010-5)
- Stevens, L.C., Little, C.C., 1954. Spontaneous Testicular Teratomas in an Inbred Strain of Mice. *Proc. Natl. Acad. Sci. U. S. A.* 40, 1080–1087.
- Sun, J., Luo, Q., Liu, L., Zhang, B., Shi, Y., Ju, Y., Song, G., 2016. Biomechanical profile of cancer stem-like cells derived from MHCC97H cell lines. *J. Biomech.* 49, 45–52. <https://doi.org/10.1016/j.jbiomech.2015.11.007>

- Sun, Y., Li, H., Chen, Q., Luo, Q., Song, G., 2021. The distribution of liver cancer stem cells correlates with the mechanical heterogeneity of liver cancer tissue. *Histochem. Cell Biol.* 156, 47–58. <https://doi.org/10.1007/s00418-021-01979-w>
- Sun, Z., Guo, S.S., Fässler, R., 2016. Integrin-mediated mechanotransduction. *J. Cell Biol.* 215, 445–456. <https://doi.org/10.1083/jcb.201609037>
- Suresh, S., Spatz, J., Mills, J.P., Micoulet, A., Dao, M., Lim, C.T., Beil, M., Seufferlein, T., 2005. Connections between single-cell biomechanics and human disease states: gastrointestinal cancer and malaria. *Acta Biomater.* 1, 15–30. <https://doi.org/10.1016/j.actbio.2004.09.001>
- Swaminathan, V., Gloerich, M., 2021. Decoding mechanical cues by molecular mechanotransduction. *Curr. Opin. Cell Biol., Cell Dynamics* 72, 72–80. <https://doi.org/10.1016/j.ceb.2021.05.006>
- Swaminathan, V., Mythreye, K., O'Brien, E.T., Berchuck, A., Blobe, G.C., Superfine, R., 2011. Mechanical Stiffness Grades Metastatic Potential in Patient Tumor Cells and in Cancer Cell Lines. *Cancer Res.* 71, 5075–5080. <https://doi.org/10.1158/0008-5472.CAN-11-0247>
- Tachibana, K., Haghparast, S.M.A., Miyake, J., 2015. Inhibition of cell adhesion by phosphorylated Ezrin/Radixin/Moesin. *Cell Adhes. Migr.* 9, 502–512. <https://doi.org/10.1080/19336918.2015.1113366>
- Takamura, M., Ichida, T., Matsuda, Y., Kobayashi, M., Yamagiwa, S., Genda, T., Shioji, K., Hashimoto, S., Nomoto, M., Hatakeyama, K., Ajioka, Y., Sakamoto, M., Hirohashi, S., Aoyagi, Y., 2004. Reduced expression of liver–intestine cadherin is associated with progression and lymph node metastasis of human colorectal carcinoma. *Cancer Lett.* 212, 253–259. <https://doi.org/10.1016/j.canlet.2004.03.016>
- Takebe, T., Zhang, B., Radisic, M., 2017. Synergistic Engineering: Organoids Meet Organs-on-a-Chip. *Cell Stem Cell* 21, 297–300. <https://doi.org/10.1016/j.stem.2017.08.016>
- Tan, Y., Tajik, A., Chen, Junwei, Jia, Q., Chowdhury, F., Wang, L., Chen, Junjian, Zhang, S., Hong, Y., Yi, H., Wu, D.C., Zhang, Y., Wei, F., Poh, Y.-C., Seong, J., Singh, R., Lin, L.-J., Doğanay, S., Li, Y., Jia, H., Ha, T., Wang, Y., Huang, B., Wang, N., 2014. Matrix softness regulates plasticity of tumour-repopulating cells via H3K9 demethylation and Sox2 expression. *Nat. Commun.* 5, 4619. <https://doi.org/10.1038/ncomms5619>
- Tanimoto, H., Sano, M., 2014. A Simple Force-Motion Relation for Migrating Cells Revealed by Multipole Analysis of Traction Stress. *Biophys. J.* 106, 16–25. <https://doi.org/10.1016/j.bpj.2013.10.041>
- Tauriello, D.V.F., Calon, A., Lonardo, E., Batlle, E., 2017. Determinants of metastatic competency in colorectal cancer. *Mol. Oncol.* 11, 97–119. <https://doi.org/10.1002/1878-0261.12018>

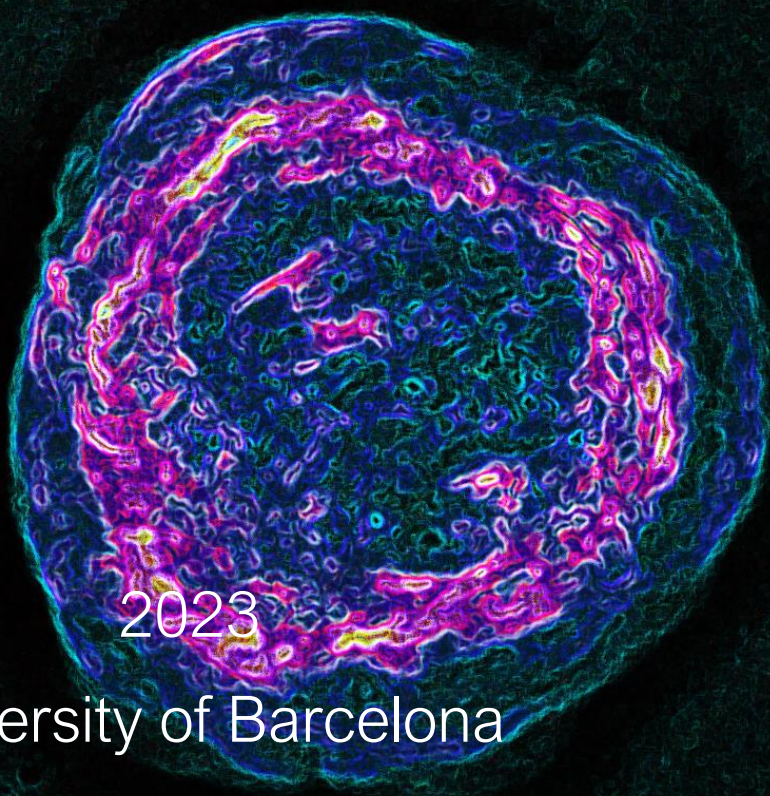
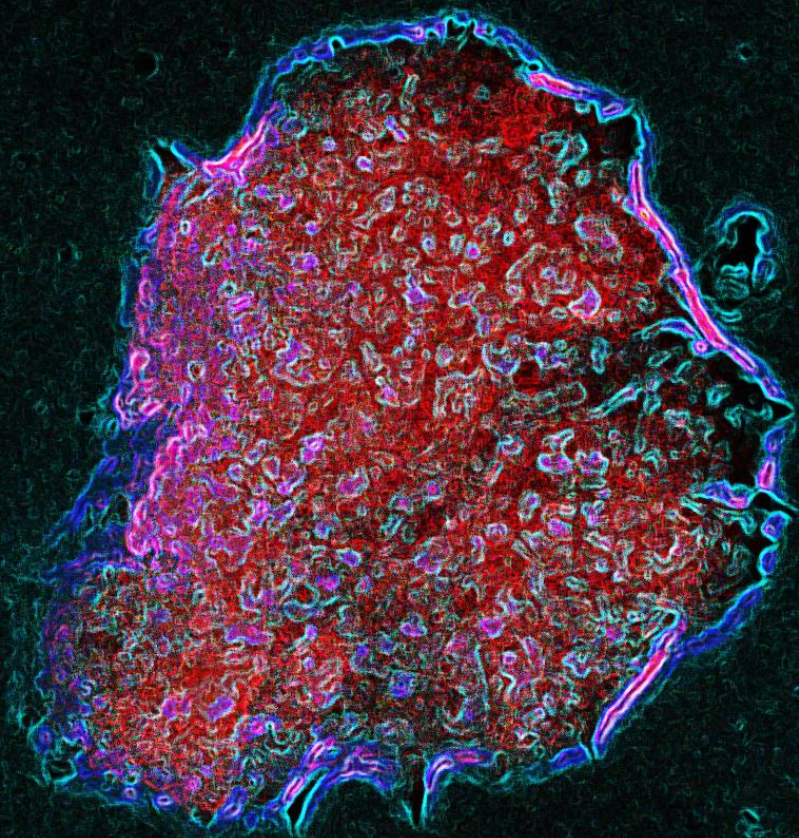
- Thorne, C.A., Chen, I.W., Sanman, L.E., Cobb, M.H., Wu, L.F., Altschuler, S.J., 2018. Enteroid Monolayers Reveal an Autonomous WNT and BMP Circuit Controlling Intestinal Epithelial Growth and Organization. *Dev. Cell* 44, 624–633.e4. <https://doi.org/10.1016/j.devcel.2018.01.024>
- Tian, B., Luo, Q., Ju, Y., Song, G., 2019. A Soft Matrix Enhances the Cancer Stem Cell Phenotype of HCC Cells. *Int. J. Mol. Sci.* 20, 2831. <https://doi.org/10.3390/ijms20112831>
- Tiriac, H., Belleau, P., Engle, D.D., Plenker, D., Deschênes, A., Somerville, T.D.D., Froeling, F.E.M., Burkhart, R.A., Denroche, R.E., Jang, G.-H., Miyabayashi, K., Young, C.M., Patel, H., Ma, M., LaComb, J.F., Palmaira, R.L.D., Javed, A.A., Huynh, J.C., Johnson, M., Arora, K., Robine, N., Shah, M., Sanghvi, R., Goetz, A.B., Lowder, C.Y., Martello, L., Driehuis, E., LeComte, N., Askan, G., Iacobuzio-Donahue, C.A., Clevers, H., Wood, L.D., Hruban, R.H., Thompson, E., Aguirre, A.J., Wolpin, B.M., Sasson, A., Kim, J., Wu, M., Bucobo, J.C., Allen, P., Sejpal, D.V., Nealon, W., Sullivan, J.D., Winter, J.M., Gimotty, P.A., Grem, J.L., DiMaio, D.J., Buscaglia, J.M., Grandgenett, P.M., Brody, J.R., Hollingsworth, M.A., O’Kane, G.M., Notta, F., Kim, E., Crawford, J.M., Devoe, C., Ocean, A., Wolfgang, C.L., Yu, K.H., Li, E., Vakoc, C.R., Hubert, B., Fischer, S.E., Wilson, J.M., Moffitt, R., Knox, J., Krasnitz, A., Gallinger, S., Tuveson, D.A., 2018. Organoid Profiling Identifies Common Responders to Chemotherapy in Pancreatic Cancer. *Cancer Discov.* 8, 1112–1129. <https://doi.org/10.1158/2159-8290.CD-18-0349>
- Tomasetti, C., Vogelstein, B., 2015. Variation in cancer risk among tissues can be explained by the number of stem cell divisions. *Science* 347, 78–81. <https://doi.org/10.1126/science.1260825>
- Trepat, X., Wasserman, M.R., Angelini, T.E., Millet, E., Weitz, D.A., Butler, J.P., Fredberg, J.J., 2009. Physical forces during collective cell migration. *Nat. Phys.* 5, 426–430. <https://doi.org/10.1038/nphys1269>
- Troyanova-Wood, M., Meng, Z., Yakovlev, V.V., 2016. Elasticity-based identification of tumor margins using Brillouin spectroscopy, in: *Biophysics, Biology, and Biophotonics: The Crossroads*. Presented at the Biophysics, Biology, and Biophotonics: the Crossroads, SPIE, pp. 72–77. <https://doi.org/10.1117/12.2213268>
- Tsai, J.H., Donaher, J.L., Murphy, D.A., Chau, S., Yang, J., 2012. Spatiotemporal Regulation of Epithelial-Mesenchymal Transition Is Essential for Squamous Cell Carcinoma Metastasis. *Cancer Cell* 22, 725–736. <https://doi.org/10.1016/j.ccr.2012.09.022>
- Tuveson, D., Clevers, H., 2019. Cancer modeling meets human organoid technology. *Science* 364, 952–955. <https://doi.org/10.1126/science.aaw6985>
- Uckun, F.M., Sather, H., Reaman, G., Shuster, J., Land, V., Trigg, M., Gunther, R., Chelstrom, L., Bleyer, A., Gaynon, P., Crist, W., 1995. Leukemic Cell Growth in SCID Mice as a Predictor of Relapse in High-Risk B-Lineage Acute

- Lymphoblastic Leukemia. *Blood* 85, 873–878. <https://doi.org/10.1182/blood.V85.4.873.bloodjournal854873>
- Urbanska, M., Rosendahl, P., Kräter, M., Guck, J., 2018. Chapter 10 - High-throughput single-cell mechanical phenotyping with real-time deformability cytometry, in: Piel, M., Fletcher, D., Doh, J. (Eds.), *Methods in Cell Biology, Microfluidics in Cell Biology Part B: Microfluidics in Single Cells*. Academic Press, pp. 175–198. <https://doi.org/10.1016/bs.mcb.2018.06.009>
- Vakoc, B.J., Lanning, R.M., Tyrrell, J.A., Padera, T.P., Bartlett, L.A., Stylianopoulos, T., Munn, L.L., Tearney, G.J., Fukumura, D., Jain, R.K., Bouma, B.E., 2009. Three-dimensional microscopy of the tumor microenvironment in vivo using optical frequency domain imaging. *Nat. Med.* 15, 1219–1223. <https://doi.org/10.1038/nm.1971>
- Valdman, A., Fang, X., Pang, S.-T., Nilsson, B., Ekman, P., Egevad, L., 2005. Ezrin expression in prostate cancer and benign prostatic tissue. *Eur. Urol.* 48, 852–857. <https://doi.org/10.1016/j.eururo.2005.03.013>
- van de Wetering, M., Sancho, E., Verweij, C., de Lau, W., Oving, I., Hurlstone, A., van der Horn, K., Batlle, E., Coudreuse, D., Haramis, A.-P., Tjon-Pon-Fong, M., Moerer, P., van den Born, M., Soete, G., Pals, S., Eilers, M., Medema, R., Clevers, H., 2002. The β -Catenin/TCF-4 Complex Imposes a Crypt Progenitor Phenotype on Colorectal Cancer Cells. *Cell* 111, 241–250. [https://doi.org/10.1016/S0092-8674\(02\)01014-0](https://doi.org/10.1016/S0092-8674(02)01014-0)
- Venkatesh, S.K., Yin, M., Glockner, J.F., Takahashi, N., Araoz, P.A., Talwalkar, J.A., Ehman, R.L., 2008. MR Elastography of Liver Tumors: Preliminary Results. *Am. J. Roentgenol.* 190, 1534–1540. <https://doi.org/10.2214/AJR.07.3123>
- Venturini, V., Pezzano, F., Català Castro, F., Häkkinen, H.-M., Jiménez-Delgado, S., Colomer-Rosell, M., Marro, M., Tolosa-Ramon, Q., Paz-López, S., Valverde, M.A., Weghuber, J., Loza-Alvarez, P., Krieg, M., Wieser, S., Ruprecht, V., 2020. The nucleus measures shape changes for cellular proprioception to control dynamic cell behavior. *Science* 370, eaba2644. <https://doi.org/10.1126/science.aba2644>
- Verissimo, C.S., Overmeer, R.M., Ponsioen, B., Drost, J., Mertens, S., Verlaan-Klink, I., Gerwen, B. van, van der Ven, M., Wetering, M. van de, Egan, D.A., Bernards, R., Clevers, H., Bos, J.L., Snippert, H.J., 2016. Targeting mutant RAS in patient-derived colorectal cancer organoids by combinatorial drug screening. *eLife* 5, e18489. <https://doi.org/10.7554/eLife.18489>
- Vermeulen, L., de Sousa e Melo, F., Richel, D.J., Medema, J.P., 2012. The developing cancer stem-cell model: clinical challenges and opportunities. *Lancet Oncol.* 13, e83–e89. [https://doi.org/10.1016/S1470-2045\(11\)70257-1](https://doi.org/10.1016/S1470-2045(11)70257-1)
- Vermeulen, L., Snippert, H.J., 2014. Stem cell dynamics in homeostasis and cancer of the intestine. *Nat. Rev. Cancer* 14, 468–480. <https://doi.org/10.1038/nrc3744>
- Vlachogiannis, G., Hedayat, S., Vatsiou, A., Jamin, Y., Fernández-Mateos, J., Khan, K., Lampis, A., Eason, K., Huntingford, I., Burke, R., Rata, M., Koh, D.-M., Tunariu,

- N., Collins, D., Hulkki-Wilson, S., Ragulan, C., Spiteri, I., Moorcraft, S.Y., Chau, I., Rao, S., Watkins, D., Fotiadis, N., Bali, M., Darvish-Damavandi, M., Lote, H., Eltahir, Z., Smyth, E.C., Begum, R., Clarke, P.A., Hahne, J.C., Dowsett, M., de Bono, J., Workman, P., Sadanandam, A., Fassan, M., Sansom, O.J., Eccles, S., Starling, N., Braconi, C., Sottoriva, A., Robinson, S.P., Cunningham, D., Valeri, N., 2018. Patient-derived organoids model treatment response of metastatic gastrointestinal cancers. *Science* 359, 920–926. <https://doi.org/10.1126/science.aao2774>
- Vleminckx, K., Vakaet, L., Mareel, M., Fiers, W., Van Roy, F., 1991. Genetic manipulation of E-cadherin expression by epithelial tumor cells reveals an invasion suppressor role. *Cell* 66, 107–119. [https://doi.org/10.1016/0092-8674\(91\)90143-M](https://doi.org/10.1016/0092-8674(91)90143-M)
- Vogelstein, B., Papadopoulos, N., Velculescu, V.E., Zhou, S., Diaz, L.A., Kinzler, K.W., 2013. Cancer Genome Landscapes. *Science* 339, 1546–1558. <https://doi.org/10.1126/science.1235122>
- Voutouri, C., Polydorou, C., Papageorgis, P., Gkretsi, V., Stylianopoulos, T., 2016. Hyaluronan-Derived Swelling of Solid Tumors, the Contribution of Collagen and Cancer Cells, and Implications for Cancer Therapy. *Neoplasia* 18, 732–741. <https://doi.org/10.1016/j.neo.2016.10.001>
- Wang, H.-J., Zhu, J.-S., Zhang, Q., Sun, Q., Guo, H., 2009. High level of ezrin expression in colorectal cancer tissues is closely related to tumor malignancy. *World J. Gastroenterol.* 15, 2016–2019. <https://doi.org/10.3748/wjg.15.2016>
- Wang, Q., Shi, Y., Zhou, K., Wang, L., Yan, Z., Liu, Y., Xu, L., Zhao, S., Chu, H., Shi, T., Ma, Q., Bi, J., 2018. PIK3CA mutations confer resistance to first-line chemotherapy in colorectal cancer. *Cell Death Dis.* 9, 1–11. <https://doi.org/10.1038/s41419-018-0776-6>
- Wang, S., Li, E., Gao, Y., Wang, Y., Guo, Z., He, J., Zhang, J., Gao, Z., Wang, Q., 2013. Study on invadopodia formation for lung carcinoma invasion with a microfluidic 3D culture device. *PloS One* 8, e56448. <https://doi.org/10.1371/journal.pone.0056448>
- Wang, Z.A., Mitrofanova, A., Bergren, S.K., Abate-Shen, C., Cardiff, R.D., Califano, A., Shen, M.M., 2013. Lineage analysis of basal epithelial cells reveals their unexpected plasticity and supports a cell-of-origin model for prostate cancer heterogeneity. *Nat. Cell Biol.* 15, 274–283. <https://doi.org/10.1038/ncb2697>
- Welf, E.S., Miles, C.E., Huh, J., Sapoznik, E., Chi, J., Driscoll, M.K., Isogai, T., Noh, J., Weems, A.D., Pohlkamp, T., Dean, K., Fiolka, R., Mogilner, A., Danuser, G., 2020. Actin-Membrane Release Initiates Cell Protrusions. *Dev. Cell* 55, 723–736.e8. <https://doi.org/10.1016/j.devcel.2020.11.024>
- West, J., Schenck, R.O., Gatenbee, C., Robertson-Tessi, M., Anderson, A.R.A., 2021. Normal tissue architecture determines the evolutionary course of cancer. *Nat. Commun.* 12, 2060. <https://doi.org/10.1038/s41467-021-22123-1>

- Winkler, J., Abisoye-Ogunniyan, A., Metcalf, K.J., Werb, Z., 2020. Concepts of extracellular matrix remodelling in tumour progression and metastasis. *Nat. Commun.* 11, 5120. <https://doi.org/10.1038/s41467-020-18794-x>
- Xu, W., Mezencev, R., Kim, B., Wang, L., McDonald, J., Sulchek, T., 2012. Cell Stiffness Is a Biomarker of the Metastatic Potential of Ovarian Cancer Cells. *PLOS ONE* 7, e46609. <https://doi.org/10.1371/journal.pone.0046609>
- Yamauchi, K., Yang, M., Jiang, P., Yamamoto, N., Xu, M., Amoh, Y., Tsuji, K., Bouvet, M., Tsuchiya, H., Tomita, K., Moossa, A.R., Hoffman, R.M., 2005. Real-time *In vivo* Dual-color Imaging of Intracapillary Cancer Cell and Nucleus Deformation and Migration. *Cancer Res.* 65, 4246–4252. <https://doi.org/10.1158/0008-5472.CAN-05-0069>
- Yang, J., Weinberg, R.A., 2008. Epithelial-Mesenchymal Transition: At the Crossroads of Development and Tumor Metastasis. *Dev. Cell* 14, 818–829. <https://doi.org/10.1016/j.devcel.2008.05.009>
- Yankaskas, C.L., Bera, K., Stoletov, K., Serra, S.A., Carrillo-Garcia, J., Tuntithavornwat, S., Mistriotis, P., Lewis, J.D., Valverde, M.A., Konstantopoulos, K., 2021. The fluid shear stress sensor TRPM7 regulates tumor cell intravasation. *Sci. Adv.* 7, eabh3457. <https://doi.org/10.1126/sciadv.abh3457>
- Yao, Y., Xu, X., Yang, L., Zhu, J., Wan, J., Shen, L., Xia, F., Fu, G., Deng, Y., Pan, M., Guo, Q., Gao, X., Li, Y., Rao, X., Zhou, Y., Liang, L., Wang, Y., Zhang, J., Zhang, H., Li, G., Zhang, L., Peng, J., Cai, S., Hu, C., Gao, J., Clevers, H., Zhang, Z., Hua, G., 2020. Patient-Derived Organoids Predict Chemoradiation Responses of Locally Advanced Rectal Cancer. *Cell Stem Cell* 26, 17–26.e6. <https://doi.org/10.1016/j.stem.2019.10.010>
- Yoshida, K., Fujikawa, T., Tanabe, A., Sakurai, K., 1993. Quantitative analysis of distribution and fate of human lung cancer emboli labeled with 125I-5-iodo-2'-deoxyuridine in nude mice. *Surg. Today* 23, 979–983. <https://doi.org/10.1007/BF00308973>
- Yu, F.-X., Zhao, B., Guan, K.-L., 2015. Hippo Pathway in Organ Size Control, Tissue Homeostasis, and Cancer. *Cell* 163, 811–828. <https://doi.org/10.1016/j.cell.2015.10.044>
- Yu, L., Zhao, L., Wu, H., Zhao, H., Yu, Z., He, M., Jin, F., Wei, M., 2019. Moesin is an independent prognostic marker for ER-positive breast cancer. *Oncol. Lett.* 17, 1921–1933. <https://doi.org/10.3892/ol.2018.9799>
- Yuki, K., Cheng, N., Nakano, M., Kuo, C.J., 2020. Organoid Models of Tumor Immunology. *Trends Immunol.* 41, 652–664. <https://doi.org/10.1016/j.it.2020.06.010>
- Zajac, O., Raingeaud, J., Libanje, F., Lefebvre, C., Sabino, D., Martins, I., Roy, P., Benatar, C., Canet-Jourdan, C., Azorin, P., Polrot, M., Gonin, P., Benbarche, S., Souquere, S., Pierron, G., Nowak, D., Bigot, L., Ducreux, M., Malka, D., Lobry, C., Scoazec, J.-Y., Eveno, C., Pocard, M., Perfettini, J.-L., Elias, D., Dartigues, P., Goéré, D., Jaulin, F., 2018. Tumour spheres with inverted polarity

- drive the formation of peritoneal metastases in patients with hypermethylated colorectal carcinomas. *Nat. Cell Biol.* 20, 296–306. <https://doi.org/10.1038/s41556-017-0027-6>
- Zanconato, F., Cordenonsi, M., Piccolo, S., 2016. YAP/TAZ at the Roots of Cancer. *Cancer Cell* 29, 783–803. <https://doi.org/10.1016/j.ccell.2016.05.005>
- Zhang, C., Samanta, D., Lu, H., Bullen, J.W., Zhang, H., Chen, I., He, X., Semenza, G.L., 2016. Hypoxia induces the breast cancer stem cell phenotype by HIF-dependent and ALKBH5-mediated m6A-demethylation of NANOG mRNA. *Proc. Natl. Acad. Sci.* 113, E2047–E2056. <https://doi.org/10.1073/pnas.1602883113>
- Zhang, S., Balch, C., Chan, M.W., Lai, H.-C., Matei, D., Schilder, J.M., Yan, P.S., Huang, T.H.-M., Nephew, K.P., 2008. Identification and Characterization of Ovarian Cancer-Initiating Cells from Primary Human Tumors. *Cancer Res.* 68, 4311–4320. <https://doi.org/10.1158/0008-5472.CAN-08-0364>
- Zhang, Y.S., Aleman, J., Shin, S.R., Kilic, T., Kim, D., Mousavi Shaegh, S.A., Massa, S., Riahi, R., Chae, S., Hu, N., Avci, H., Zhang, W., Silvestri, A., Sanati Nezhad, A., Manbohi, A., De Ferrari, F., Polini, A., Calzone, G., Shaikh, N., Alerasool, P., Budina, E., Kang, J., Bhise, N., Ribas, J., Pourmand, A., Skardal, A., Shupe, T., Bishop, C.E., Dokmeci, M.R., Atala, A., Khademhosseini, A., 2017. Multisensor-integrated organs-on-chips platform for automated and continual in situ monitoring of organoid behaviors. *Proc. Natl. Acad. Sci.* 114, E2293–E2302. <https://doi.org/10.1073/pnas.1612906114>
- Zhao, Z., Chen, X., Dowbaj, A.M., Sljukic, A., Bratlie, K., Lin, L., Fong, E.L.S., Balachander, G.M., Chen, Z., Soragni, A., Huch, M., Zeng, Y.A., Wang, Q., Yu, H., 2022. Organoids. *Nat. Rev. Methods Primer* 2, 1–21. <https://doi.org/10.1038/s43586-022-00174-y>
- Zhou, W., Lv, R., Qi, W., Wu, D., Xu, Y., Liu, W., Mou, Y., Wang, L., 2014. Snail Contributes to the Maintenance of Stem Cell-Like Phenotype Cells in Human Pancreatic Cancer. *PLoS ONE* 9, e87409. <https://doi.org/10.1371/journal.pone.0087409>
- Zhu, T.S., Costello, M.A., Talsma, C.E., Flack, C.G., Crowley, J.G., Hamm, L.L., He, X., Hervey-Jumper, S.L., Heth, J.A., Muraszko, K.M., DiMeco, F., Vescovi, A.L., Fan, X., 2011. Endothelial cells create a stem cell niche in glioblastoma by providing NOTCH ligands that nurture self-renewal of cancer stem-like cells. *Cancer Res.* 71, 6061–6072. <https://doi.org/10.1158/0008-5472.CAN-10-4269>
- Zomer, A., Ellenbroek, S.I.J., Ritsma, L., Beerling, E., Vrisekoop, N., Van Rheenen, J., 2013. Brief Report: Intravital Imaging of Cancer Stem Cell Plasticity in Mammary Tumors. *Stem Cells* 31, 602–606. <https://doi.org/10.1002/stem.1296>
- Zuela-Sopilniak, N., Lammerding, J., 2022. Can't handle the stress? Mechanobiology and disease. *Trends Mol. Med.* 28, 710–725. <https://doi.org/10.1016/j.molmed.2022.05.010>



2023

University of Barcelona